Steinar Liebe Harneshaug
Lars Otto Lofthus Ose

Modelling of laminated glass

June 2020

Master's thesis

Master's thesis

2020

Steinar Liebe Harneshaug, Lars Otto Lofthus Ose

NTNU
Norwegian University of
Science and Technology
Faculty of Engineering
Department of Structural Engineering

NTNU
Norwegian University of
Science and Technology

NTNU
Norwegian University of
Science and Technology

NTNU
Norwegian University of
Science and Technology

Modelling of laminated glass

Steinar Liebe Harneshaug
Lars Otto Lofthus Ose

Department of Structural Engineering
Faculty of Engineering
NTNU – **Norwegian University of Science and Technology**

MASTER THESIS 2020

SUBJECT AREA:	DATE:	NO. OF PAGES:
Computational Mechanics	June 11th, 2020	7 + 80 + 37

TITLE:

Modelling of laminated glass

Modellering av laminert glass

BY:

Steinar Liebe Harneshaug

Lars Otto Lofthus Ose

SUMMARY:

Automobile windshields are optimized for protecting vulnerable road users from head injury in case of a head impact. The windshields should additionally protect the occupants from the outer environment and free-flying objects. Accurate and efficient numerical tools for simulating the behaviour of laminated glass exposed to different loading are therefore demanded by the industry. This thesis will review how existing and commercially available tools in the finite element (FE) code Abaqus are able to simulate the structural behaviour of laminated glass. The simulations will be compared with low-velocity impact tests and quasi-static punch tests.

Experimental tests have been performed in order to investigate typical responses and failure modes of monolithic and laminated glass exposed to dynamic and quasi-static loading. Dynamic tests were performed in a drop tower on both monolithic and laminated glass. All tests were run with a 6.551 kg half-spherical shaped impactor with a radius of 50 mm. Tests with impact velocities of 2 m/s and 4 m/s were performed on monolithic glass, and 1 m/s, 2 m/s, 6 m/s and 10 m/s on laminated glass. Quasi-static punch tests were performed on laminated glass with a loading rate of 3 mm/min. Digital cameras and 3D DIC were used to detect the position of fracture initiation and to measure the displacement of selected points on the glass panes during the experiments. All experiments showed similar fracture behaviour with initial radial fractures followed by circumferential fractures.

Explicit non-linear FE simulations of the experiments were performed in Abaqus. The built-in Brittle Cracking model in Abaqus was used together with element erosion to model glass failure. A series of factorial design studies were performed in order to investigate how changes in different parameters influenced the numerical results and how changes in different parameters interacted with each other. The simulations were able to reproduce the general trends in the failure modes of glass. The best performing simulation of laminated glass with an impact velocity of 5.8 m/s deviated 16.2% from the experiment in HIC_{15} value. Head impact simulations on a laminated windshield were performed as a case study. A major numerical challenge with Brittle Cracking and element erosion was the slow fracture growth and a limited amount of fractures. The experiments showed extremely fast fracture growth, which reduced the stiffness of the glass immediately after fracture initiation. This effect proved to be a numerical challenge.

RESPONSIBLE TEACHER: Professor Tore Børvik

SUPERVISORS: Professor Tore Børvik, Postdoctoral fellow Karoline Osnes,
PhD-candidate Jonas Rudshaug

CARRIED OUT AT: Department of Structural Engineering, NTNU

Institutt for konstruksjonsteknikk
Fakultet for ingeniørvitenskap
NTNU – **Norges teknisk-naturvitenskapelige universitet**

MASTEROPPGAVE 2020

FAGOMRÅDE:	DATO:	ANTALL SIDER:
Beregningsmekanikk	11. Juni 2020	7 + 80 + 37

TITTEL:

Modellering av laminert glass

Modelling of laminated glass

UTFØRT AV:

Steinar Liebe Harneshaug

Lars Otto Lofthus Ose

SAMMENDRAG:

Frontruter på biler er optimalisert for å beskytte myke trafikanter mot hodeskader ved påkjørsler. Frontrutene skal i tillegg beskytte fører og passasjerer mot ytre omgivelser og flyvende objekter. Industrien etterspør nøyaktige og effektive numeriske verktøy for å simulere oppførselen til laminert glass under ulike typer belastninger. Denne avhandlingen vil undersøke hvordan eksisterende og kommersielt tilgjengelige verktøy i elementmetodeprogrammet Abaqus er i stand til å simulere den strukturelle oppførselen til laminert glass. Simuleringene vil sammenlignes med fallverksforsøk og kvasistatiske trykktester.

Eksperimentelle tester har blitt utført for å undersøke typisk respons og bruddmekanismer i monolittisk og laminert glass som er påført dynamiske og kvasistatiske laster. Dynamiske tester ble utført på monolittiske og laminerte glassplater i et fallverk. En halvsfæriskformet dor med radius på 50 mm og masse på 6.551 kg ble benyttet i alle forsøkene. Hastigheter på 2 m/s og 4 m/s ble benyttet på monolittiske glassplater, og 1 m/s, 2 m/s, 6 m/s og 10 m/s ble benyttet på laminerte glassplater. Kvasistatiske tester ble utført på laminerte glassplater med en hastighet på 3 mm/min. Digitale kameraer og 3D DIC ble benyttet for å oppdage hvor bruddet startet og for å måle deformasjonen til utvalgte punkter på glassplaten underveis i forsøket. Alle eksperimentene viste den samme bruddoppførselen med radielle brudd i starten etterfulgt av sirkulære brudd.

Det ble utført Ikke-lineære eksplisitte elementmetodesimuleringer av forsøkene i Abaqus. Den innbygde bruddmodellen Brittle Cracking i Abaqus ble brukt sammen med elementerosjon for å modellere sprekkdannelsen i glasset. Fullstendige parameterstudier ble utført der både virkningen av en parameter og vekselvirkningen mellom ulike parametere ble undersøkt. Simuleringene var i stand til å gjenskape de samme trendene som ble observert i forsøkene. Simuleringen som presterte best hadde et avvik på 16.2% i HIC_{15} fra eksperimentelle forsøk. Denne simuleringen ble utført med en støthastighet på 5.8 m/s. Simuleringer av hodestøt mot frontrute ble utført som en eksempel-studie. Treg bruddvekst og et begrenset antall brudd var en gjennomgående utfordring i simuleringene med Brittle Cracking og elementerosjon. Det ble observert veldig rask bruddvekst i eksperimentene, noe som medførte en rask reduksjon i stivheten etter initiering av første brudd. Denne mekanismen viste seg å være vanskelig å simulere.

FAGLÆRER: Professor Tore Børvik

VEILEDERE: Professor Tore Børvik, Postdoktor Karoline Osnes, PhD-kandidat Jonas Rudshaug

UTFØRT VED: Institutt for konstruksjonsteknikk, NTNU

Department of Structural Engineering
FACULTY OF ENGINEERING
NTNU – Norwegian University of Science and Technology

MASTER'S THESIS 2020

for

Steinar Liebe Harneshaug and Lars Otto Lofthus Ose

Modelling of laminated glass

1. INTRODUCTION

Laminated glass is widely used in security glazing and as windshields in vehicles. The laminated glass normally consists of two soda-lime glass sheets bonded together with a polymer interlayer, preferably polyvinyl butyral (PVB). Laminated glass reduces the risk of free-flying glass fragments by retaining them on the PVB interlayer after glass failure. Additionally, the use of a PVB interlayer increases the structural integrity of the laminated glass, mainly because PVB can withstand large strains.

To optimise the laminated glass design towards different type of loadings, it is important to understand the behaviour of the glass, the polymer, and the component as a whole. Special attention must be paid to the conditions for and the types of failure mechanisms in the glass. Due to existing microscopic flaws in the glass surface, the strength will have a large scatter when exposed to extreme loading. Numerical simulations of failure in laminated glass have received considerable attention in recent years and are of large interest to several industries.

2. OBJECTIVES

The main objective of this master's thesis is to study how laminated glass components behave under low-velocity impact loading. Numerical models will be made to examine the response of the components by use of the finite element methods. Some experiments in a drop-tower will be used to validate the numerical models and to examine to which extent they can predict the response of the laminated glass under dynamic loading conditions.

3. A SHORT DESCRIPTION OF THE RESEARCH PROJECT

The main topics in the research project will be as follows:

1. A literature review ("state-of-the-art") shall be conducted to understand the role of laminated glass as a safety component. Additionally, the behaviour and numerical modelling of glass and PVB exposed to various loading scenarios shall be reviewed in some detail.
2. A few impact tests in a drop-tower will be conducted to expose plain glass and laminated glass to various loading scenarios. The experiments, together with data from the literature, shall be used to investigate typical responses and failure modes of glass and PVB exposed to low-velocity impact loads.
3. Digital cameras will be used to measure the displacement field by 3D-DIC and the position of failure initiation of the glass specimens in the experiments.
4. Non-linear finite element simulations of the experiments using Abaqus and commercially available material models will be performed, and the numerical results shall be compared and discussed based on the experimental findings.

Supervisors: Tore Børvik (NTNU), Karoline Osnes (NTNU) and Jonas Rudshaug (NTNU).

The thesis must be written according to current requirements and submitted to the Department of Structural Engineering, NTNU, no later than June 11th, 2020.

NTNU, January 15th, 2020.

Tore Børvik
Professor

Acknowledgement

<div align="center">
Trondheim, June 11th 2020
</div>

Abstract

Automobile windshields are optimized for protecting vulnerable road users from head injury in case of a head impact. The windshields should additionally protect the occupants from the outer environment and free-flying objects. Accurate and efficient numerical tools for simulating the behaviour of laminated glass exposed to different loading are therefore demanded by the industry. This thesis will review how existing and commercially available tools in the finite element (FE) code Abaqus are able to simulate the structural behaviour of laminated glass. The simulations will be compared with low-velocity impact tests and quasi-static punch tests.

Experimental tests have been performed in order to investigate typical responses and failure modes of monolithic and laminated glass exposed to dynamic and quasi-static loading. Dynamic tests were performed in a drop tower on both monolithic and laminated glass. All tests were run with a 6.551 kg half-spherical shaped impactor with a radius of 50 mm. Tests with impact velocities of 2 m/s and 4 m/s were performed on monolithic glass, and 1 m/s, 2 m/s, 6 m/s and 10 m/s on laminated glass. Quasi-static punch tests were performed on laminated glass with a loading rate of 3 mm/min. Digital cameras and 3D DIC were used to detect the position of fracture initiation and to measure the displacement of selected points on the glass panes during the experiments. All experiments showed similar fracture behaviour with initial radial fractures followed by circumferential fractures.

Explicit non-linear FE simulations of the experiments were performed in Abaqus. The built-in Brittle Cracking model in Abaqus was used together with element erosion to model glass failure. A series of factorial design studies were performed in order to investigate how changes in different parameters influenced the numerical results and how changes in different parameters interacted with each other. The simulations were able to reproduce the general trends in the failure modes of glass. The best performing simulation of laminated glass with an impact velocity of 5.8 m/s deviated 16.2% from the experiment in HIC_{15} value. Head impact simulations on a laminated windshield were performed as a case study. A major numerical challenge with Brittle Cracking and element erosion was the slow fracture growth and a limited amount of fractures. The experiments showed extremely fast fracture growth, which reduced the stiffness of the glass immediately after fracture initiation. This effect proved to be a numerical challenge.

Contents

1. Introduction

1.1 Motivation

Pedestrian safety has received increased attention in the automotive industry in recent years. Windshields are optimized to protect vulnerable road users from serious injury. The windshields should additionally protect the occupants from the outer environment and free-flying objects.

New car assessment programmes (NCAP), such as Euro NCAP, tests and verifies the safety of new cars [1]. The purpose of the programmes is to give the consumers an independent review of new cars safety. Euro NCAP gives the cars a score based on the safety performance within the four categories: adult occupant protection, child occupant protection, vulnerable road user protection and safety assistance technology [2]. A five-star rating system represents the final score, where five stars are the best rating. The test protocols are continuously improved, and the requirements to get the best score are progressively more challenging. Five tests determine the score within the category vulnerable road user protection: Head impact, upper leg impact, lower leg impact, autonomous emergency brakes for pedestrian and cyclists. The first test imitates a pedestrian impacting a bonnet or a windshield with the head in 40 km/h. The score in the test is given by the measured Head Injury Criterion (HIC) value in the impact. HIC is a measurement on the protection against brain damage and skull fracture [3, 4]. The criterion is calibrated from experimental tests on cadaver heads, and the value gives information about the likelihood of head injury. HIC is defined in Equation 1.1 [5].

$$HIC = \max_{t_1,t_2} \left(\left[\frac{1}{t_2 - t_1} \int_{t_1}^{t_2} \sqrt{a_i a_i} dt \right]^{2.5} \left(t_2 - t_1 \right) \right) \tag{1.1}$$

Where t_1 and t_2 are two instances in the impact, and $\sqrt{a_i a_i}$ is the resultant translational acceleration of the centre of gravity of the head during impact. The acceleration is measured in units of standard gravity. t_1 and t_2 are chosen such that the HIC-measurement is maximized. In the HIC_{15} measurement, the maximum duration of interest, t_2 - t_1, is 15 ms.

It is of great importance for a car manufacturer to achieve the best score in an NCAP test to be competitive and sell cars. Increased use of numerical tools, such as the finite element method, instead of physical testing, will save the industry for time and money, in addition to saving the environment. Accurate and predictable numerical tools for simulating the structural behaviour of laminated glass are therefore crucial for design and verification of safe windshields.

1.2 Background

Laminated glass is a composite material consisting of two or more glass layers with polymer interlayer in-between. There exist several variations with regard to glass and interlayer type. Each variation yields different behaviour. Soda-lime-silica glass and polyvinyl butyral (PVB) interlayer are the most commonly used components of an automobile windshield.

There exist two extreme bounds on the characteristic behaviour of laminated glass which can be categorized as the upper bound and lower bound. The upper bound postulates a behaviour from classical Euler-Bernoulli beam theory. This behaviour implies that cross-sections perpendicular to the neutral axis remain plane and perpendicular to the neutral axis during bending. The upper glass layer will hence be in pure compression and the lower glass be in pure tension. The lower bound assumes that the two glass layers behave as distinctly separate units and the interlayer only acts as a spacing between the glass layers [6]. Real laminated glass plates behave somewhere in between the two bounds, and the behaviour is determined by the interlayers ability to transfer shear forces. The material used as interlayer is often a thermoviscous polymer, which implies that the interlayer stiffness is dependent on both strain rate and temperature [7, 8].

The advantage of laminated glass in windshields lies in the post-fracture behaviour, which is defined by fractures in all glass panes. In the post-fracture phase, the fractured glass shards are bonded to the interlayer and the elastic interlayer offer greater post-fracture energy absorption compared to monolithic glass [9]. The failure process of laminated glass is fairly complex due to the interaction between glass and interlayer. The process can be idealized and is summarized below in five steps according to Larcher et al. [10], and is shown in Figure 1.1.

1. Elastic behaviour

2. The first glass layer fails, the second is intact. The interlayer is undamaged.

3. The second glass layer fails. The interlayer behaves elastically.

4. The interlayer deforms plastically while retaining the shards.

5. The interlayer fails by reaching ultimate tensile capacity or by tearing from shards.

The same idealized behaviour shown in Figure 1.1 can also be seen in dynamic impacts on laminated glass. Alter et al. [11] described the failure process in dynamic impact by the three phases shown in Figure 1.2, which also corresponds to the three first phases described by Larcher et al. The two latter phases in Figure 1.1 may also be present in a low-velocity impact.
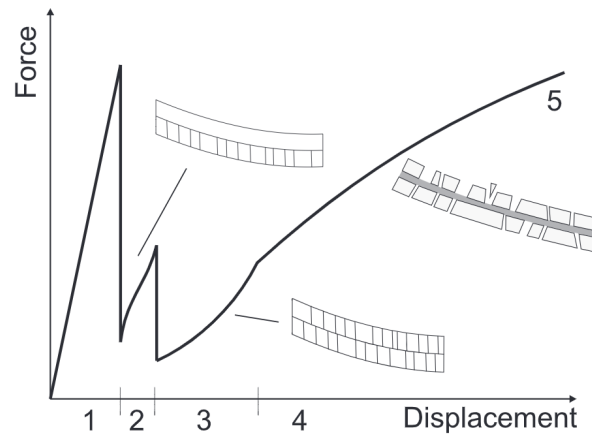
Figure 1.1: Idealized failure process of laminated glass. Adapted from [10].
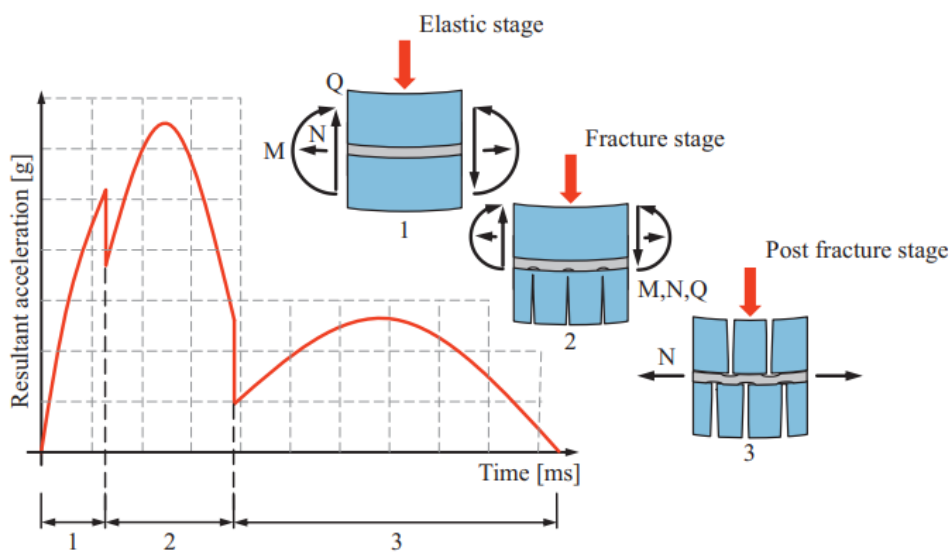
Figure 1.2: Idealized failure process of laminated glass exposed to impact loading with the resultant acceleration of the impactor on the y-axis. Adapted from [11].

Delamination properties are essential for the behaviour of laminated glass under extreme loading. The adhesive strength is controlled by many factors, such as the materials used and the autoclave process [12]. The strength of the adhesion between glass and interlayer controls the amount of delamination. Two cases can be considered. First, if the level of adhesion is low, then the glass will detach from the interlayer and produce dangerous high-velocity shards. Since the amount of adhesion is low, the size of shards is large and comparable with impact on a monolithic glass. Second, if the level of adhesion is high, then little delamination will occur and the glass will break into smaller pieces while being attached to the polymer. This will lead to large strains in the interlayer since the area subject to straining becomes relatively small and may lead to early tearing of the interlayer. In an ideal world, both of the characteristics of high and low adhesion levels are preferable. A polymer interlayer that is able to break the glass into small fragments and absorb large amounts of energy by straining

would be beneficial. Therefore, the amount of adhesion is a trade-off between fragmentation and energy absorption.

The structural behaviour of glass is dominated by brittle behaviour. The strength is determined by the presence of surface cracks. The cracks are randomly distributed in size, density and orientation, which causes the glass strength to be probabilistic. The point of initiated failure in the glass is therefore not necessarily the point of maximum stress. Beason and Morgan [13] described the probabilistic behaviour and proposed a failure prediction model for laterally loaded glass plates. They also suggested that the probability of glass failure was Weibull distributed.

Yankelevsky [14] proposed a new model to predict the strength of annealed glass plates in 2014. This model has been further developed by Osnes et al. [15]. The model aims to predict failure in a glass plate based on the stress history and a log-normal distribution of surface cracks in both size and orientation. The distribution of surface cracks is assigned to a flaw map. By running a Monte Carlo simulation with different flaw maps, the model gives a probability distribution of the glass strength and the position of crack initiation. This enables the model to include the probabilistic behaviour of glass.

The PVB polymer is a commonly used interlayer material in laminated glass for automotive applications [7]. Authors in the literature have investigated the mechanical behaviour of PVB, and the material response was found to be highly non-linear and strain rate-dependent. The material response is also dependent on temperature and UV-light [16, 17]. PVB material models used in simulations of laminated glass are usually fitted to experimental tests on plain PVB [18, 19, 20].

Simulating failure in brittle materials is considered as a challenging task due to the highly non-linear and abrupt change in material response in the event of failure. The low fracture energy in glass introduces additional challenges in terms of modelling since it causes the fractures to grow fast.

Element erosion is a method to model failure in a FE model, which is easy to implement. When a certain criterion is reached within an element, the element erodes from the FE mesh when using element erosion. This causes removal of mass, which could affect the energy balance. The element erosion method is efficient since it does not introduce any new equations in the computations after failure. Failure in brittle materials is dominated by extensive fragmentation. Element erosion could therefore result in an unrealistic failure behaviour when combined with large element sizes and brittle material behaviour. Great care must be taken when choosing an erosion criterion and material model in order to obtain reliable results [21]. Pelfrene et al. [22] simulated glass exposed to a low-velocity impact by using element

erosion. The study showed that element erosion could give realistic results when sufficiently small elements were used. They used the commercially available Brittle Cracking model in Abaqus to model the material behaviour and as erosion criterion. The Brittle Cracking model is based on the Fictitious Crack Model proposed by Hillerborg et al. [23], which was originally developed for brittle fracturing in concrete. This model includes a tension softening phase with reduction of stiffness before deletion of the element. Pelfrene et al. observed slower crack propagation than in the experiment.

Node-splitting is another method for modelling failure in a FE model. The node-splitting technique split the nodes in the FE mesh rather than removing the element when a failure criterion is met. The mass is therefore conserved, and the energy balance is maintained. The splitting of nodes introduces new degrees of freedom, which increase the number of equations to solve [24]. Osnes et al. [25] simulated laminated glass plates exposed to blast load with the FE code IMPETUS Afea Solver. A node-splitting technique was used for modelling the fractures in the glass, and the simulation predicted a realistic fracture pattern.

The intrinsic cohesive zone approach has also been used for modelling glass failure. Regions of glass elements are divided by cohesive zones in the cohesive zone model. The fractures are represented by separation of the cohesive zones, and the fractures are initiated by following a traction separation law [21]. Gao et al. [26] simulated head impacts on automobile windshield by using the cohesive zone approach. Abaqus was used, and the results were compared with simulations where element erosion had been used. Acceleration measurements of the head shaped impactor from the cohesive zone model were comparable with the element erosion model. The cohesive zone model produced more realistic fracture patterns.

The extended finite element method (XFEM) is an approach for simulation of evolving cracks in a FE model. The XFEM method enriches elements with higher-order shape functions, such that they can catch the high stresses at the crack tip. This allows the FE model to follow evolving cracks without the need of a very refined mesh around the crack tip. The crack itself is usually displayed in the FE model by deleting elements. Due to the computational cost from the enrichment of the shape functions, the XFEM approach is usually most suited for following a single crack rather than multi-fracture cases [21]. Xu et al. [27] used the XFEM approach to simulate a head impact on a windshield. The XFEM simulations were able to recreate both the radial and the circumferential fractures that Xu et al. have observed in experiments.

Yang et al. [28] used combined discrete element (DE)/finite element code for modelling low-velocity impact behaviour of laminated glass. Experimental drop hammer tests were also conducted. The glass was modelled with discrete elements and a cohesive model to describe the bonding between the glass particles. The PVB interlayer was modelled with 3D finite

elements. A penalty-based approach was used to model the adhesion between the discrete glass particles and interlayer finite elements. The results from the simulations predicted a realistic fracture behaviour and the numerical values of the impactor acceleration was nearly coinciding with the experimental results.

Wei et al. [29] combined a Taylor–Chen–Kuszmaul (TCK) model in tension for describing the rate-dependent damage behaviour of glass and a Johnson-Holmquist Ceramic (JH2) model in compression. The model used the volumetric strain within an element to determine the appropriate material model. They further implemented the model as a user-defined subroutine in Abaqus and compared the simulation results to experimental tests conducted in a drop tower. The simulation results were promising both in terms of global response and crack pattern.

Pyttel et al. [30] proposed a non-local failure criterion for laminated glass, which has been further improved by Alter et al. [11]. The criteria were implemented in the finite element solvers PAM-CRASH and LS-DYNA, respectively. Simulations of head impacts on laminated automobile windshields were performed and compared with experimental tests. Simulations with both criteria were able to replicate the sudden drop in acceleration experienced by a headform during a head impact on a laminated automobile windshield.

LS-DYNA [31, 32] have implemented a material model, MAT_GLASS (MAT_280). The model lets the user assign a laminated glass section to a shell element mesh. The glass is modelled as shell elements and the PVB interlayer is modelled as solid elements. Three different stress-based failure criteria are available in the model: Rankine, Mohr-Columb and Drucker-Prager. The stress in tension is reduced to a user-specified level in a failed element, but the element does not erode from the mesh. The model is thus able to simulate crack closure effects and transfer compressive forces after glass fracture. A non-local criterion motivated by Pyttel et al. [30] is also included in the model in the R11.0 version of LS-DYNA. The non-local criterion also includes strain-rate dependent tensile strength, which has been observed in glass by Osnes et al. [33], among others.

There has been considerable research on the strength and the behaviour of the bonding between glass and interlayer in laminated glass. Much of the valuable properties of a composite, such as laminated glass, are determined by the adhesion between layers. Several experimental tests have been used in an attempt to determine the characteristic behaviour, such as through-cracked tension test (TCT), pummel test, compressive shear test and 90° peel test [34]. Samieiana et al. [35] investigated the effect of temperature and strain rate on the adhesion between glass and interlayer. It was found that the adhesion level is insensitive to temperatures between 20 and 60 degrees Celsius at constant load rates. The adhesion level displayed a significant loading rate dependency for a constant temperature. The finite

element simulations successfully reproduced the experimental results. Linz et al. [16] used the TCT test on laminated glass in order to investigate the delamination behaviour of PVB and glass under high deformation rates. Finite element simulations were used to estimate the delamination energies and speeds.

There are different methods for modelling the bonding between the glass and the interlayer. Two of the most common are shared nodes and penalty based methods. The latter includes both extrinsic and intrinsic descriptions by traction-separation laws. By using shared nodes, the bonding between the glass and the interlayer is complete and relative displacements between them are not allowed. This approach is viable for simulating the pre-fracture response of laminated glass [33]. Penalty based methods maintain the bonding between glass and interlayer by imposing penalty forces through traction-separation laws. The stiffness of the bonding can be adjusted by changing the penalty stiffness [36]. Chen et al. [37] performed numerical simulations of impact on laminated glass with an intrinsic cohesive formulation and compared it with simulations where shared nodes were used. Simulations with intrinsic cohesive formulation gave the most physically correct damage pattern both in terms of delamination and crack propagation in the glass.

1.3   Scope of thesis

This thesis will focus on the behaviour of laminated glass subjected to low-velocity impact loading. The behaviour will be examined in experimental tests and simulations by use of the FE solver Abaqus.

The experimental work will consist of quasi-static and dynamic tests. Quasi-static tests will be performed as punch tests on laminated glass. Dynamic tests will be performed in a drop tower on both monolithic and laminated glass. All glass plates will be clamped along its edges. A half spherical-shaped impactor with a radius of 50 mm will be used. During the experiments, digital cameras will measure the displacement at selected points on the glass, and a load cell will measure the contact force. The experiments shall investigate typical responses and failure modes in glass. They shall additionally give information about what results that can be expected from the simulations.

The main scope of the thesis is to explore and investigate the capabilities of simulating both pre- and post-cracking behaviour of glass with tools available in Abaqus [38]. Several factorial design studies will be performed with the motivation to investigate how changes in different parameters influence the numerical results and how changes in different parameters interact with each other.

2. Experimental work

The experimental work in this thesis consists of dynamic low-velocity impact tests and quasi-static punch tests. The dynamic tests were performed on monolithic and laminated glass, while the quasi-static tests only included laminated glass. The motivation for performing the quasi-static tests was to understand the behaviour of laminated glass better. In a quasi-static test, the dynamic forces are not present and each phase of the fracture process in Figure 1.1 is easy to recognize.

2.1 Dynamic tests

2.1.1 Methods

Prior to the tests, a coordinate system was defined on each glass plate. The thickness was measured along the edge at the eight points shown in Figure A.1 in Appendix A and the measurements are presented in Table A.1 in Appendix A. The laminated glass plates had a nominal thickness of 9.12 mm, where the PVB interlayer had a nominal thickness of 1.52 mm and each of the glass plates had a nominal thickness of 3.8 mm. The monolithic glass plates had a nominal thickness of 3.8 mm. All plates showed a standard deviation in thickness of less than 0.02 mm. All visible defects were noted. Optical targets were painted on the glass plates and their position in the defined coordinate system was measured. The targets were needed for the 3D DIC measurements. The positions of the targets are shown in Figure A.2 in Appendix A.

The low-velocity impact tests were performed in an Instron CEAST 9350 drop tower at the Structural Engineering Laboratory at NTNU in Trondheim. This drop tower can simulate impacts from dropped objects with kinetic energy up until 1800 J [39].

The force, P, in the striker was measured by a load cell with a sampling rate of 1 MHz. The load cell was positioned approximately 225 mm from the bottom of the impactor. For calculating the contact force, F, between the glass and the impactor, the mass below the load cell needs to be taken into account. This can be done by using dynamic equilibrium as described by Reyes et al. [40] and defined in Equation 2.1.

$$F = \left(1 + \frac{m_2}{m_1}\right) P \tag{2.1}$$

Where m_1 and m_2 is the mass above and below the load cell, respectively. Striker velocity, v and displacement w during the impact can be found from the numerical integration schemes

in Equation 2.2.

$$v_{n+1} = v_n + \left(\frac{F_{n+1} + F_n}{2m_p} - g\right)\Delta t, \quad w_{n+1} = w_n + \left(\frac{v_{n+1} + v_n}{2}\right)\Delta t \qquad (2.2)$$

Where $g = 9.81$ m/s^2 is the gravitational acceleration, m_p is the total mass of the impactor and striker, n and $n+1$ denotes the values at time t_n and t_{n+1} respectively, and $\Delta t = t_{n+1} - t_n$.

The test programme is shown in Table 2.1. The glass plates were divided into five series, where each series was intended to be used at one impact velocity. Four tests with laminated glass at 2 m/s were carried out because there was a mistake with the force measurements in the first test.

Table 2.1: Test programme

Impact velocity	Glass type	Number of tests	Series
2.00 m/s	Monolithic	3	1
4.00 m/s	Monolithic	3	2
0.77 m/s	Laminated	1	5
0.90 m/s	Laminated	1	5
0.95 m/s	Laminated	1	5
1.00 m/s	Laminated	2	5
1.20 m/s	Laminated	1	5
2.00 m/s	Laminated	3 (4)	3
6.00 m/s	Laminated	3	4
10.0 m/s	Laminated	1	5

Four cameras were used during the tests, as shown in Figure 2.1. Two Phantom V1610 high-speed cameras with 25 kHz sampling rate captured the optical targes on the plate during the impact. One Photron Fastcam APX-RS camera with 25 kHz sampling rate detected the movement of the impactor and actuated the two Phantom v1610 high speeds cameras. One Photron Fastcam APX-RS camera with 5 kHz sampling rate captured the movement of the drop tower during the impact. The digital image correlation (DIC) software eCorr [41, 42] was used to track the optical targets on the glass plate. Pictures for the tracking were provided by the two Phantom V1610 high-speed cameras.

The glass plates were clamped between two 25 mm thick aluminium plates similar to the setup in the study done by Osnes et al. [15]. Four rubber strips with a thickness of 4 mm were applied to the aluminium clamping plates, such that only the rubber was in contact with the glass. The reason for this was to avoid fracture initiation at the boundary during setup. The glass plates, both monolithic and laminated, had the dimension 400 × 400 mm^2. They were clamped in a 50 mm distance from the edge, such that an area of 300 × 300 mm^2

was visible. Twelve equidistant M24 bolts were tightened to 100 Nm for clamping the glass plates. Steel stoppers were used between the aluminium clamping plates as shown in Figure 2.2, such that the clamping pressure was ensured to be 0.14 MPa ± 0.03 MPa according to the European Standard for testing and classification of security glazing [43]. The thickness of the stoppers was chosen to obtain the required clamping pressure.
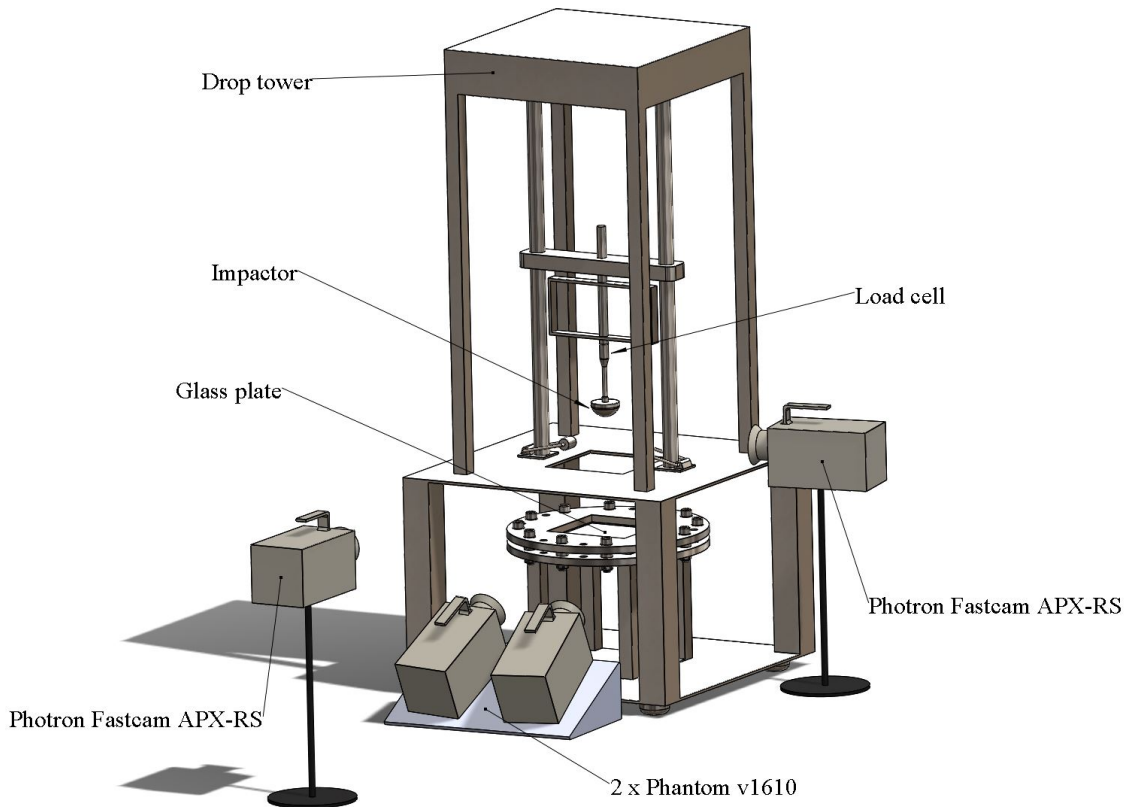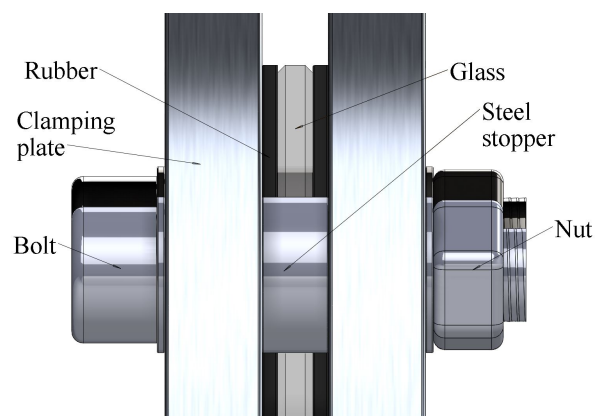

**Figure 2.1:** Experimental setup.

Figure 2.2: Glass clamping mechanism.

The impactor nose used in the experiments was made out of aluminium and had a half-spherical shape with a radius of 50 mm. The impactor nose geometry is shown in Figure A.3 in Appendix A. The total mass, m_p, of the impactor was 6.551 kg, where $m_1 = 5.243$ kg and $m_2 = 1.308$ kg in accordance with Equation 2.1. In an attempt to avoid high stress peaks in the measurements, the impactor was covered with a thin layer of rubber coating.

2.1.2 Results

The measured impact velocities differed from the prescribed values for both monolithic and laminated glass. Measured velocities for each test are given in Table A.2 in Appendix A. The impact velocity is referred to as the prescribed value.

All tests on monolithic glass resulted in glass failure. The general trend observed experimentally for the monolithic glass plates can be described by three phases. The initial phase involves fracture initiation in the vicinity of the impactor. Thereby, the propagation of radial cracks from the initiation site, followed by the propagation of one or several circumferential cracks. The crack propagation for Monolithic 1-1 with a prescribed impact velocity of 2 m/s is shown in Figure 2.3.

**(a)** $t = 2.12$ ms   **(b)** $t = 2.28$ ms   **(c)** $t = 31.16$ ms
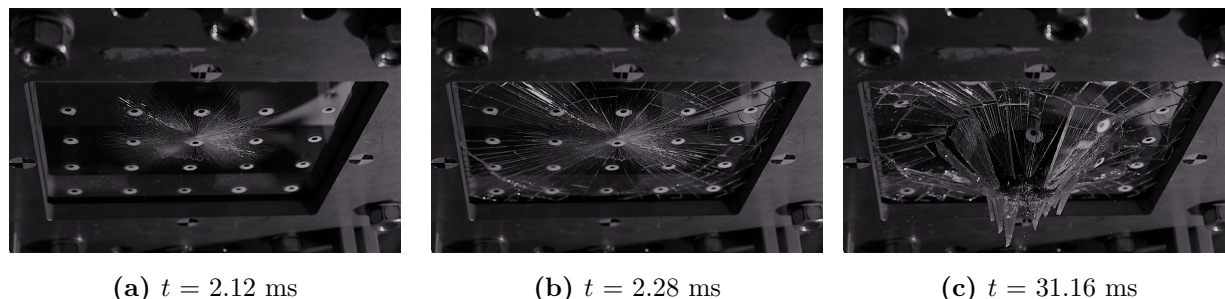
Figure 2.3: Pictures of test 1-1 with monolithic glass and prescribed impact velocity of 2 m/s.

The force versus time history from the experiments on monolithic glass series 1 and 2 is presented in Figures 2.4 and 2.5, respectively. The force shown in the figures is the contact force, found from Equation 2.1, and the velocity is obtained by Equation 2.2 while utilizing a starting velocity, v_0, found from the photocell in the drop tower. All three plates in series 1 fractured at approximately the same time and force level. The velocity for all tests decreased while there was contact between the glass and the impactor. At fracture, the velocity shows a slight increase since the glass provides no resistance after failure. This is also observed as a sudden drop in force levels at fracture and oscillation around zero afterwards. Similar behaviour is observed in series 2. The time at fracture initiation appears to be earlier than series 1, which is to be expected as the velocity is doubled.

(a) Force versus time

(b) Velocity versus time
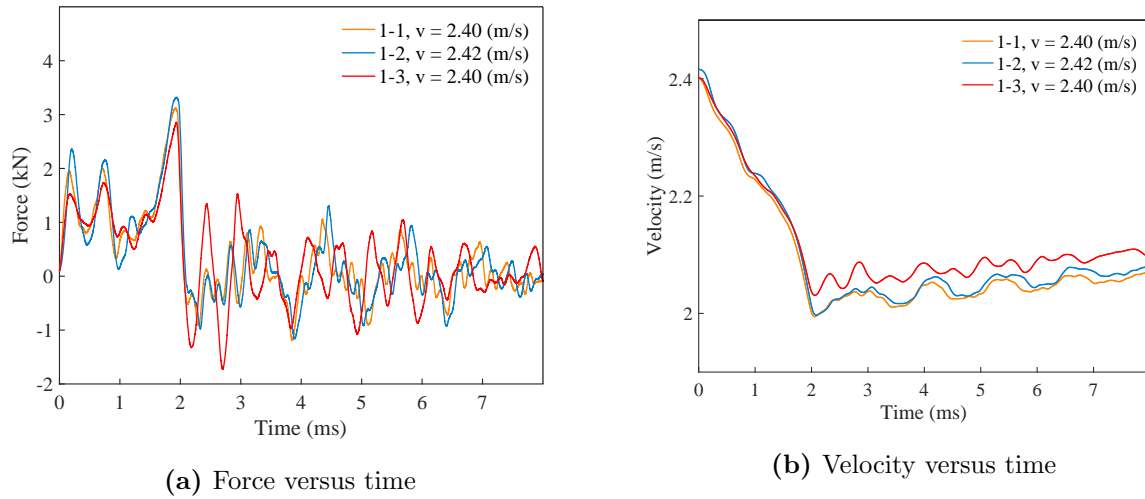
Figure 2.4: Force versus time (a) and velocity versus time (b) for monolithic glass series 1 with a prescribed velocity of 2 m/s. The measured impact velocities are given in the legends.


(a) Force versus time

(b) Velocity versus time
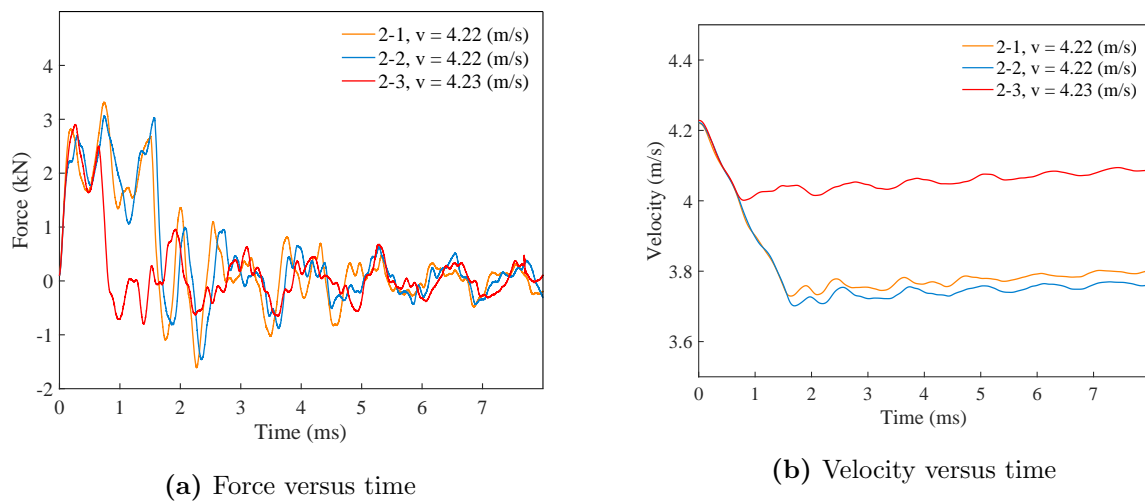
Figure 2.5: Force versus time (a) and velocity versus time (b) for monolithic glass series 2 with a prescribed velocity of 4 m/s. The measured impact velocities are given in the legends.

All tests with laminated glass at impact velocities of 2 m/s, 6 m/s and 10 m/s resulted in glass failure. The tests with impact velocities of 6 m/s and 10 m/s yielded considerably more fragmentation and deformation, compared to 2 m/s. The crack propagation and the level of fragmentation for tests with 2 m/s and 6 m/s are shown in Figures 2.6 and 2.7, respectively. Failure in the PVB interlayer was observed in the test with an impact velocity of 10 m/s. One sample with an impact velocity of 1 m/s experienced fractures in the lower glass, while the upper glass was undamaged. The other samples with impact velocity around 1 m/s did not fail. Resulting fracture patterns from the four different impact velocities that resulted in glass failure are shown in Figure 2.8.

(a) $t = 1.68$ ms   **(b)** $t = 2.28$ ms   **(c)** $t = 7.6$ ms
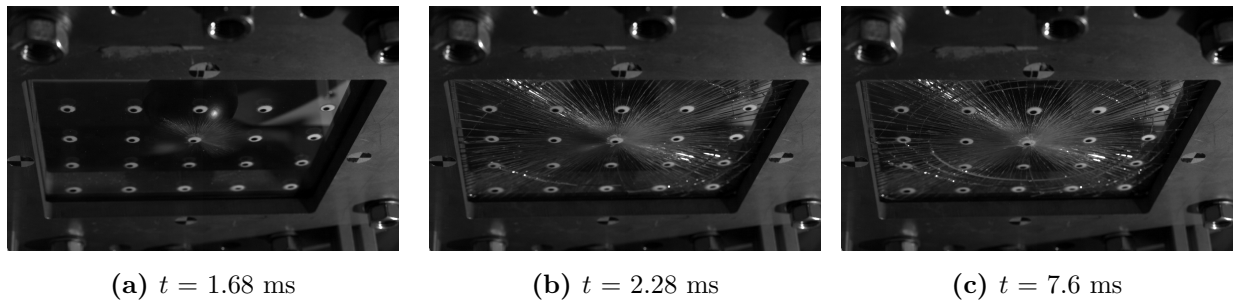
Figure 2.6: Pictures of test 3-1 with laminated glass and a prescribed impact velocity of 2 m/s.

(a) $t = 0.24$ ms   **(b)** $t = 1.00$ ms   **(c)** $t = 13.04$ ms
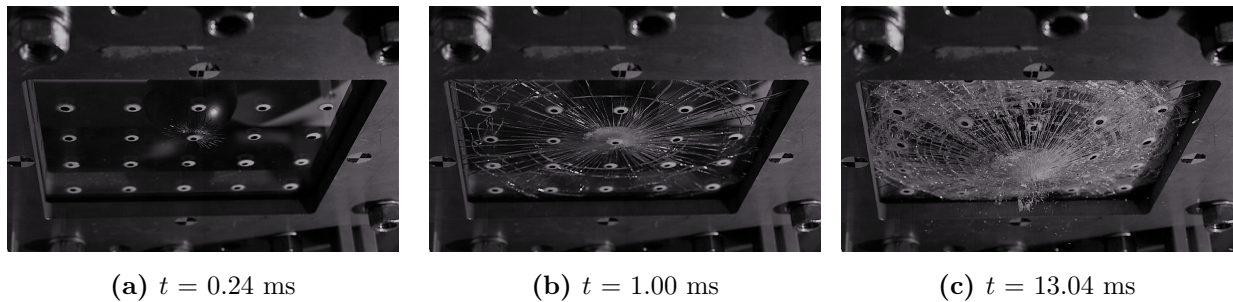
Figure 2.7: Pictures of test 4-1 with laminated glass and a prescribed impact velocity of 6 m/s.

As for the monolithic glass, the failure of laminated glass can be described by the three phases previously explained. More circumferential cracks were observed in the laminated glass, compared to the monolithic. The glass fractured into smaller pieces as the impact velocity increased. The velocity of the initial radial fractures was found to be around 2000 m/s in all tests. A higher sampling rate on the high-speed cameras is needed to determine whether the fracture velocity in the laminated glass is different from the monolithic.

The force versus displacement and velocity versus time histories from series 3 are presented in Figure 2.9. All three specimens fractured in both glass plates, while the interlayer remained intact and not allowing perforation. The time of zero velocity was found from Figure 2.9b and this was determined as the time of maximum impactor displacement. The force versus displacement curves, shown in Figure 2.9a, illustrates several of the characteristics of laminated glass. All three specimens behaved similarly up until fracture. The strength of glass is probabilistic, which can be seen in differences in time at fracture. The total deformation of the laminated glass is dependent on the time at fracture initiation. The maximum displacement is seen to lie between 6.0 mm and 10.7 mm.

The force versus displacement and velocity versus time histories for series 4 is presented in Figure 2.10. The prescribed velocity was 6 m/s. As for series 3, all specimens fractured in both glass panes. There was no indication that the interlayer ruptured. In contrast to series 3, all plates fractured approximately at the same time. This resulted in total displacement between 42.8 mm and 43.9 mm for the three specimens.
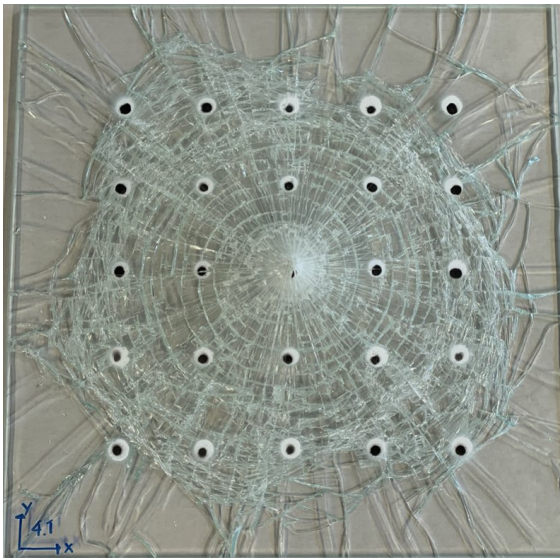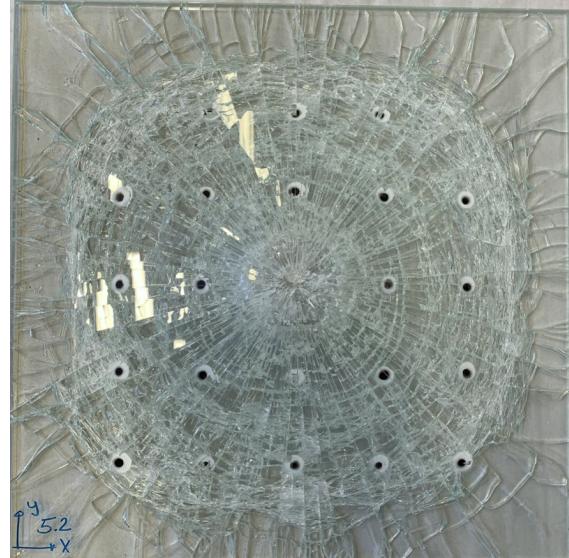
(a) Impact velocity = 1.72 m/s
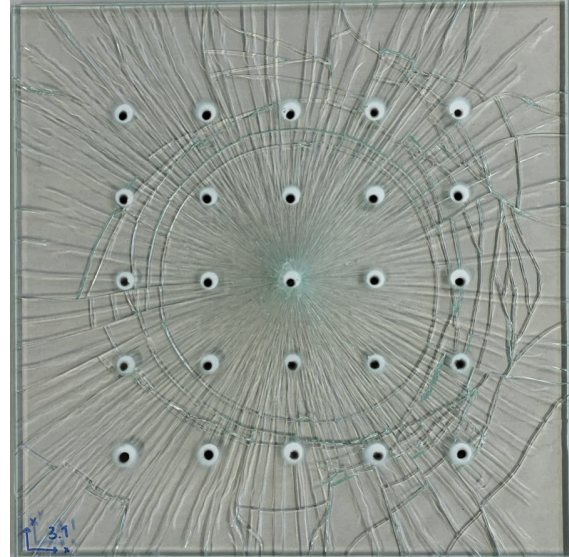
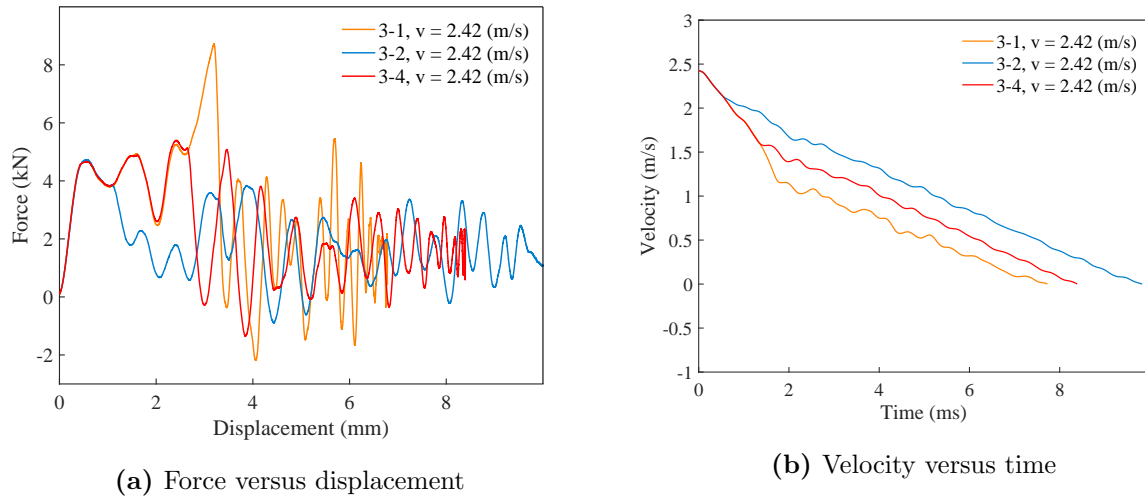**(b)** Impact velocity = 2.42 m/s
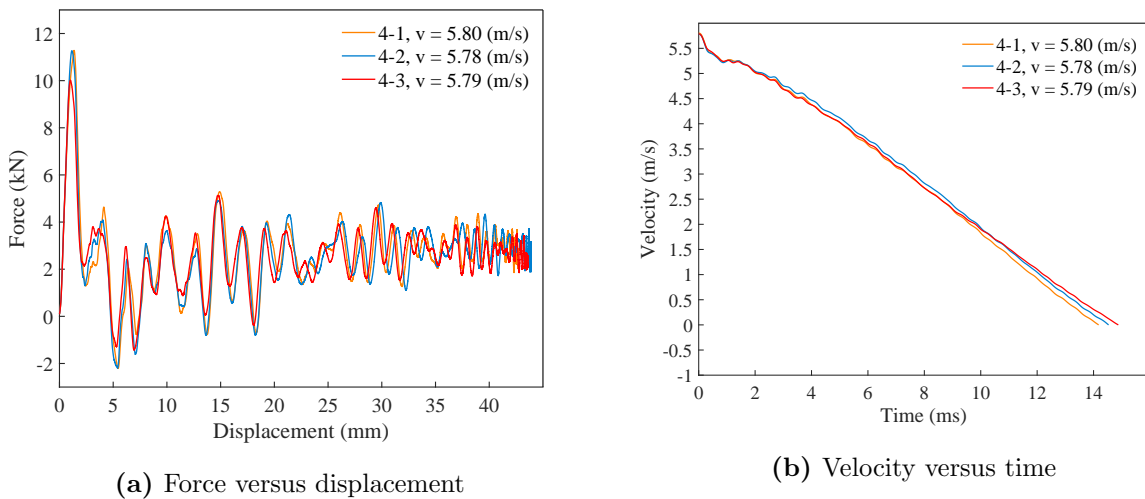
(c) Impact velocity = 5.8 m/s

(d) Impact velocity = 9.8 m/s

Figure 2.8: Fracture patterns from low-velocity impact tests on laminated glass.

The midpoint displacement in the test with a prescribed velocity of 1.2 m/s is presented in Figure 2.11a. This test did not end in glass failure. The displacement measurements are obtained from 3D DIC of the plate, 2D DIC of the movement of the impactor and by integration of the force measurements as shown in Equation 2.2. Since the two latter measurements follow the impactor and not the plate, the displacement measurements are only valid when the impactor is in contact with the plate. The displacement of the clamping plate and the drop tower for the two tests are shown in Figure 2.11b.

(a) Force versus displacement

(b) Velocity versus time

Figure 2.9: Curves for (a) force versus displacement and (b) velocity versus time for laminated glass series with a prescribed velocity of 2 m/s. The measured impact velocity is given in the legends.

(a) Force versus displacement


(b) Velocity versus time

Figure 2.10: Curves for (a) force versus displacement and (b) velocity versus time for laminated glass series with a prescribed velocity of 6 m/s. The measured impact velocity is given in the legends.

2.1.3 Discussion

It is important to highlight that the failure of glass is highly probabilistic. The limited amount of tests performed is not sufficient to conclude anything with statistical significance and should be treated with caution. The general trends observed from the results will therefore only be discussed.

All impact tests that ended in glass failure showed a similar failure behaviour. The fractures initiated in the vicinity of the impact area, and were followed by the development of radial

(a) Displacement versus time

(b) Displacement versus time
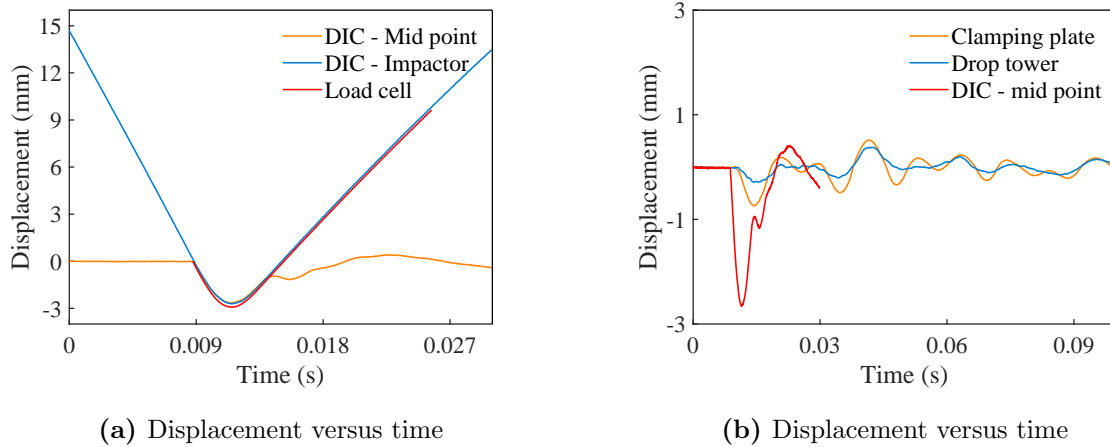
Figure 2.11: Displacement measurements for (a) glass plate midpoint and (b) drop tower and clamping plate for laminated glass with a prescribed velocity of 1.2 m/s.

cracks before circumferential cracks. The position of failure initiation in the glass will be dependent on the combination of density, size and orientation of surface flaws, and the stress history. Osnes et al. [33] performed quasi-static punch tests on laminated glass with two different impactor geometries. One of the impactors had identical geometry to the one used in this thesis, while the other had a larger contact area. The fractures initiated in the centre in all tests with an impactor identical to the one used in this thesis. The fractures initiated in both the centre and at the boundary in the tests where an impactor with a larger contact area was used. Low-velocity impact tests introduce high stresses in the glass close to the impactor immediately after impact. It is therefore believed that it is most likely for failure to initiate in the centre of the plate when it is exposed to low-velocity impacts. As seen in the work done by Osnes et al., the impactor geometry also influence whether or not the fracture initiates in the centre or at the boundary.

As seen in Figure 2.8, around 50 radial fractures were observed in the experiments with laminated glass. Almost all these fractures reached the edge of the glass before the development of circumferential fractures. The laminated glass plate will hence experience a rapid drop in stiffness when the radial fractures reach the glass edge. The large amount of glass shards created by the radial fractures implies that the glass can only transfer tensile forces in the radial directions. Remember that there are small deformations at the onset of radial fractures and the glass will be the major load-carrying component in the laminate. Each glass shards will hence behave similarly to a cantilever beam with a point load, and the first circumferential fractures take place around the positions of the maximum moment, i. e. close to the clamped boundary. After the development of the first circumferential fracture, the glass plate will possibly again experience a drop in the stiffness. The glass shards are bonded to the interlayer, and it will force the glass to further deformation and fragmentation. The ability to transfer compressive forces through the crack plane in the glass is possibly an

important mechanism for the further fragmentation. Otherwise, all the deformation would have been localized in the interlayer.

There are small variations in the force versus displacement history in the pre-fracture phase when comparing tests with equal impact velocity, as seen in Figures 2.4, 2.5, 2.9 and 2.10. This is a valuable property which can be useful for verifying the boundary conditions in the numerical model. The post-failure behaviour of the force versus displacement curves depends on the displacement at fracture initiation. Since the displacement at fracture initiation varies between the tests due to probabilistic behaviour of glass, the test results should not be used as a goal or standard for the simulations. The pre-fracture response gives valuable information on the elastic behaviour and the post-fracturing give insight to the structural response of laminated glass and propagation of fractures.

The displacement was measured in three different ways during the impact. The two DIC measurements coincide, as seen in Figure 2.11a. The displacement obtained from the force measurement is slightly larger than the DIC measurements in absolute value. This might be explained by an inaccurate calibration of the load cell. Inaccurate camera calibration performed by the user in the DIC software is another possible source of error.

As seen in Figure 2.11, both the drop tower and the clamping plate are moving during the impact. The displacement measurements of the glass therefore need to be adjusted. The movement of the drop tower and the clamping plates lag behind the movement of the glass, and the lag increases with increasing impact velocity. The maximum midpoint displacement of the glass plate is therefore nearly unaffected by the movement of the drop tower and the clamping plate. It is not straightforward to correct the force versus time curve for the drop tower movements. The movement of testing setup, including drop tower and clamping plate, needs to be taken into account when comparing experimental results with simulations.

The impactor was covered with a thin layer of rubber coating. It is difficult to know if and how this coating affects the results. To include it in the simulations is also a challenging task because of unknown geometric and material properties.
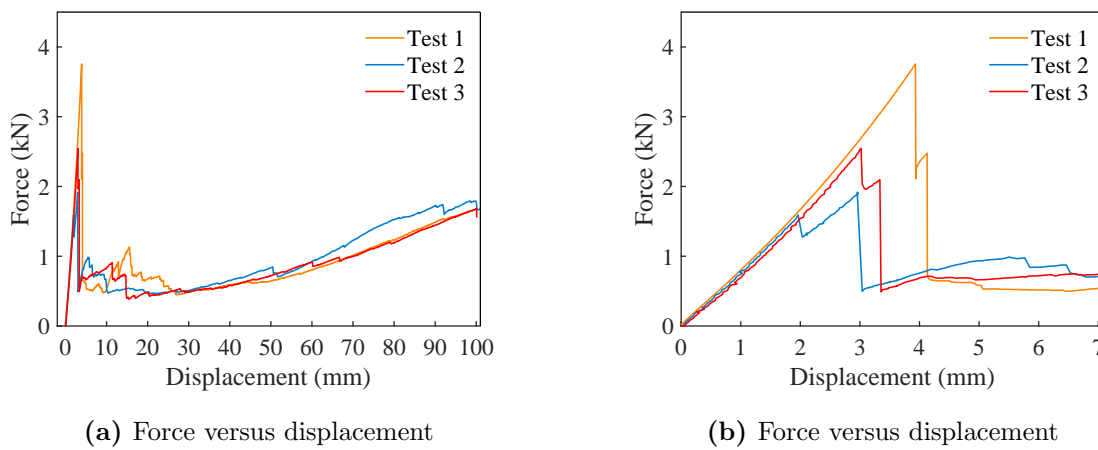
2.2 Quasi-static tests

2.2.1 Methods

The quasi-static tests were performed in an Instron 5985 universal testing machine with a 250 kN load cell at the Material Testing Laboratory at SINTEF in Trondheim. The loading rate was set to 3 mm/min and the total deformation limit was set to 100 mm. The glass was

clamped in the same way as in the dynamic tests described in Section 2.1. The impactor
and the laminated glass plates were also the same as used in the dynamic tests. Two AVT
Proscilla GC2450 cameras were used to capture the displacement of optical targets on the
plate with 3D DIC. Force measurements were provided by the testing machine. Displacement
was provided by both the testing machine and from 3D DIC.

2.2.2   Results

The force versus displacement histories from the three tests are presented in Figure 2.12.
All three plates failed in the centre. The general trends in the failure mode were similar
to the behaviour observed in the dynamic tests, with initially radial fractures followed by
circumferential fractures.

(a) Force versus displacement

(b) Force versus displacement

Figure 2.12: Force versus displacement for quasi-static tests on laminated glass. Complete test
in (a) and first 7 mm of displacement in (b).

Pictures during the test from test 3 are presented in Figure 2.13.

(a) d = 3.02 mm

(b) d = 3.36 mm

(c) d = 100 mm
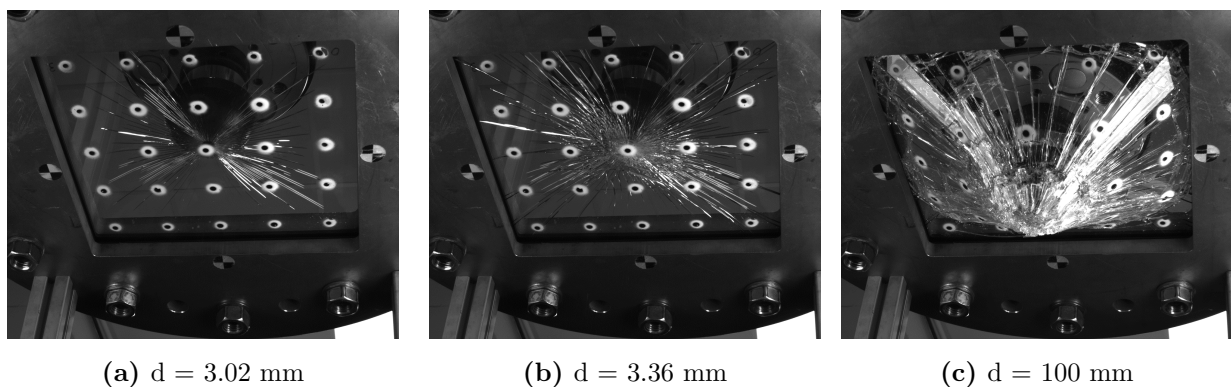
Figure 2.13: Pictures of quasi-static test 3 with the corresponding displacement of impactor.
Undeformed (a), fracture in first plate (b), fracture in both plates (c) and end of test (d).

2.2.3 Discussion

The same idealized failure process of laminated glass seen in Figure 1.1 is observed in Figure 2.12a. The behaviour was linear elastic until the fracture of the first plate in the laminate. The force then dropped before the behaviour was linear elastic again with a lower stiffness than the initial pre-failure stiffness. After the failure of both plates in the laminate, the force dropped to a certain level and then started to increase with increasing impactor displacement. The increase in force was caused by membrane stretching of the PVB interlayer. The small peaks in the force, which can be seen between 5 and 20 mm displacement in Figure 2.12a, is believed to be caused by the failure of larger glass fragments.

The failure load in the three tests deviated between 1.59 kN in test 2 and 3.76 kN in test 1. All three tests were performed under the same conditions. The failure initiated in the centre in all three tests. Early failure caused by edge imperfections can thus be neglected as the reason for the deviation in failure loads. It is therefore believed that the deviation in failure load is caused by the stochastic behaviour of glass. Such large deviations in fracture load implicate that three tests are not sufficient to determine the mean failure load for laminated glass. Yankelevsky [14] proposed that 5000 repetitions of experimental tests on glass is needed to describe the statistical variance. The results from the tests can not be used to verify the strength of glass, but it gives information about how laminated glass behaves under quasi-static loading.

By comparing Figures 2.7 and 2.13, it may be seen that the dynamic tests produced small glass shards and a large amount of fragmentation. The quasi-static tests on laminated glass resulted in significantly larger shards and less fragmentation. The dynamic tests on laminated glass with an impact velocity of 6 m/s resulted in a mean peak force of 10.7 kN, while the highest force from the quasi-static tests was only 3.76 kN. Since the forces are higher in the dynamic tests, it appears reasonable that the shards are smaller and more fragmentation occurs because of momentum transfer in the impact. The PVB interlayer is strain rate-dependent [17]. The stresses in the PVB will hence be lower in the quasi-static tests than in the dynamic tests, because of the differences in strain rate. The strength of glass is also rate-dependent, and the strength increases with increasing strain rate [33]. Because of the increased strength, the glass in the dynamic tests can store more elastic strain energy up until fracture than in the quasi-static tests. The release of elastic strain energy at fracture may result in more fracturing. The rate-dependency of the PVB and the glass strength may therefore be other reasons for the observed differences between the dynamic and the quasi-static tests.

# 3. Preliminary numerical work

This chapter presents the preliminary work on finite element (FE) simulation of monolithic and laminated glass. The finite element model used will be presented along with the results. The main focus of this chapter is to recreate the pre-fracture response observed in the experiments realistically and cost-effectively. Glass behaves as a linear-elastic isotropic material before fracture initiation. The initiation of fracture determines the strength of glass in a specimen, but should not influence the stiffness before fracture. This chapter aims to model the boundary conditions and verify that the FE simulations can reproduce the pre-fracture response. A small parametric study will investigate the effects of numerical integration, interlayer material model and which parts from the test setup that needs to be included to ensure accurate results.

3.1   Finite element model

The difference in terms of modelling monolithic and laminated glass is the inclusion of a polymer interlayer and an additional glass pane. As a preliminary study, the bonding between the glass and interlayer is modelled with a simple technique. A surface-to-surface tie constraint between glass and polymer is utilized to model the bonding. The polymer interlayer is the soft underlying material and therefore chosen to be the slave surface. Since the main focus of the preliminary study is to model the pre-fracture behaviour, it is assumed that there is complete adhesion between glass and polymer. Delamination effects are only relevant in the post-fracture phase.

Modelling of the full test setup, as described in Section 2.1 and shown in Figure 2.1, is complicated and costly in terms of processing time. The cost would be far greater than the benefits. This introduces the need to simplify the modelling of boundary conditions and striker. The striker includes both the impactor and bar above, illustrated in Figure 3.1. The bar is modelled as steel with linear-elastic material properties. Linear truss elements, T3D2, with a characteristic length of 2 mm is used. The extra weight of the beam connecting the striker to the columns is modelled as a point mass of $m = 4.47$ kg added to the bar. The motivation behind modelling the striker is to compare the force from the loadcell with simulations. The contact force found from the experimental tests is derived from dynamic equilibrium, shown in Equation 2.1. Still, the contact force is just the force measured in the loadcell multiplied by a factor. The contact force from the FE simulations is validated by comparing the sensor force from the loadcell in the experiments and the force extracted from a truss element at the same location in the FE simulations. It is also possi-

ble to obtain the contact force from the interaction between glass and impactor in Abaqus. The use of this contact force allows for simpler modelling of the impactor without the striker.
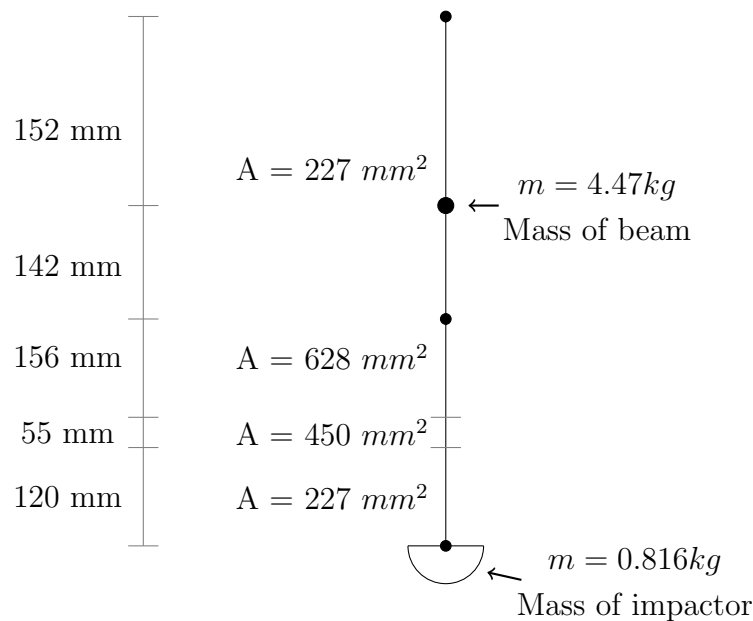
Figure 3.1: Idealization of the striker with impactor and bar. A is the section area of the bar. The figure is not drawn in scale.

Several simplifications are introduced in the FE model. Glass is treated as an isotropic linear-elastic material with Youngs's modulus of 70000 MPa, Poisson's ratio of 0.2 and a density of 2500 kg/m³. The rubber strips are idealized as a purely linear-elastic material with Young's Modulus of 2 MPa and Poisson's ratio of 0.46 and a density of 1100 kg/m³. The simplification of the rubber is justified by the work done on laminated glass exposed to blast loading in the work by Osnes et al. [15]. The rubber strips are glued to the clamping frame made of solid aluminium. The outer surface of the rubber strips is therefore fixed in all directions throughout the FE simulation. The contact between the glass and the rubber is modelled by using surface-to-surface contact with kinematic constraint enforcement found in Abaqus, which is illustrated in Figure 3.2. The slave surface is chosen to be the rubber because of the large difference in stiffness between glass and rubber. Each part of the FE model is assigned an element type and element dimension, shown in Table 3.1. The effect of reduced or full integration is checked in the parametric study for the glass and the PVB.

The output from the experiments used to validate the numerical model is the contact force, the sensor force and the displacement of three optical targets on the lowest glass pane. The optical targets chosen are denoted P0, P1 and P2. A full visual description of the optical targets can be found in Figure A.2 in Appendix A.

The testing setup is a complex dynamic system. Therefore great care was taken to isolate

Table 3.1: Numerical properties in the parametric study on preliminary FE simulations.

Part	Type	Element	Size (mm)
Glass	Shell	S4R	$5 \times 5 \times 3.8$
	Shell	S4	$5 \times 5 \times 3.8$
PVB	Solid	C3D8	$5 \times 5 \times 0.5$
	Solid	C3D8R	$5 \times 5 \times 0.5$
Rubber	Solid	C3D8	$5 \times 5 \times 4$
Impactor	Discrete Rigid	R3D4	0.25×0.25 in centre

the displacement of the glass from the rest of the system. The dynamic coupling between systems is previously elaborated in Section 2.1. The displacements used to validate the FE simulations are corrected to account for displacement of the clamping frame and the test machine. The reader should note that the contact force used for validation of the numerical results is not corrected and incorporates the whole system, including test component, clamping frame and drop tower.
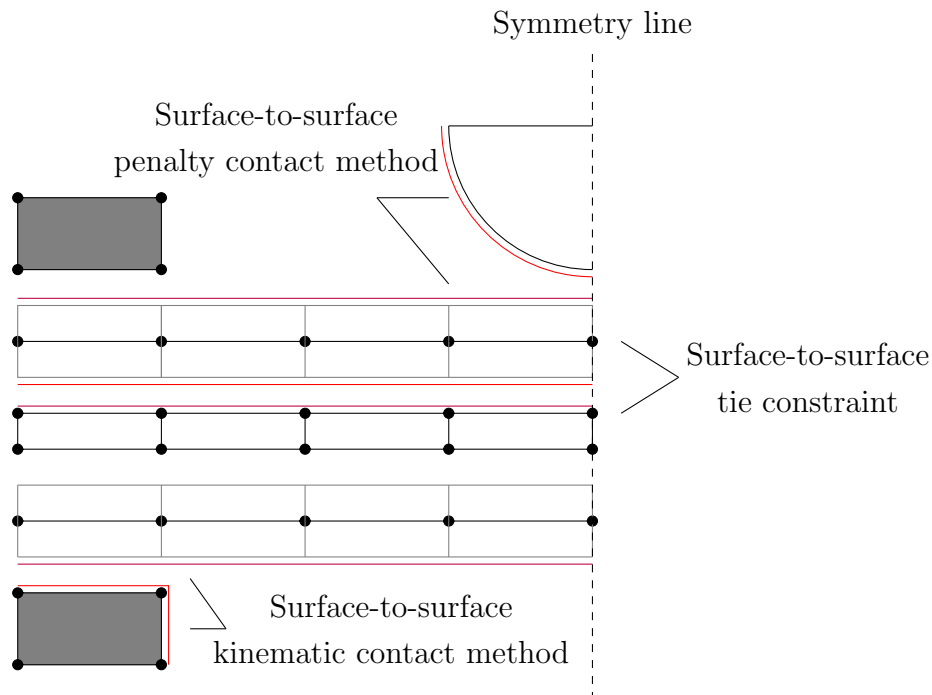
Figure 3.2: Schematic view of the finite element model of laminated glass.

3.2 PVB material models

Laminated glass is manufactured by an autoclave process with high temperature and pressure [12]. The calibration of a material model for the PVB is performed on the polymer before the autoclave process. After the autoclave process is finished, some uncertainty is in-

troduced to the calibrated model since the autoclave process involves high temperatures and pressure. A common approach is to fit the PVB material model to a plain PVB [18, 19, 20].

The first model is a non-linear viscoelastic material model composed of hyperelastic and viscoelastic behaviour described by the Arruda-Boyce model and Bergström-Boyce creep model, respectively. Input parameters, found in Table 3.2, are based on the work done by Osnes et al. [33] and a thorough description of the complete model can be found in [44]. Since the model describes both hyper- and viscoelasticity, it is believed that it can model the complete response during impact, especially the elastic response without fractures.

Table 3.2: Input parameters to the non-linear viscoelastic model.

μ	λ_m	D_1	A	m	C	E
4.177	2	0.01	0.001	3	-1	0.01

The second model represents a simplified, but a well-known approach for modelling polymers [45]. The model combines linear-elasticity with strain rate-dependent Mises plasticity. The linear-elastic behaviour uses a Young's Modulus of 500 MPa and Poisson's ratio of 0.45 and in-house values for the strain rate-dependent Mises plasticity. The strain rate-dependent Mises plasticity is implemented as a plastic material with isotropic hardening for several different equivalent plastic strain rates. The stress versus equivalent plastic strain curves are shown in Figure 3.3. A limiting factor in the elastic-plastic model is that the plastic strains are non-reversible, which can cause the unloading response in an impact to be inaccurate. Bergström suggests that a plasticity model can be efficient for monotonic loading [45]. The impact situation up to maximum displacement could be described efficiently by a plasticity model. The second model will hereafter be denoted Mises plasticity model.

3.3   Pre-failure simulations of laminated glass

The numerical results from the parametric study are validated against an experimental test that did not end in fracture. The impact velocity was 1.83 m/s in this experimental test. The variables that are included in the parametric study are repeated for clarity: integration order of the glass and the PVB, and material models for the PVB. The simulations with corresponding variables are listed in Table 3.3 and simulation results in terms of displacement versus time and force versus time histories are shown in Figures 3.4a and 3.5b, respectively.

The main results in Figure 3.4 can be summarized as follows: There is no difference between the integration order of glass and PVB when the non-linear viscoelastic PVB model is used. The Mises plasticity PVB model overestimates the displacements and underestimates the
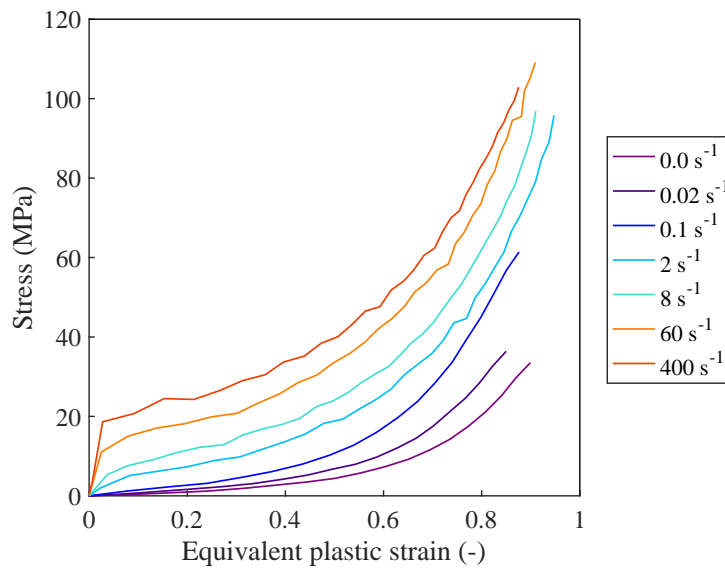
Figure 3.3: Stress versus equivalent plastic strain curves in the Mises plasticity PVB material model. The legend denotes the equivalent plastic strain rates.

Table 3.3: Simulation parameters in the parametric study on the elastic response.

Simulation	Glass	PVB	PVB material model
1	S4	C3D8	non-linear viscoelastic
2	S4R	C3D8	non-linear viscoelastic
3	S4	C3D8	Mises plasticity
4	S4R	C3D8	Mises plasticity
5	S4	C3D8R	non-linear viscoelastic
6	S4R	C3D8R	non-linear viscoelastic

contact force. All simulations in Figure 3.4 are performed with simplified modelling of the test setup, i.e. only the impactor is modelled and the total mass, m_p, was 6.551 kg. The contact force is extracted from the interaction between glass and impactor in Abaqus.

Practically no difference was observed between the integration order of either the glass or the PVB interlayer. The total energy output of the simulation with S4R, C3D8R and a non-linear viscoelastic PVB material model remained approximately constant throughout the analysis. The analysis results were deemed satisfactory with regards to the simplified modelling approach with an impactor. The best results was obtained by using: S4R, C3D8R and a non-linear viscoelastic PVB material model.

A numerical model was built according to Figure 3.1 and the best result from the parametric study on integration order in Figure 3.4. The results are shown in Figure 3.5.
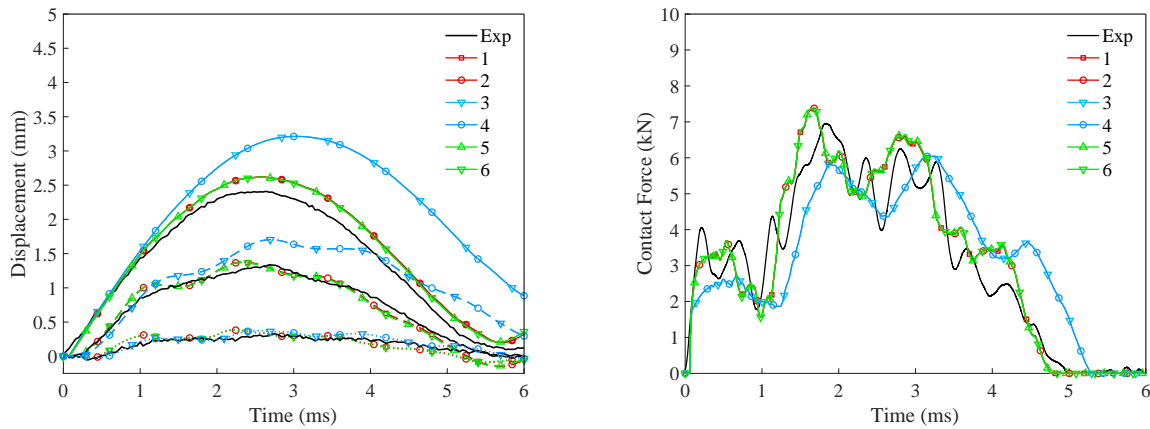
(a) Displacement versus time. The solid line is P0, dashed is P1 and dotted line is P2.

(b) Contact force versus time.

Figure 3.4: Simulations results versus experiments. The impact velocity is 1.83 m/s. Note that no fracture occurred in the experiment. The numbering in the legends corresponds with Table 3.3.
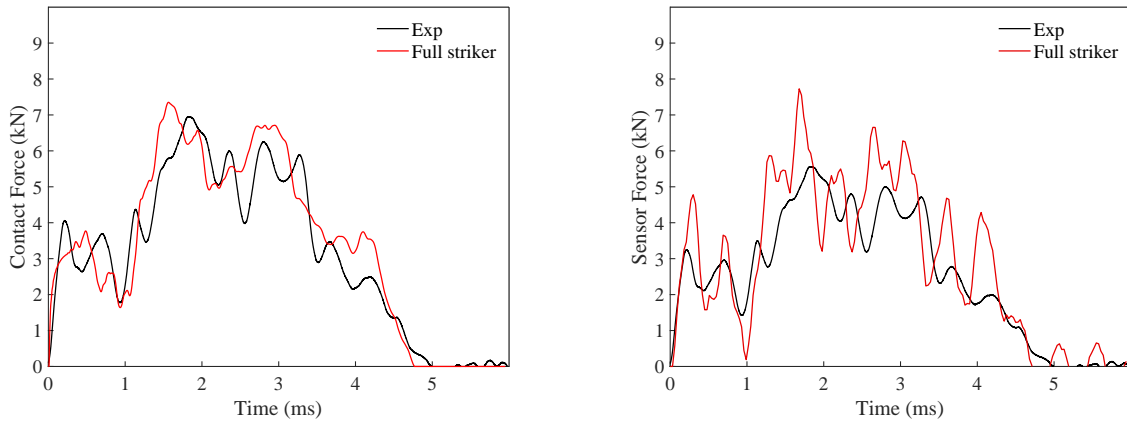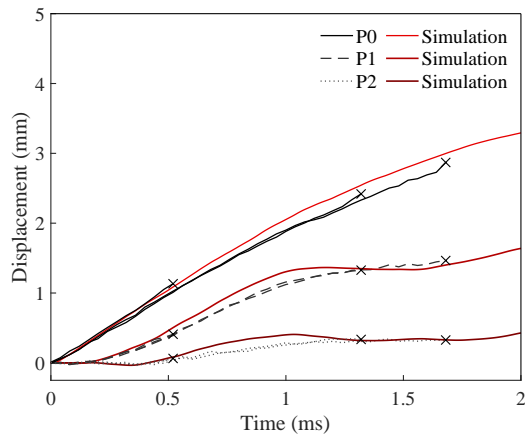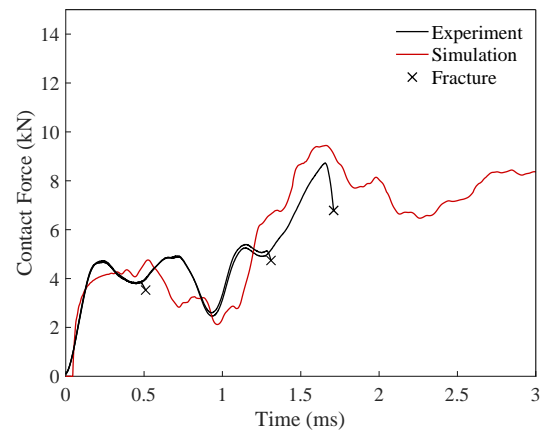

(a) Contact force versus time.

(b) Sensor force versus time.

Figure 3.5: Comparison of (a) contact force and (b) sensor force from simulation with S4R, C3D8R, non-linear viscoelastic PVB model and full modelling of striker. The impact velocity is 1.83 m/s.

The best configuration from the parametric study was verified against the experimental series 3 and 4. The results are only verified until fracture occurred. The start of fracture in the experiments is visualized with a black cross. The full results are shown in Figures 3.6 and 3.7.

(a) Displacement versus time.

(b) Contact force versus time.

Figure 3.6: Simulation for laminated glass with a velocity of 2.4 m/s. The experimental results in (a) and (b) are from series 3.
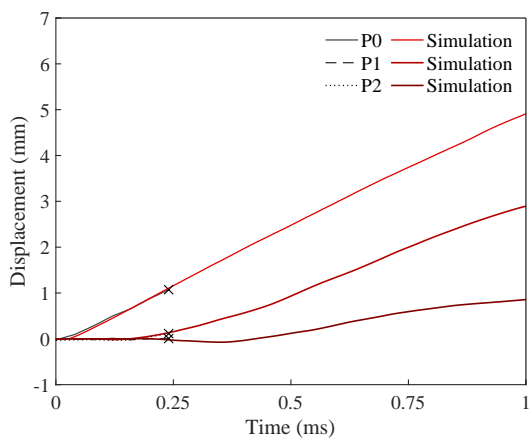

(a) Displacement versus time
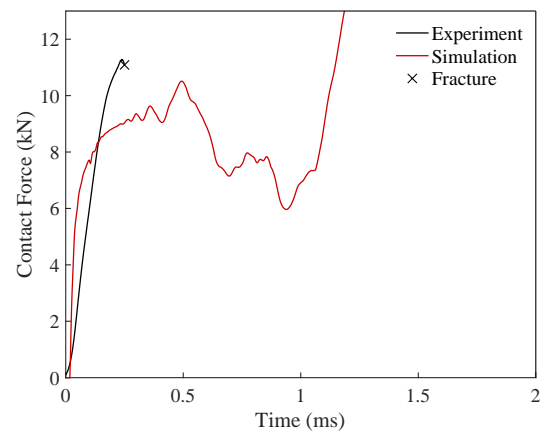
(b) Contact force versus time.

Figure 3.7: Simulation for laminated glass with an impact velocity of 5.8 m/s. Only one of the tests from series 4 is shown due to very similar behaviour, as noted in Section 2.1.

It was also made an attempt to model the impactor as deformable with the elastic properties of aluminium. No improvements in the results were observed, but it resulted in increased computational cost.

3.4   Pre-failure simulations of monolithic glass

Simulations of monolithic glass were verified against the experimental series 1 and 2. The results are presented as displacement versus time and force versus time histories from the simulations and the experiments. The contact force was extracted from the interaction between glass and impactor. Figures 3.8 and 3.9 presents the results for impact velocity of 2.4 m/s and 4.2 m/s, respectively. The start of fracture in the experiments is visualized with a black cross. The behaviour in the simulations is initially too stiff, but converge to the experiment over time.

(a) Time vs displacement.   **(b)** Time vs contact force.
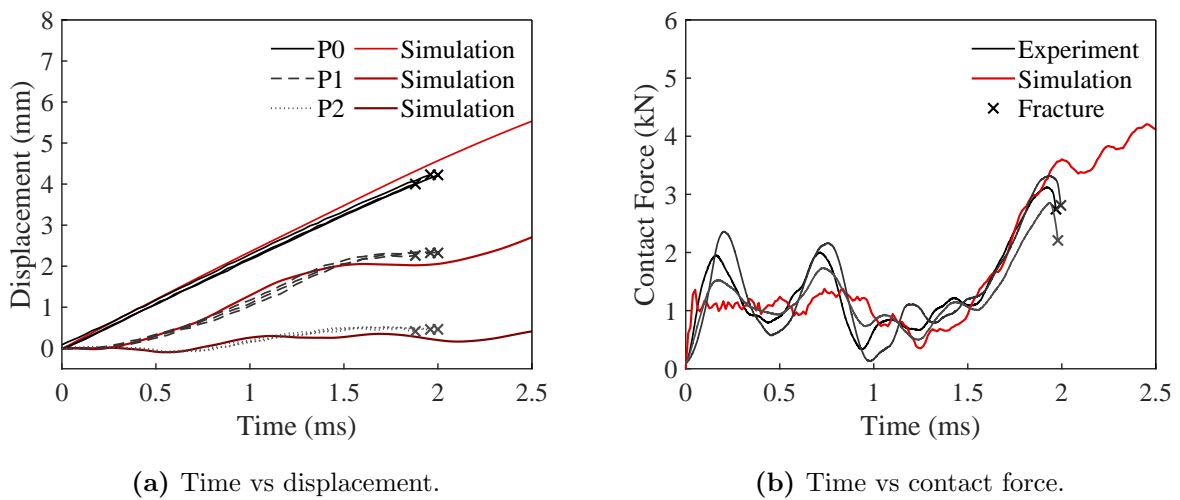
Figure 3.8: Simulation for monolithic glass with an impact velocity of 2.4 m/s.

(a) Time vs displacement.   **(b)** Time vs contact force.
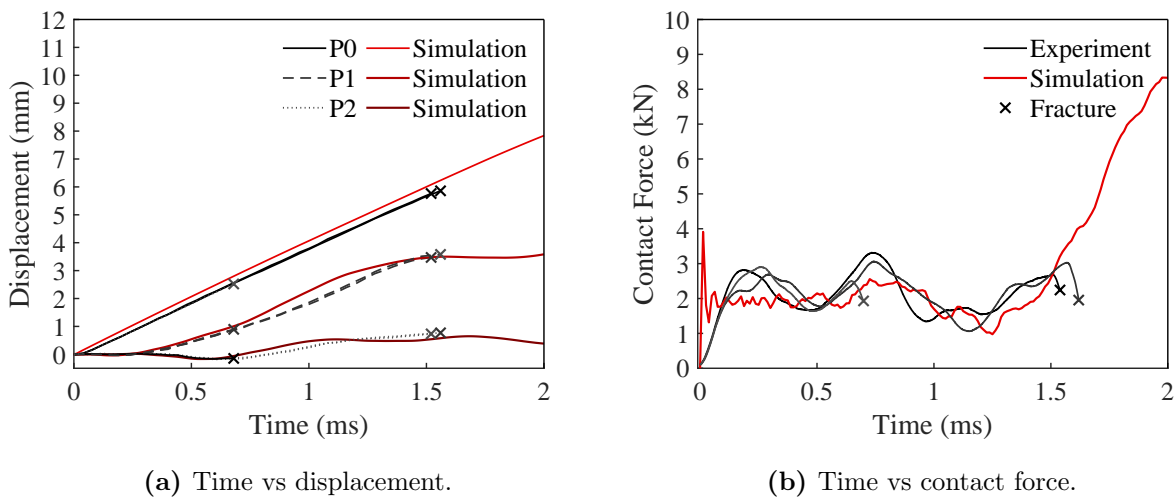
Figure 3.9: Simulation for monolithic glass with an impact velocity of 4.2 m/s.

3.5 Discussion

The preliminary numerical study's primary objectives were to establish a FE model that was able to recreate the boundary conditions and the pre-fracture response. The numerical results obtained were in good agreement with the experimental results for both the monolithic and laminated glass for all impact velocities simulated. The simplification of boundary conditions introduced with fixing the rubber and idealizing the material behaviour as linear-elastic appear to be sufficient and accurate.

The most considerable discrepancy between numerical results was between the non-linear viscoelastic PVB model and the Mises plasticity PVB model. Figure 3.4a demonstrates that both material models are accurate in describing the first part of the impact, while the Mises plasticity PVB model deviates from 1 ms and overestimates the displacement at P0 and P1. The obvious explanation of the discrepancy between PVB models is that Mises plasticity is a plasticity model. Hence a large amount of the strain in the PVB interlayer is plastic and non-reversible, which can explain the large discrepancy in the unloading response. Another possible source of error is that the Mises plasticity model is calibrated before the autoclave process, which can affect the material properties. For further numerical work, the Mises plasticity model can function well in simulating glass fracture and large displacements, while providing computational efficiency over the non-linear viscoelastic PVB model [20].

Modelling the full striker, including the impactor and the bar, was done to verify that the contact force extracted from the interaction was accurate enough. Figures 3.5a and 3.5b show the contact force for only the impactor and the full striker, respectively. The numerical results are coinciding and follow the contact force from the experiments. The sensor force from the numerical simulation in Figure 3.5 is also coinciding with the experimental results, but show heavy oscillations. Since the bar is modelled with linear truss elements, the stress in the bar is one-dimensional. The beam connecting the striker to the drop tower is modelled as a point mass, which is also a considerable simplification. Grue and Kjernlie reported similar challenges when modelling the full striker in the same test setup [46]. Based on the findings, it was concluded that modelling only the impactor as discrete rigid with a mass, $m_p = 6.551$ kg, was sufficient for further numerical work.

4. Numerical work - Monolithic glass

This chapter will present the numerical work on monolithic glass. The purpose of simulating impact on monolithic glass, is to investigate the behaviour of glass as a single component. This work will provide knowledge about the material model that describes the failure of glass in Abaqus. This knowledge will further be utilized in the simulation of laminated glass in Chapter 5.

Factorial design studies have been performed in order to investigate the behaviour of the build-in Brittle Cracking model in Abaqus and how different meshing techniques and element formulations influence the fragmentation of glass. A factorial design is a method to investigate how different independent variables influence a single output variable. Instead of only investigate the response from one variable at a time, the factorial design approach also investigates the interactions between different independent variables [47].

It is not expected that the simulations will reproduce the exact behaviour. However, it is of interest to optimize the variables such that simulations and experiments match as close as possible.

4.1 The Brittle Cracking model

The built-in material model Brittle Cracking in Abaqus is based on Hillerborgs Fictitious crack model [48, 49]. The Fictitious crack model [23] is originally developed for modelling brittle fracture and crack growth in concrete. The model is based on energy balance, and the crack is not displayed explicitly in the finite element model. Cracking starts when the stress reaches the tensile strength of an element. The fictitious crack opens in the direction of maximum principal stress. The model includes a softening phase after crack initiation. The stress in the element decreases with increasing crack opening. When the work performed on the element reaches the mode I fracture energy, the stress is equal to zero in tension. The element can therefore still carry loads in compression. The shear stiffness in the crack plane decreases with increasing crack opening, and becomes zero at a specified value.

The post-cracking behaviour is determined by the user. One method is to specify the critical mode I fracture energy, G_{IC}, and the critical stress σ_0. It is then assumed that the stress decreases linearly with increasing crack opening and that the area under the stress versus displacement curve is equal to the specified critical mode I fracture energy, as seen in Figure 4.1a. Note that the mode I fracture energy in the Brittle Cracking model includes the elastic

strain energy. Since only mode I cracking will be considered, the mode I fracture energy will further be referred to as the fracture energy. The displacement at failure, u_f, will be dependent on the specified fracture energy. The specified fracture energy therefore needs to be sufficiently large such that $u_f > u_0$ is ensured. Since the strain energy within the element is dependent on the element size, the fracture energy will therefore also be element size-dependent and needs to fulfil the requirement in Equation 4.1 [22].

$$G_{IC} \geq \frac{h_e \sigma_0^2}{2E} \tag{4.1}$$

Where E is the modulus of elasticity. h_e is a characteristic element length, and the longest distance across an element in the reference plane for a shell element and longest distance through a volume element. The fracture energy of glass is approximately 0.008 N/mm, [22]. Element sizes for practical purposes will therefore result in too large fracture energy when the minimum requirement is fulfilled. The fracture energy in the Brittle Cracking model should be treated as a numerical value and is not directly comparable with the physical property.

Another way to define the post-cracking behaviour is to specify the stress versus strain relationship, as shown in Figure 4.1b. The user also needs to define the shape of the curve, which describes the reduction of shear stiffness in the cracking plane. The curves go from the initial shear stiffness of the uncracked material to zero at a given displacement, u_s, as shown in Figure 4.1c.

For deleting an element, the displacement within the element needs to reach a specified level defined as Brittle Failure displacement. If the Brittle Failure displacement is less than u_f, the element will fail before the stress drops to zero. Similarly, if the Brittle Failure displacement is less than u_0, the element will fail immediately after the crack initiation criterion is reached.

(a) Mode I fracture energy   (b) Stress versus strain   (c) Shear stiffness reduction
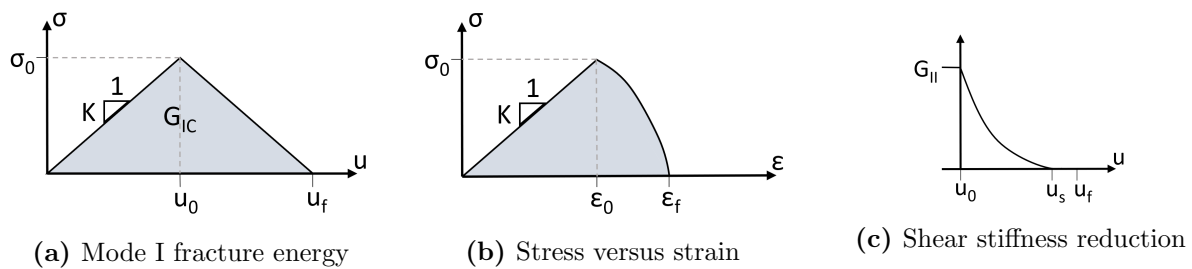
Figure 4.1: Input parameters for the built-in Brittle Cracking model in Abaqus.

4.2   Base Model

The model developed in Chapter 3 will be used as the Base Model. This Base Model consists of a glass pane modelled as a shell with 5 mm structured mesh and a supporting rubber band

modelled with $5 \times 5 \times 4$ mm^3 volume elements. The impactor is modelled as analytical rigid. The built-in Brittle Cracking model in Abaqus was used to model glass failure. Critical stress, fracture energy and failure displacement in the model were chosen to be 118 MPa, 0.27 N/mm and 0.001 mm respectively. These parameters are based on previous in-house work. The impact velocity was chosen to be 2.4 m/s. This allows for direct comparison between simulations and experiments on monolithic series 1 in Chapter 2.

The contact force from the Base Model simulation is plotted against time in Figure 4.2a and compared with the contact force from the experiments. The force versus time data from the simulation is filtered by using a channel frequency class filter (CFC) [50]. Two significant differences between the Base Model and the experiments may be found from 4.2a, which include too early fracture initiation and too slow fracture growth. Too early fracture initiation at 1.73 ms makes the Base Model incapable of catching the peak force from the experiments and too slow fracture growth makes it incapable of reproducing the rapid drop in the force after the initial failure. The velocity of the initial radial fractures was measured to be around 50 m/s in the simulations and 2000 m/s in the experiments.
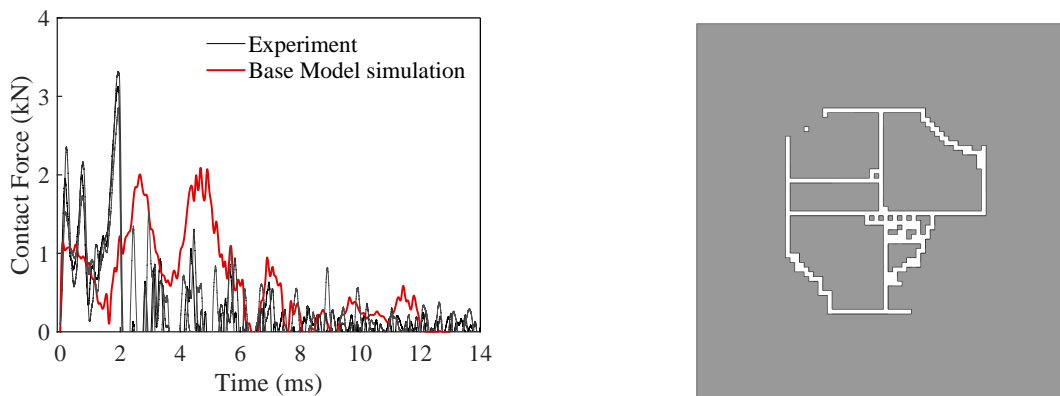
(a) Contact force versus time for a impact velocity of 2.4 m/s.

(b) Fracture pattern

Figure 4.2: Results from Base Model simulation.

As seen from Figure 4.2b, the Base Model is able to reproduce the general behaviour from the experiment with radial fractures out from centre followed by circumferential fractures. However, the fractures do not reach the edge of the glass and there are far less fractures in the simulation compared to the experiments.

4.3   Factorial design - Brittle Cracking and mesh

A factorial design study was conducted in order to investigate the influence of and the interaction between different input parameters in the built-in Brittle Cracking model in Abaqus. The influence of the mesh type and the element size was also included in the study.

The finite element model developed in Section 4.2 was used as a basis for the factorial design study. Linear shell elements with reduced integration were used with five integration points over the thickness. The glass was meshed with two different techniques, structured and free meshing. The structured mesh had equally sized square, four noded elements. The free mesh had similarly sized elements. Most of the elements were quadrilaterals with four nodes, while three noded, triangular elements were used in some regions by the meshing software in Abaqus to avoid elements with large distortions. The model with the free mesh was partitioned into circular sections, such that the mesh was oriented along radial lines out from the glass plate centre. This mesh will be referred to as circular free. The reason for making such a mesh was to trigger the fracture growth in the glass in the same way as in the experiment. Two different element sizes were used with each of the meshing techniques, such that four different meshes were studied in total. The four meshes are shown in Figure B.1 in Appendix B.

The fracture energy-based criteria in the Brittle Cracking model was used. In order to simplify the factorial design study, only the critical stress, fracture energy and failure displacement were chosen as factors. The influence of shear stiffness relaxation was considered negligible, based on initial studies. Three different values for critical stress and fracture energy, and two different values for failure displacement were considered. There were performed 72 individual simulations in total. The numerical values for the different factors and levels are presented in Table 4.1.

Table 4.1: Numerical values in the factorial design of Brittle Cracking.

Level	Mesh type	Critical stress	Fracture energy	Failure displacement
1	3 mm circular free	100 MPa	0.27 N/mm	0.001 mm
2	3 mm structured	118 MPa	0.50 N/mm	0.010 mm
3	5 mm circular free	140 MPa	0.70 N/mm	
4	5 mm structured			

Four different parameters from the simulation results were used to evaluate the performance of each simulation. The first parameter is the time at the first fracture. The second parameter is the time from the first fracture until complete glass failure. The first and the second parameter are obtained from visual inspection of the ODB output file in Abaqus. The third parameter is based on a qualitative evaluation of the fracture pattern. A jury of four, including the authors and supervisors of this thesis, gave a grade between 1 and 10 on the fracture pattern in each simulation. Grade 1 corresponds to no fracture and grade 10 corresponds to a fracture pattern equal to the physical experiments. The average grade was used as the third parameter. The fourth parameter is the HIC_{15} value which is obtained from the impactor acceleration. The HIC_{15} value is obtained by calculating the integral in

Equation 1.1 for different values of t_1 and t_2 while searching for the maximum.

The performance measurements from the Base Model simulation and the experiment are presented in Table 4.2.

**Table 4.2:** Simulation results from the Base Model.

	Base Model	Experiment
Time at fracture initiation	1.73 ms	2.0 ms
Fracture growth	11.3 ms	0.4 ms
HIC	7.29 $g^{2.5}s$	4.68 $g^{2.5}s$
Fracture pattern	3.5	10

The results from the factorial design study are presented as interaction plots in Figures 4.3, 4.5, 4.7 and 4.8. The results that the interaction plots are obtained from is presented in Tables B.1 - B.4 in Appendix B. The y-axis in the figures shows the mean deviation from the Base Model, while the x-axis shows the different input parameters in the factorial design. The diagonal plots show the main effect of changing one parameter, which is the average of the off-diagonal plots in the same column in the figure. The off-diagonal plots show the interaction effect between different input parameters. The gradient of the curve corresponds to the influence on the performance measurement when changing the input parameter. A flat curve means no influence and a steep curve means considerable influence. The interaction plots are obtained from the means of several simulation results. The different simulation results included in the means are not consistent. A complete statistical analysis is not performed, and the plots do not give any information about the significance of each result. The average computational times per simulated time are presented in Table 4.3 for the different meshes.

Table 4.3: Computational time from factorial design study of Brittle Cracking.

Mesh	Average computational time per simulated time
3 mm structured	136 s/ms
5 mm structured	27 s/ms
3 mm circular free	616 s/ms
5 mm circular free	52 s/ms

In a typical simulation with a structured mesh, the fractures started to grow in a cross pattern. The fractures grew in the direction which the mesh is oriented. When the fracture got close to the rubber edge, new fractures perpendicular to the original started to grow. In some simulations, these fractures grew such that they formed a circular crack. The resulting fracture patterns consist of mostly quadrilateral shaped pieces, or quadrilaterals with one
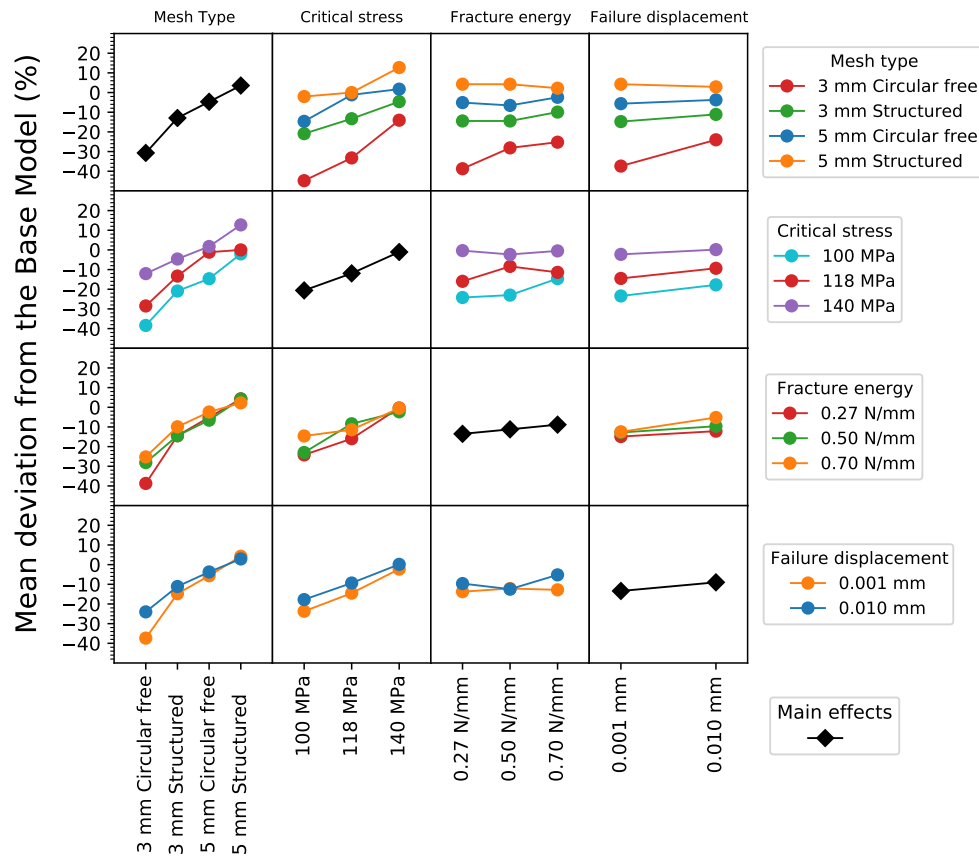
Figure 4.3: Interaction plots from the factorial design study for the performance measurement fracture initiation.

rounded edge. In a typical simulation with circular free mesh, the fractures started to grow in four or more radial directions. After the development of radial fractures, one or more circumferential fractures took place. The resulting fracture pattern consisted of circular sector-shaped pieces, and the size of the pieces was generally smaller than with the structured mesh. Fracture patterns from all simulations can be shown in Tables B.5 - B.12 in Appendix B. Typical fracture patterns from the different meshes are additionally shown in Figure 4.4. In some simulations, the fractures did not grow fast enough to develop fragments within the simulation time. The time at complete failure for these simulations was set to 13 ms, which is recognized as the time when the simulations finished.

High-frequency acceleration peaks and oscillations were observed in some of the simulations. The oscillations occurred typically after rapid changes, such as the initial contact between the impactor and the glass and when several elements failed. Remedies to overcome this problem were tried, such as using fully integrated elements, adjusting the shape of the impactor, turn off contact thickness reduction in the contact formulation for shell elements, and changing boundary conditions from clamped by the rubber to simply supported. None of these remedies provided any improvements on the oscillations problem. The problems disappeared when element erosion was turned off. It is believed that element erosion was

| (a) 3 mm Structured | (b) 5 mm Structured | (c) 3 mm Circular | (d) 5 mm Circular |
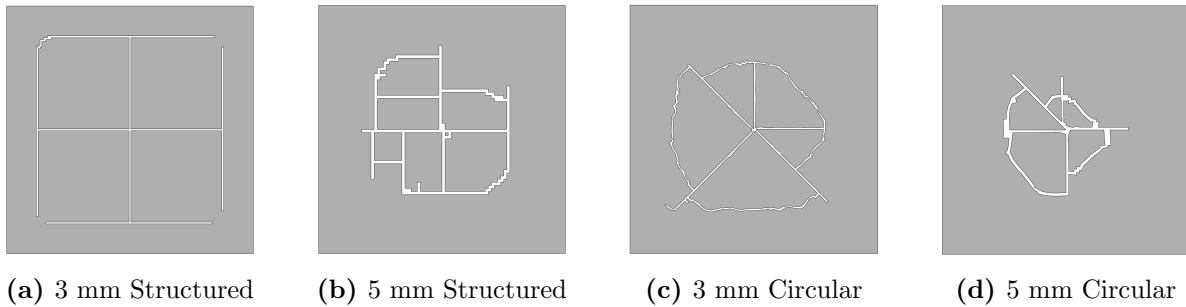
Figure 4.4: Fracture pattern from typical simulations with different meshes.

the reason for the high-frequency noise. Turning off element erosion resulted in a way to stiff behaviour of the glass even though the stress in the glass was set to zero by the Brittle Cracking model. Reducing the penalty stiffness by a factor of 100 in the contact formulation removed the oscillations. Too low penalty stiffness should be avoided since it will produce more penalty work, and affect the total energy balance. In addition, a low penalty stiffness will cause an inaccurate representation of the contact constraint. It is assumed that a few high-frequency acceleration peaks do not have a large influence on the fracture growth, fracture pattern and HIC_{15} value. The time at fracture initiation might be affected due to high stress peaks caused by high force peaks.

The energy balance was checked for each simulation. Figure B.2 in Appendix B shows the energy balance for a typical simulation in the factorial design study. Increases in the artificial strain energy and the viscous dissipation energy were observed when several elements eroded simultaneously. The total energy output was constant for all the simulations and the artificial strain energy was maximum 3% of the total energy output.

As shown in the plots in Figure 4.3, the mesh and the critical stress influence the time at fracture initiation the most. It can also be seen that the time at fracture initiation increases with increasing fracture energy and failure displacement. Nevertheless, the increase is small and it is hard to judge whether or not it is significant without a complete statistical analysis. The Brittle Cracking model uses a stress based criteria and smaller elements allow for better representation of high stress gradients. It is therefore reasonable that a refined mesh and reduction of the critical stress will cause earlier fracture initiation. The time at fracture initiation was around 2 ms in the experiment, as seen in Figure 2.4, and 1.73 ms in the Base Mode simulation, as shown in Table 4.2. All the simulations are generally underestimating the time at fracture initiation, and refinement of mesh leads to further underestimation. The strength of glass is highly stochastic. The limited amount of experimental tests are not sufficient for calibrating the critical stress. The simulation results should therefore give something similar to the experimental behaviour, but there will not be made any effort for calibrating the critical stress such that the fracture initiates at the same time as in the experiments.
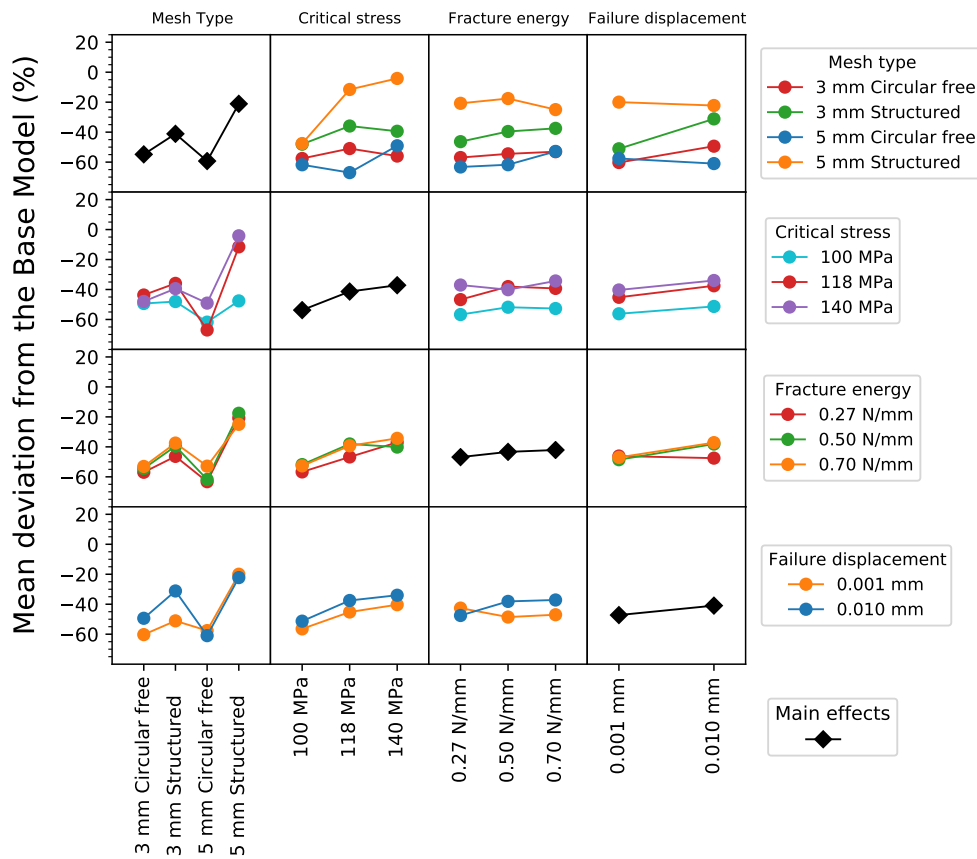
Figure 4.5: Interaction plots from the factorial design study for the performance measurement fracture growth.

The fracture growth was also highly dependent on the mesh, as seen in Figure 4.5. The circular mesh had a faster fracture growth than the structured mesh. The 5 mm circular free mesh had a faster fracture growth than 3 mm structured mesh. The difference between the 3mm circular mesh and the 5 mm circular mesh was small. It was observed more radial fractures in the simulations with circular mesh than with structured mesh. In addition, it was easier to develop circumferential cracks when the elements were oriented as in the circular mesh. It is believed that this is one of the reasons for faster fracture growth with circular mesh. Increasing critical stress also leads to slower fracture growth. This is reasonable since it was observed that increasing critical stress also leads to later fracture initiation.

The time from the first fracture until complete glass failure was around 0.4 ms in the experiments. This process took 3 ms in the simulation with the fastest fracture growth, and 11.3 ms in the simulation of the Base Model. Fractures in glass grow because of the stress intensity at the crack tip. They grow fast because of the low fracture energy in glass, such that only a small amount of energy is needed to create new surfaces. Extremely small elements are necessary for catching the stress intensity at the crack tip. Impact loads on glass results in a lot of fractures and the fractures grow all over the glass pane, such that the crack

tips can be anywhere. Extremely small elements all over the glass pane are thus necessary for catching the physical behaviour of fracture growth in glass. Such small elements are not feasible for practical purposes with the computer power available today. The FE model is not able to catch the stress intensity at the crack tip with the element sizes that have been used in this factorial design study. The mechanism that controls the fracture growth in the simulations with Brittle Cracking is that the stress reaches a critical level within an element. The element then erodes from the mesh. The fracture that initiated in one element can not grow beyond the element and propagate to neighbouring elements. The stress in the neighbouring elements needs to reach the critical level as well in order to get eroded. This process is a lot slower than the actual mechanism, where the fracture initiates and the low fracture energy offer little resistance against further growth. The differences between the fractures modelled with the Brittle Cracking model and the actual behaviour is illustrated in Figure 4.6.

(a) Fracture growth in the simulations

(b) Idealized fracture behaviour of glass
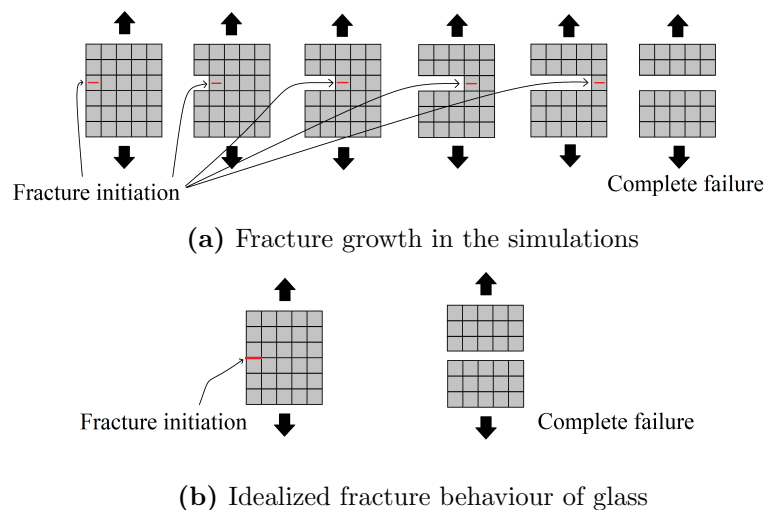
Figure 4.6: Illustration of the differences between fracture growth with Brittle Cracking (a) and the idealized behaviour (b).

In some simulations, several elements in the centre of the plate failed simultaneously. In these cases, the contact between impactor and glass also disappear for a short period of time. When the contact disappears, the glass loses its momentum and the stress decreases. The stress can further increase when the impactor reestablishes contact with the glass. This could also be a reason for slow fracture growth in the simulations compared to the experiments.

As seen in Figure 4.7, the mesh type had the largest influence on the fracture pattern and the circular free mesh was performing significantly better than the structured mesh. The difference between 3mm and 5mm element size is only minor compared to the difference in the mesh type. A circular oriented mesh seems to trigger a more physically correct fracture pattern. The fracture pattern also seems to look better with decreasing critical stress. This

might be expected since lower critical stress results in faster fracture growth and earlier fracture initiation. This allows more elements to fail, and fracture patterns that resemble the experiments are more probably. There are in general too few fractures in the simulations compared to the experiments. Most of the simulations are regardless capable of describing the underlying mechanisms of failure in glass exposed to impact loading.
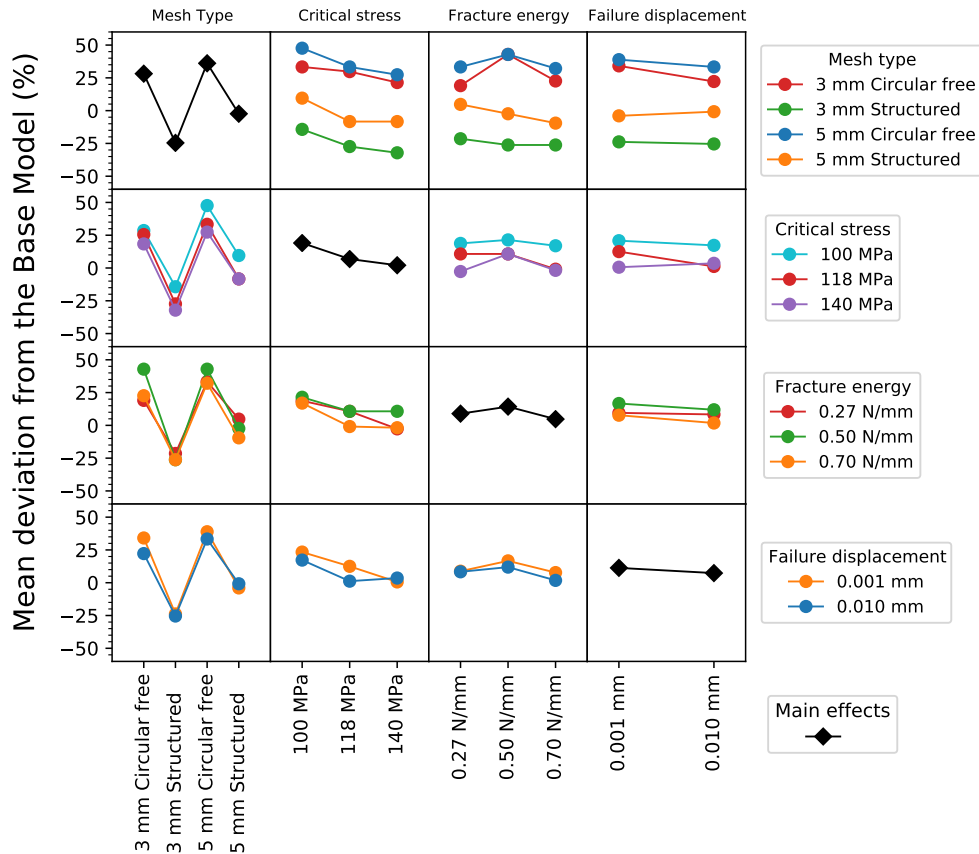
Figure 4.7: Interaction plots from the factorial design study for the performance measurement fracture pattern.

The HIC_{15} value is also highly dependent on the mesh and the critical stress, as seen in Figure 4.8. It is seen that there is less consistency between the different simulations from the off-diagonal plots. The simulations with critical stress equal to 140 MPa have a different response to the other input parameters than the simulations with critical stress equal to 100 and 118 MPa. Fracture stress equal to 140 MPa resulted in high HIC_{15} values in general. This is possibly because increased critical stress results in higher impactor acceleration. The HIC_{15} value is dependent on both the acceleration during the impact and the duration of the impact. The pre-failure phase dominates the acceleration versus time curve from the experiments. The acceleration oscillates around zero in the post-failure phase. The acceleration is significant both before and after the first fracture in the simulations because of the slow fracture growth. The duration of the impact is then significantly longer in the simulation than in the experiment. It is therefore reasonable that the HIC_{15} value is overestimated in

the simulations.
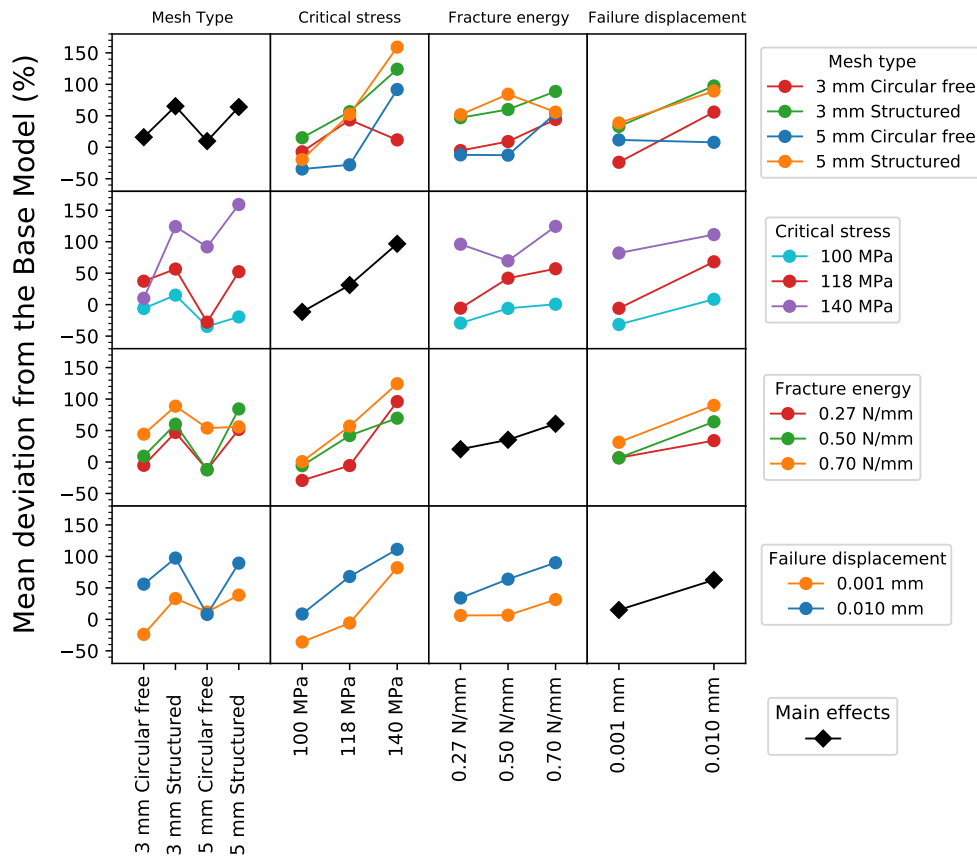
Figure 4.8: Interaction plots from the factorial design study for the performance measurement HIC_{15}.

The mesh seems to be the most critical parameter for all the performance measurements in this factorial design study. The circular free mesh showed generally better performance than structured mesh. Due to the large differences in computational time between 3 mm and 5 mm circular free mesh and small differences in performance, it is recommended to use the 5 mm circular free mesh for further analysis. The second most critical parameter is the critical stress. Fracture stress equal to 140 MPa gave both too high HIC_{15} values and too slow fracture growth, while the time at fracture initiation was closer to the experiment. The combination of critical stress equal 118 MPa and 5 mm circular free mesh performed well in all of the four performance measurements, and is recommended to use for further analysis.

Fracture energy and failure displacement showed only a minor influence on the performance measurements. It was observed larger dissipation energy in the simulations where the fracture energy requirement in Equation 4.1 was not met. It is also most physically correct to use a value of the failure displacement, which corresponds to the displacement when the stress is equal to zero. It is recommended to adjust the fracture energy and failure displacement for the given element size, which will require a mesh with similarly sized elements. The re-

quirement of similarly sized elements may be overcome by using an user-defined subroutine, which adjusts the material parameters for the characteristic element length [51]. However, this subroutine will not be used in further studies, since it is not commercially available in Abaqus.

4.4 Integration order and number of integration points

A parametric study was performed in order to investigate how the number of integration points over the thickness and how the use of fully or reduced integrated elements influence the results. The finite element model with 5 mm circular free mesh from Section 4.3 was used as a basis. The critical stress, fracture energy and failure displacement were set to 118 MPa, 0.59 N/mm and 0.01 mm, respectively. Simulations with 5, 7 and 9 integration points over the thickness were tested, and the HIC_{15} value was used as a performance measurement.

HIC_{15}-estimations versus number of integration points are shown in Figure 4.9. Fracture patterns and the numerical HIC_{15} values are presented in Tables B.13 and B.14 in Appendix B. The computational time for the different simulations are presented in Table B.15 in Appendix B. Increasing the number of integration points by two, resulted in an approximately 15% increase in computational time. Changing from reduced to fully integrated elements, increased the computational time by a factor of approximately three.
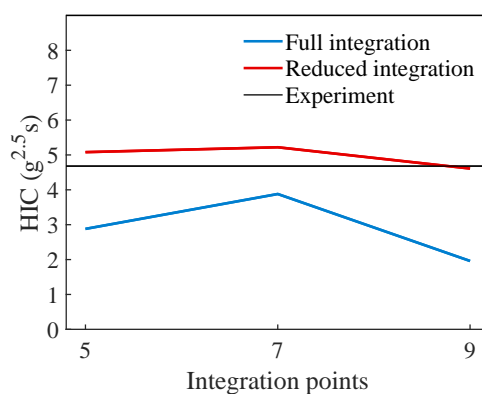
Figure 4.9: HIC_{15}-estimations versus the number of integration points.

From Figure 4.9, it is observed that fully integrated elements result in lower HIC_{15} values compared to reduced integration. Simulations with fully integrated elements underpredicted the HIC_{15} value in general. The stress is calculated at four points in all planes corresponding to the integration points when fully integrated elements are used. Reduced integrated elements only calculate the stress at one point for each integration point. High stress peaks can thus easier be detected when fully integrated elements are used, and earlier fracture initiation may be expected. Increasing the number of integration points will also make it

easier to detect high stress peaks. The combination of fully integrated elements and nine integration points may be a reason for the especially low HIC_{15} value provided from the simulation with that combination. A weakness in the use of a pure stress-based cracking criterion, which is implemented in the Brittle Cracking model, is that artificially induced high stress peaks may initiate the cracking too early. It may therefore be argued that the use of both fully integrated elements and nine integration points in combination with a pure stress-based criterion should be avoided. Form Figure 4.9, it may also be argued that reduced integrated elements provide better HIC_{15} estimations than fully integrated elements.

There is some lack of consistency in the results. HIC_{15} increases when going from five to seven integration points, but decreases when going from seven to nine. It should maybe be expected a monotonic change in HIC_{15}, when increasing the number of integration points. There seems to be a correlation between the fracture pattern and the HIC_{15} value, as seen in Tables B.13 and B.14. The highest HIC_{15} values were observed in simulations with a large radius on the circumferential fractures. This can be explained by the fact that the fractures must go further before complete failure. This leads to a longer duration of the impact and a higher HIC_{15} estimation. It is important to highlight that it is preferable that both the HIC_{15} estimation and the fracture behaviour resemble the experiment. A correct HIC_{15} estimation alone will not be useful if it is obtained from an unphysical behaviour. It is hard to draw conclusions on the best practice in terms of the number of integration points because of the inconsistency in the results. Five integration points will be used in further studies, motivated by the computational efficiency and the small influence on the results when used in combination with reduced integrated elements.

4.5 Volume elements

A series of simulations where the glass was modelled with cubic C3D8R volume elements were run. The purpose of these simulations was to investigate how volume elements perform compared to shell elements. Simulations with three different element sizes were performed. The material parameters in the Brittle Cracking model were customized for each mesh such that the parameters fulfilled the requirement in Equation 4.1. Table B.16 in Appendix B presents the different element dimensions and the Brittle Cracking material parameters. The rubber and the impactor were modelled in the same way as in Section 4.2. The impact velocity was 2.4 m/s.

The results from the simulations with volume elements are presented as contact force versus time histories and as fracture patterns in Figure 4.10. The computational time per simulated time was 688 s/ms, 6208 s/ms and 56480 s/ms for Mesh 1, 2 and 3, respectively. In the simulation with Mesh 1, the fracture did not develop into a hole in the glass pane and the

impactor was pushed back upwards.

(a) Contact force versus time

(b) Mesh 1   (c) Mesh 2   (d) Mesh 3
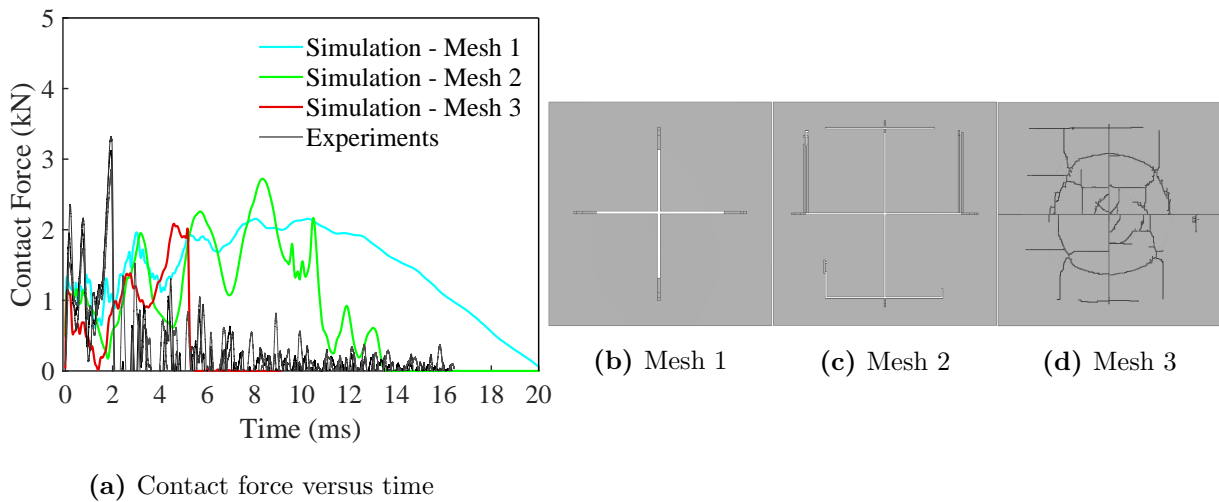
Figure 4.10: Results from simulations with volume elements. Force versus time histories in (a) and fracture patterns in (b), (c) and (d).

As seen from both the force versus time curves and from the fracture patterns in Figure 4.10, it is necessary with small elements for obtaining proper results with volume elements. The simulation with Mesh 3 is performing well, and the time from the first fracture until complete failure is in line with the best simulations with shell elements. The force gets a rapid drop at around 5 ms which is caused by a quick formation of a circumferential fracture. This behaviour resembles the physical behaviour, but the computational cost of obtaining such results are high. The computational time with Mesh 3 is around 1000 times longer than with the recommended 5 mm circular free mesh with shell elements from Section 4.3.

The material parameters in the Brittle Cracking model need to be customized for the element size, and it is only possible to do it for one characteristic element length. Mesh 3 has an element geometry which is close to cube-shaped. The material perimeters are therefore optimized for cracking in all three directions. This might be one of the reasons for Mesh 3 to perform better than Mesh 1 and 2. Abaqus is only providing linear interpolated volume elements and a sufficient number of elements over the thickness is necessary in order to represent bending. If cube-shaped elements are necessary to obtain proper results with volume elements together with the Brittle Cracking model, the elements need to be small in order to represent bending.

Volume elements can provide satisfactory results, but do not yield advantages over shell elements. Shell elements are significantly more efficient than volume elements with respect to computational cost. Further studies will only include shell elements for glass.

5. Numerical work - Laminated glass

5.1 Introduction

The composite sandwich construction of laminated glass introduces several complex numerical challenges, which include modelling of the polymer interlayer, bonding between components and fracturing of glass. The basic laminated glass model, developed in Chapter 3, is used as a starting point for the numerical work in the following section.

A study on the numerical performance of laminated glass covers a wide range of factors that can influence the results. Some initial exclusions of factors are therefore necessary to minimize the numerical work. An important factor which is neglected is the possible delamination between the glass and the interlayer. When utilizing the element deletion method, there are usually two preferred methods for simulating the bonding between glass and interlayer. The simplest method is to assume a rigid and unbreakable bond by using a shared node technique [9, 52]. A more refined method involves using tie-break constraints between glass and interlayer to simulate debonding. The tie-break method has been used with the element deletion method on blast loaded laminated glass but resulted in unstable simulations [7]. A similar technique is used in combination with novel methods like cohesive zone model (CZM) and node-splitting [46, 25, 53]. These novel methods of simulating glass fracture represent more physical fracture behaviour in line with experimental observations. Since CZM and node-splitting involve splitting elements, rather than eroding them, the width of the cracks will be substantially smaller compared to cracks from eroded elements. As a result, the strains in the interlayer will become far too large without some form of debonding behaviour. Following this argument, it is believed that a simple tie constraint between glass and interlayer can be efficient in combination with relatively large element sizes and element deletion method.

The model developed in Chapter 3 will function as the Base Model. Key components of the Base Model include a 5 mm structured mesh of the glass panes, 5 mm structured mesh of the polymer interlayer with three elements over the thickness, surface-to-surface contact (STS) and a non-linear viscoelastic PVB material model. An impact velocity of 5.8 m/s was chosen in the numerical model, which allows for validation against the experimental tests in series 4 described in Chapter 2. The experimental data revealed large mid-point displacements and substantial glass fractures while the interlayer remained intact. This was deemed as a suitable challenge for the numerical study on laminated glass.

5.2 Base Model

The performance of the Base Model (BM) is presented by comparing the contact force versus time in Figure 5.1a. A STS contact was defined between both the upper glass and the impactor, and between the PVB and the impactor. The total force is the sum of the contact forces extracted from the interactions with the impactor. Displacement versus time is shown in Figure 5.1b, general fracture behaviour in Figure 5.2 and predicted HIC_{15} in Table 5.1. The contact force extracted from the contact algorithm displayed large oscillations. It is believed that this is caused by element erosion and is elaborated in Section 4.3. The contact force from the numerical results is therefore filtered using a CFC method [50].

(a)

(b)
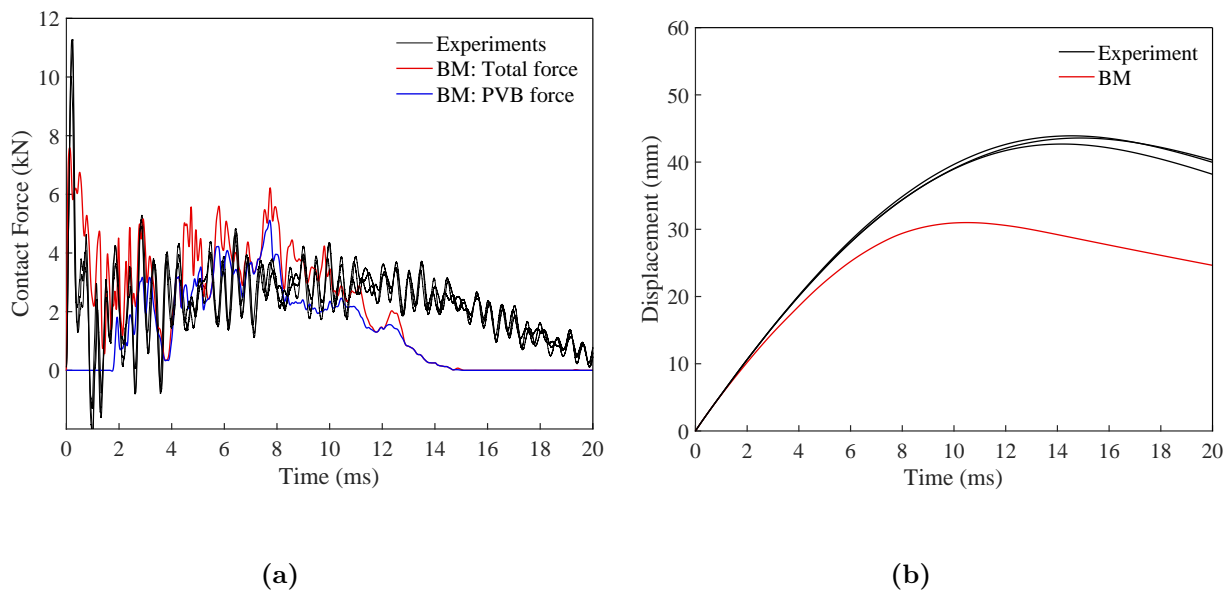
Figure 5.1: The performance of the Base Model compared to experimental results. The impact velocity is 5.8 m/s. Figure (a) displays contact force versus time and (b) display displacement versus time of impactor.

(a) 1.5 ms. **(b)** 1.5 ms. **(c)** 3.5 ms. **(d)** 3.5 ms.
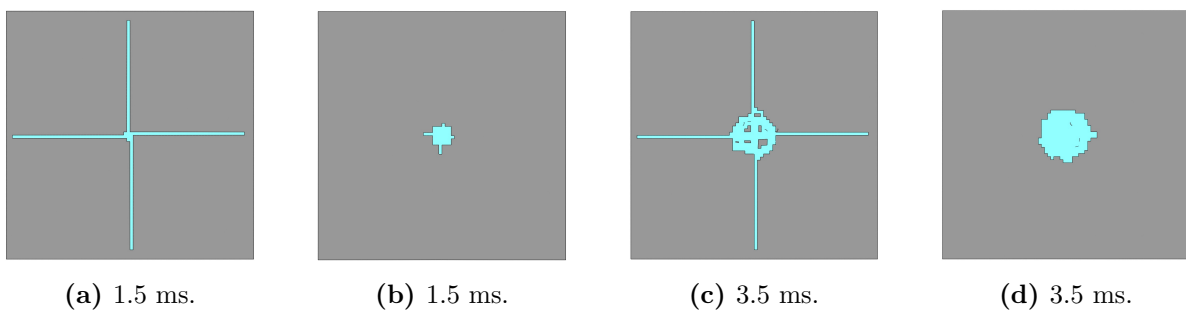
Figure 5.2: Fracture growth for the Base Model with impact velocity of 5.8 m/s. Figure (a) and (c) corresponds to the non-impacted pane, while (b) and (d) corresponds to the impacted pane.

The initial response is, to some degree, captured by the Base Model. The mean peak force from the experiments was 10.9 kN and 7.9 kN from the Base Model simulation. The lower peak force is presumably due to premature fracturing of the lower glass pane. The pre-failure simulation in Figure 3.7b captures the peak force more accurately. After the initial peak force, the lower pane fractures in a distinct cross, seen in Figure 5.2a. These fractures significantly reduce the stiffness of the laminated glass. The fractures in the lower pane are followed by fractures in the upper pane, which results in a large amount of erosion, shown in Figure 5.2d. Excessive erosion occurs around the impact area for both the panes. As a result, the PVB interlayer accounts for most of the force transfer, as there is excessive glass erosion between 2 and 4 ms. The numerical results from the Base Model indicate that the model is not able to simulate the fracturing of glass. Neither number of fractures nor the excessive erosion resembles the observed physical behaviour from the experiments.

Impactor displacement from both simulation and experiment are shown in Figure 5.1b. Simulation and experiment coincide well up to 2 ms in the impact. As noted earlier, the excessive erosion of elements in the impacted glass pane occurs at around 2 ms. Contact between interlayer and impactor is established. The intact glass elements are only in contact with the impactor through a circle at the outer perimeter of the impactor. Under these circumstances, two mechanisms will simultaneously contribute to absorbing energy from the impact. Experimental observations show that the radial cracks travel from the impact zone to the edges at a velocity of approximately 2000 m/s. Radial cracks are evenly spread from the impact zone, in the upper and lower pane. From qualitative assessment, there were observed more than 50 radial cracks developing before the onset of any circumferential cracking. The numerical model produced four radial cracks in the lower pane and none in the upper pane. It is believed that this is a contributing factor to why the numerical model underestimates the displacement by approximately 38%.

The main focus is to what extent the numerical models can predict HIC_{15} correctly. Results from the Base Model and the experiments in series 4 are given in Table 5.1. HIC_{15} is overestimated by approximately 50.9% and the general behaviour does not resemble the experiments. The following work on laminated glass will attempt to improve HIC_{15} prediction with a better numerical description of the physical behaviour of impact loaded laminated glass.

5.3   Factorial design - Main parameters

A factorial design with four factors for the laminated glass was designed to investigate possibly important factors in the numerical model. The four factors examined are Mesh, Element erosion, PVB material model and contact algorithm. The reasoning behind why the factors could be important will be elaborated. The material parameters in the Brittle Cracking

Table 5.1: HIC_{15} performance of the Base Model versus the experiments.

	HIC_{15} ($g^{2.5}s$)	t_1 (ms)	t_2 (ms)
Base Model	257.0	0.0	11.3
Laminated-4-1	180.0	0.0	15.0
Laminated-4-2	171.0	0.0	15.0
Laminated-4-3	160.0	0.0	15.0
Mean series 4	170.3	-	-

model are based on the work done in Section 4.3 and follow the recommended criterion in Equation 4.1. The chosen critical stress is 118 MPa, fracture energy is set to 0.5 N/mm and failure displacement is 0.0084 mm.

The meshing of the glass panes has shown to be important in Section 4.3, when utilizing element erosion in simulating glass fracture. Both geometrical shape and size of elements can be important factors for the effectiveness of the numerical model. The levels consist of 5 mm and 3 mm for both structured and circular free meshes. These are the same that were used in Section 4.3.

Element erosion is an easy-to-implement approach for modelling fracture in laminated glass. When element erosion is combined with a local fracture criterion, one may experience quick and localised erosion in the impacting zone [30]. Quick and localised erosion may lead to cratering of the impacted glass pane and very localised deformation. The Brittle Cracking model allows for fracture modelling without element erosion. In this regard, the failed element can no longer transfer tensile stress but can withstand compressive stress. Levels included in Element erosion is element erosion turned on for both glass panes, and element erosion turned off in the top pane. The two levels are denoted On and Top Off, respectively.

The PVB material models used in the factorial design are described in Section 3.2. Both the non-linear viscoelastic model and the Mises plasticity model will be used as levels. The Mises plasticity model was not capable of describing the unloading in an elastic response, as discussed in Section 3.5. Given that the primary objective of the numerical study is to simulate both the pre- and the post-fracture response of laminated glass, it is of interest to validate whether or not the Mises plasticity models is a viable option.

The numerical model consists of five parts, two glass panes, interlayer and two rubber clampings. Contact between each part should be enforced accurate and cost-effective. Abaqus has two contact algorithms available for dynamic explicit analysis, general contact (GC) and surface-to-surface contact (STS). STS allows for both kinematic and penalty enforcement of contact. While GC only allows for enforcement through a penalty method. Therefore, it

is of interest how the two algorithms perform in terms of solution accuracy and CPU cost. The factors and corresponding levels are summarized in Table 5.2 and the Base Model of the factorial design is 5 mm Structured, On, Non-linear viscoelastic and STS.

Table 5.2: Numerical values in factorial design of the laminated glass model.

Level	Mesh	Element erosion	PVB model	Contact
1	5 mm structured	On	Non-linear viscoelastic	GC
2	3 mm structured	Top off	Mises plasticity	STS
3	3 mm circular free			
4	5 mm circular free			

The results of HIC_{15} prediction in the factorial design of laminated glass are presented in Figure 5.3 as interaction plots. Listed values for all simulations is found in Tables C.1 and C.2 in Appendix C.
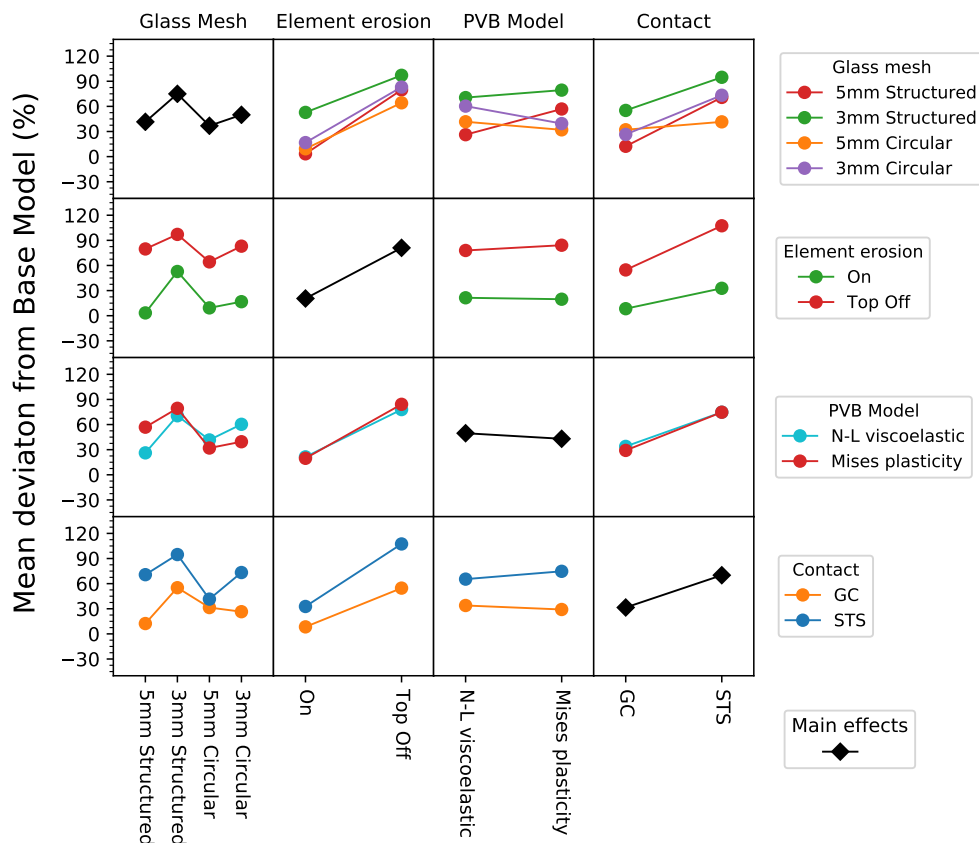
Figure 5.3: Interaction plots from the factorial design study for the performance measurement HIC_{15}. The Base model is 5mm Structured, On, Non-linear viscoelastic and STS, where each term corresponds to a level. Non-linear is abbreviated to N-L.

The main effects from the factorial design are summarized as follows:

- Glass meshing show inconsistent results. The 3 mm structured produce significantly higher HIC_{15} values compared to the three other levels.

- Element erosion: Top off leads to an increase in HIC_{15}.

- The results are close to insensitive to PVB material model.

- STS leads to higher HIC_{15} compared with GC.

Key two-way interactions are summarized as follows:

- Glass Mesh interacts with PVB Model. The structured meshes have a negative effect of using the Mises plasticity model, while the circular meshes have a positive effect.

Interpretation of the numerical results, shown in Figure 5.3, reveal several key points. First, meshing and choice of PVB material model appear to have little effect on HIC_{15} for the given impact velocity. If the impact velocity is high, such that the glass panes experience a complete fracture, the interlayer becomes the main load-carrying component by membrane forces. Since energy-absorption occurs primarily before maximum displacement, a Mises plasticity model appears adequate in describing the response. Secondly, the choice of contact algorithm is important in several ways. A major flaw with the numerical simulations done with GC was discovered. Abaqus enforces automatic shell thickness reduction when the shell area dimensions are close to the thickness dimension [54]. This does not influence the stiffness calculations, but it allows for rotation between glass panes and rubber strips. The extra rotation will therefore contribute to a softer impact. The STS contact may have problems when simulating shell elements that are eroded and unphysical bull-nose extensions may occur, which can explain why simulations with STS showed an increase in the total energy output [55].This behaviour was not observed with GC. Results indicate that GC is a better alternative with element erosion, but the automatic thickness reduction must be manually disabled. GC will be the base of further simulations.

A surprising result from the factorial design is that the meshing appears to have little effect on HIC_{15}. This could be explained by comparing the fracture growth from the Base Model in Figure 5.2 and a simulation from the factorial design. The fracture pattern in Figure 5.4 is similar to the experiments, radial cracks followed by some circumferential cracking. The main challenge is that the fracture growth is slow and the stiffness is greatly overestimated. Hence, the visually better results obtained by mesh refinements do not offer better performance in terms of predicting HIC_{15}.

The PVB material model did not influence the simulations in terms of HIC_{15} or maximum displacement of the impactor. This suggests that the simpler Mises plasticity model is able to describe the behaviour up until maximum displacement. Therefore, it would be beneficial

(a) 1.5 ms.   **(b)** 1.5 ms.   **(c)** 6.75 ms.   **(d)** 6.75 ms.
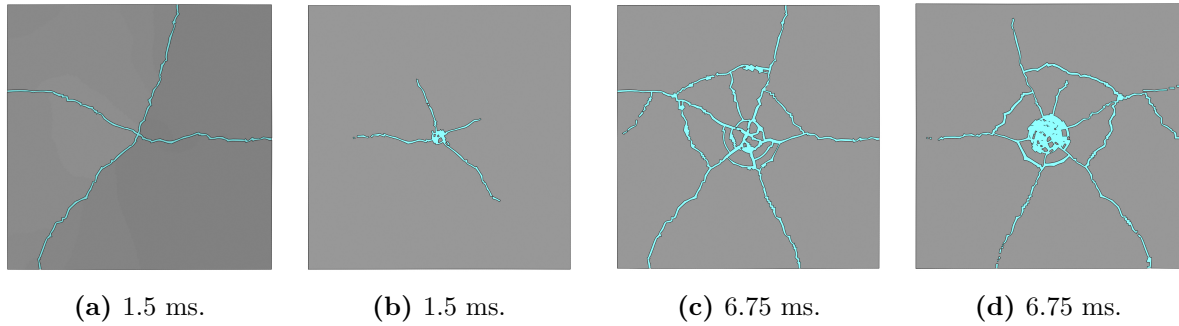
Figure 5.4: Fracture growth for 3mm Circular mesh, Brittle Failure: on, Mises plasticity and GC with an impact velocity of 5.8 m/s. Figures (a) and (c) is the non-impacted pane, while (b) and (d) is the impacted pane.

to utilize the most effective material model with regards to computational cost. Measured efficiency is presented in Figure 5.5, where the simulations with element erosion: Top Off is omitted. CPU time is normalized based on the runtime of the Base Model, which was 1.5 hour. GC performed better than STS in both energy conservation and computational efficiency. Therefore, the results were compared based on the PVB material model only, corresponding to the purple and green bars in Figure 5.5. The reduction in CPU time when changing material models, from left to right, was 23.6%, 23.4%, 42.8% and 20.0%. These results suggest that the Mises plasticity model function well for the given impact velocity and offer faster computations.
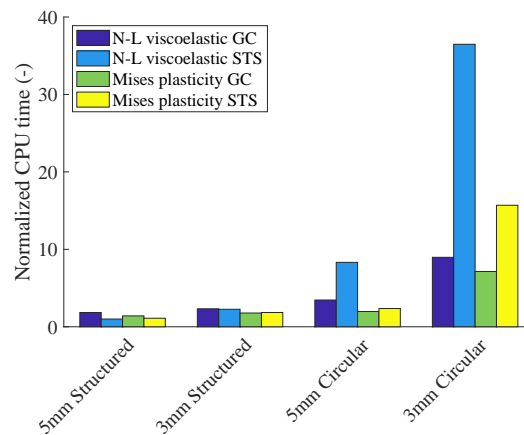
Figure 5.5: Normalized CPU time from the factorial design of laminated glass with impact velocity 5.8 m/s. The CPU time for the Base Model was approximately 1.5 hour.

5.4   Factorial design - Mesh parameters

Based on the results from the former factorial design, in Section 5.3, a new factorial design was developed. The motivation for the new design was to investigate how further mesh refinements of glass panes and interlayer can affect the performance of the numerical model. Since the numerical performance was not sensitive to the PVB material model, the Mises plasticity model was chosen for computational efficiency. GC was preferred for several reasons. The computational efficiency was better, the total energy output was approximately constant, and disabling of shell thickness reduction allowed for an accurate representation of the boundary conditions. Numerical parameters for Brittle Cracking model are given in Table 5.3. Factors and corresponding levels are presented in Table 5.4.

Table 5.3: Numerical values in Brittle Cracking for Factorial design Mesh Parameters.

Glass element size	Critical stress	Fracture energy	Failure displacement
5 mm	118 MPa	0.500 N/mm	0.0084 mm
3 mm	118 MPa	0.298 N/mm	0.0051 mm
2 mm	118 MPa	0.199 N/mm	0.0034 mm

A brief overview of the different factors is presented. The first factor is the Meshing technique and covers the glass panes. The former factorial design demonstrated that crack propagation with element erosion is an inherently mesh dependent problem [18, 56]. For this reason, two meshing techniques are used, shown in Figure 5.6. Circular free is a mesh with no induced direction for radial cracking. Radial cuts free describes a circular free mesh, but with the inclusion of eight radial cuts to trigger fractures. It is of interest whether or not the radial cuts reduce the stiffness and HIC_{15} prediction of the numerical model.

Figure 5.6: (a) is Circular free and (b) is Radial cuts free.

Size of glass elements follow the same argument as before, but with further refinement of adding 2 mm elements. A finer discretization of the interlayer allows for a better representation of the curvature around the impact zone. The main purpose of the PVB mesh is to

investigate how this may or may not influence the crack pattern and the global response of the model. The last level, NOE PVB thickness, accounts for how membrane forces in the interlayer are represented. The number of elements is abbreviated to NOE. The interlayer has negligible bending stiffness, while the membrane stiffness is considerable and is the main load-carrying component after both glass panes fracture. If the option of using one element over the interlayer thickness yields satisfying results, it would be beneficial to lower the computational cost.

Table 5.4: Numerical parameters in the Mesh parameters factorial design.

Level	Meshing technique	Glass mesh	PVB mesh	NOE PVB thickness
1	Circular free	5 mm	5 mm	1
2	Radial cuts free	3 mm	4 mm	3
3		2 mm	3 mm	
4			2 mm	

Results from the factorial design of mesh parameters of the laminated glass model are presented in Figure 5.7. Listed values for all simulations is found in Tables C.3 and C.4 in Appendix C. The energy balance was checked for each simulation and was deemed satisfactory. A typical energy balance for an simulation is found in Figure C.1 in Appendix C.

The main effects from the factorial design are summarized in the following.

- Mesh type affects the response in HIC. Introduction of radial cuts reduces HIC_{15} in general for all other factors, but the effect is small.

- Glass Size appears to reduce the stiffness and the HIC_{15}, but the effect is largest between 5 mm and 3 mm.

- PVB size appears to play an important role in determining the response. Smaller PVB element size reduces HIC_{15}.

The key interaction effects are listed below.

- The response of Mesh type is more influenced when the Glass Size decrease.

- Glass Size interacts with Mesh type. This effect is stronger as the Glass Size is reduced.

- The interaction between sizes of glass and PVB is complex. For the largest PVB size one observe a negative effect, while the effect is positive for PVB sizes between 4 mm and 2 mm.

- PVB size also interacts with Mesh type. This effect is stronger for Radial Cuts compared to Circular Free.
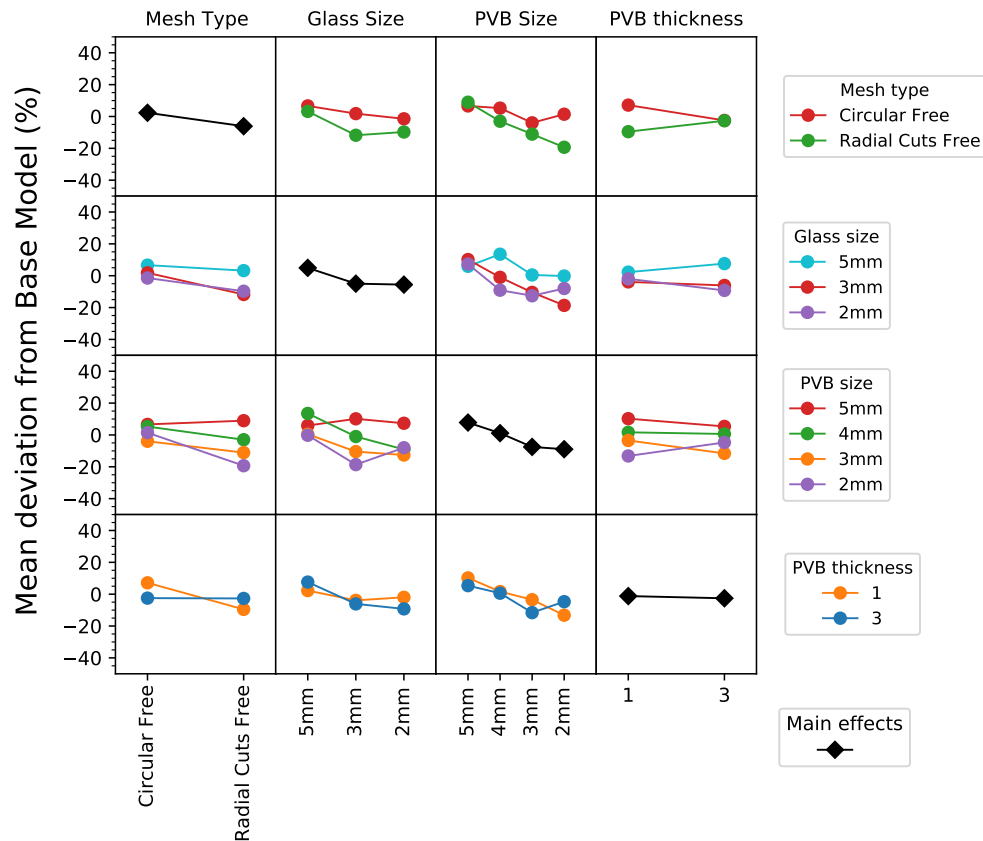
Figure 5.7: Interaction plots from the factorial design study for the performance measurement HIC_{15}. The Base Model is Circular Free-5mm-5mm-3, where each term corresponds to a level.

The factorial design of mesh parameters revealed HIC_{15} to be sensitive to both the geometrical shaping of the mesh and element sizes. The fracture behaviour of glass panes is believed to be an important factor in the global response of an impact problem with laminated glass. From a qualitative assessment of the fracture behaviour, some key findings can be summarized as follows. None of the meshing parameters in the factorial design controls the initial response and all simulations display the same behaviour. The initial cracks initiate in the lower pane at approximately 0.2 - 0.3 ms. The number of initial cracks varies between 4 and 5 and the initial peak force is approximately 6 kN for all simulations before it drops rapidly. The rapid drop in contact force observed for all simulations is believed to be caused by the initiation of fracture in the lower plate.

The secondary phase of the fracture behaviour starts after the initial cracks have reached the edges of the lower pane. The post-fracture phase is controlled by the different mesh factors. For illustrating how the fracture behaviour controls the global response, a selection of two simulations are chosen, the best and worst in terms of HIC_{15}. The results are given in Figure 5.9. As stated before, the initial response is similar until 1.5 ms. The best simulation, shown in red, display some erosion in the lower pane and continuing fracture growth in the upper pane. The contact force drops rapidly between 4 ms and 5 ms due to a growing cir-

cumferential fracture near the impact zone and near the rubber clamping. This effect causes the glass to lose load-bearing capacity and a larger portion is carried by the interlayer. The worst simulation displayed more element erosion in the impacted zone and more localised deformation. Since most of the glass is intact, the response is notably stiffer from 4 ms to 11 ms.

The results indicate that the meshing of the PVB interlayer is important for both the HIC_{15} prediction and the fracture pattern. The general trend observed, illustrated in Figure 5.8, is that larger PVB element sizes lead to localised erosion and deformation around the impact zone, especially for large discrepancies between the glass and the PVB size. Because of the tied constraint between the glass and PVB, the strains in the PVB will also occur in the glass. If several glass elements are tied to a PVB element, this can lead to erosion of several glass elements. The consequence of localised erosion is the lack of circumferential cracking, which limits the area of interlayer actively involved in absorbing the impact. Contrary, the best configurations from the factorial design are able to simulate more radial and circumferential cracking in line with the experimental observations.

There are several numerical simplifications which can affect the results. The strain rate-dependency in the glass is not accounted for explicitly. Numerical work in Chapter 4 found that the initial peak force is dependent on the critical stress, but can lead to slow fracture growth. Initial numerical work showed that the initial response was not influenced by the critical stress and could suggest that the stress in the impact zone is overestimated. The rubber coating on the impactor has unknown friction properties. Different values of friction between glass and impactor were investigated but yielded practically no difference. Delamination between layers was not included. How and if delamination combined with element erosion and the Brittle Cracking model influences the results is reserved for future work.

(a) Radial Cuts-3mm-2mm-3.

(b) Circular Free-2mm-5mm-3.
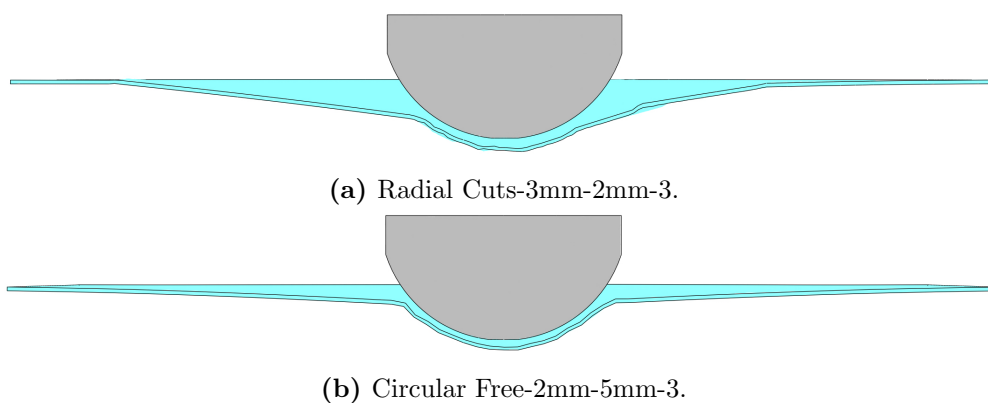
Figure 5.8: The deformation profiles for the PVB. Glass panes and supports are omitted to visualize the deformation. Both (a) and (b) are at maximum displacement at 27.5 mm and 25.1 mm, respectively. The corresponding HIC_{15} for (a) is 242 $g^{2.5}s$ and (b) is 323 $g^{2.5}s$.
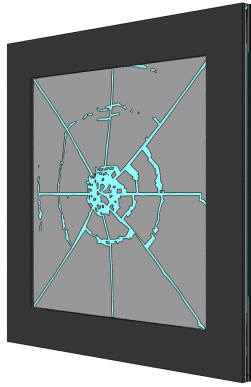
(a) Radial Cuts-3mm-2mm-1 lower view.
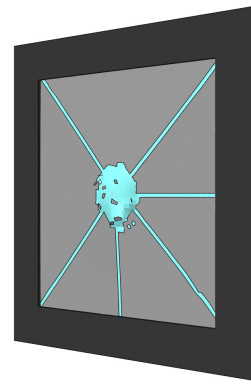
(b) Radial Cuts-5mm-4mm-3 lower view.
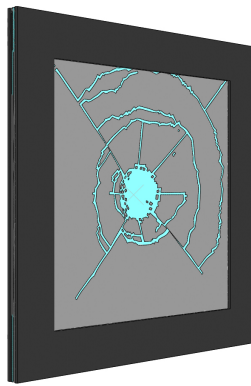
(c) Radial Cuts-3mm-2mm-1 upper view.
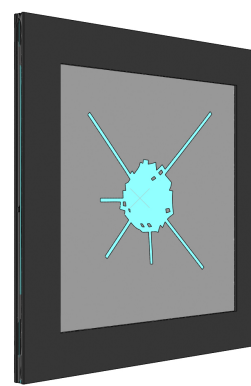
(d) Radial Cuts-5mm-4mm-3 upper view.
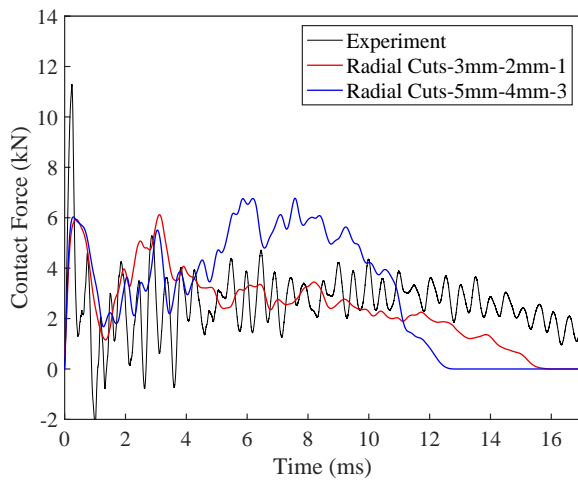
(e)
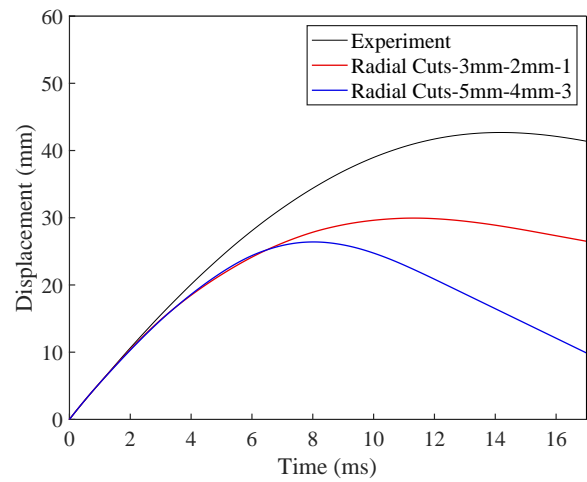
(f)

Figure 5.9: The response of the best and the worst simulation in terms of HIC_{15}. The fracture patterns at 6.8 ms are displayed for best simulation in (a),(c) and worst in (b),(d). Figure (e) display contact force versus time and (f) display displacement versus time of the impactor. The corresponding level in the factorial design is given in the legends. The red simulation predicted HIC_{15} of 198 $g^{2.5}$s and blue simulation predicted HIC_{15} of 457 $g^{2.5}$s.

5.5   Verification of best configuration

Brittle material failure is a numerical challenge, especially when coupled with the PVB interlayer. The numerical work has shown promising results in predicting HIC_{15}. The best configuration from the two former factorial designs is simulated with impact velocities of 2.4 m/s and 9.9 m/s and configuration Radial Cuts-3mm-2mm-1 from Section 5.4 is used. The numerical performance is presented in Figures 5.10 with corresponding fracture patterns in 5.11, and HIC_{15} predictions in Table 5.5.

Both simulations, with impact velocities of 2.4 m/s and 9.9 m/s, underpredicts the initial force before fracture initiates. The pre-fracture phase has a short duration and should not be the primary reason for deviations in HIC_{15}. After the initial drop in force, between 1 and 2 ms for both simulations, there is an unphysical increase in the force. Since only a small number of fractures occurs, the unphysical increase in force is presumably due to the development of the fracture patterns seen in Figure 5.11. The extra stiffness obtained from the slow fracture growth absorbs the kinetic energy faster, such that the PVB interlayer is not the main load-carrying component in the numerical simulations. If the PVB interlayer is not sufficiently activated as a membrane component, this could explain why the factorial design in Section 5.3 was insensitive to the PVB material mode. The experiment in Figure 5.11c show severe fragmentation and a fully activated PVB interlayer.
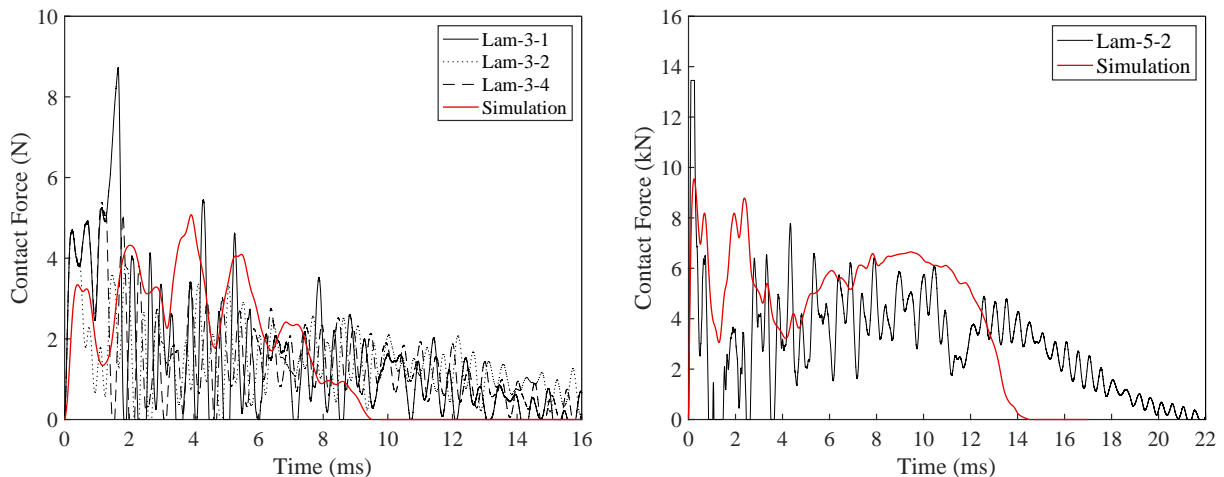
(a) Impact velocity of 2.4 m/s   (b) Impact velocity of 9.9 m/s

Figure 5.10: Contact force versus time for two different impact velocities with the best configured numerical model.

The exposed area of the laminated glass is 300×300 mm^2 and the nominal thickness of the component is 9.12 mm. Compared to an automobile windshield, the component will be much stiffer, and it is believed that this poses a greater challenge for the numerical tools used to simulate an impact. In order to properly estimate HIC$_{15}$ the model should be able to simulate fast glass fracture such that the PVB interlayer becomes the main load-carrying component by membrane forces, and not hinge-like mechanisms.

Table 5.5: HIC$_{15}$ predictions for simulations with impact velocities (IV) of 2.4 m/s and 9.9 m/s.

IV (m/s)	Type	HIC$_{15}$ (g$^{2.5}$s)	t$_1$ (ms)	t$_2$ (ms)
2.4	Simulation	108.4	0.34	7.50
	3-1	82.0	0.0	1.8
	3-2	40.3	0.0	13.7
	3-4	49.5	0.0	11.1
9.9	Simulation	931.4	0.0	12.8
	5-2	391.2	0.0	15.0

(a) 3-2   **(b)** 4-1   **(c)** 5-2

(d) Simulation   **(e)** Simulation   **(f)** Simulation
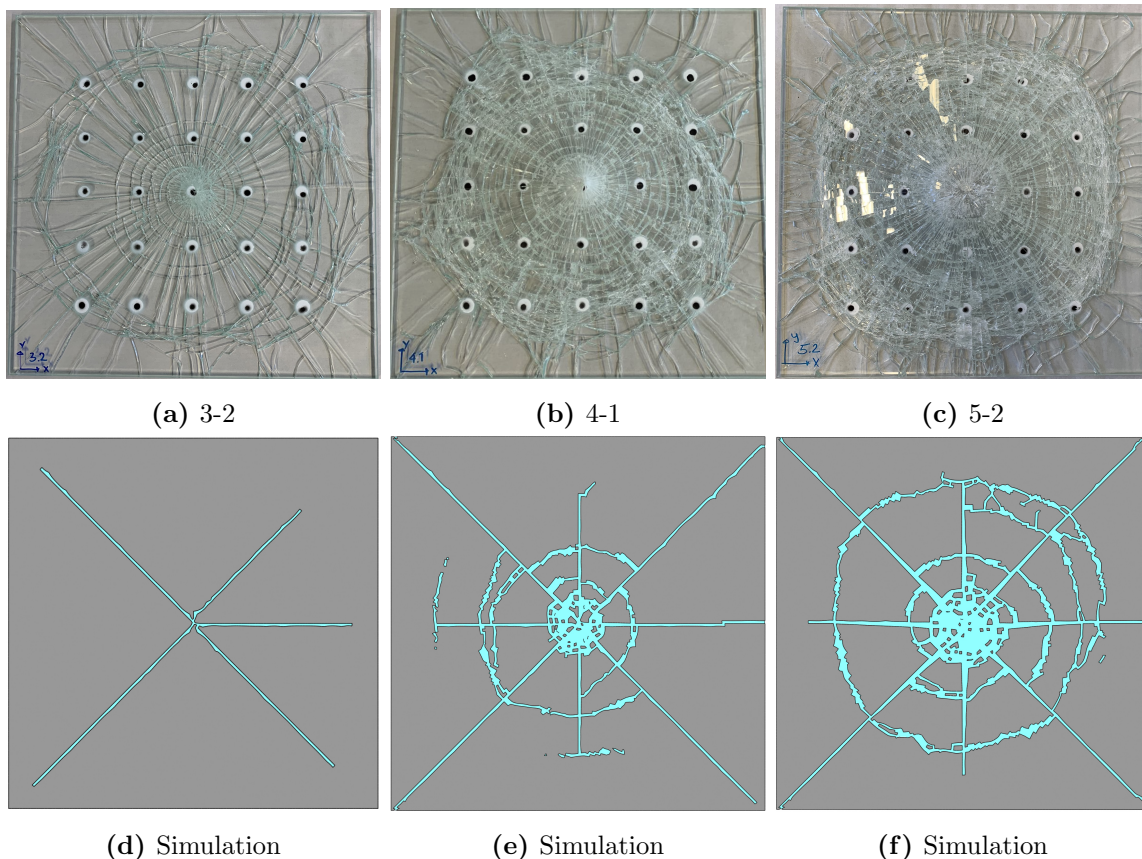
Figure 5.11: Final fracture state in the experiments and numerical simulations. (a)-(d) corresponds to impact velocity of 2.4 m/s, (b)-(e) to 5.8 m/s and (c)-(f) to 9.9 m/s.

5.6 Stress softening and material damping

The Brittle Cracking model was thoroughly investigated in Chapter 4. A small factorial design was developed to further investigate how the Brittle Cracking model can influence the laminated glass model. Motivated by the work of Pelfrene et al. [22] the effect of stress softening, material damping and mesh size is investigated. The factorial designs in Sections 5.3 and 5.4 used the minimum fracture energy criterion in Equation 4.1, referred to as Fast fracture in the following, and a small amount of stiffness dependent Rayleigh damping, $\beta = 1.7 \cdot 10^{-7}$. The material damping was added in an attempt to mitigate unwanted stress waves caused by Brittle Failure. From the industrial perspective, where efficiency is important, it is of interest whether or not the inclusion of stress softening in the Brittle Cracking model is more efficient than material damping.

The Brittle Cracking model interprets the elastic strain energy in an element as part of the fracture energy. The stress softening used in the factorial design is calculated by using the minimum fracture energy from Equation 4.1 multiplied by a factor of 1.5. The failure displacement, u_f, is adjusted according to Figure 4.1a. The numerical input, factors and levels are presented in Table 5.6.

Table 5.6: Numerical parameters in the Brittle Cracking laminated glass factorial design.

Level	Mesh	Stress model	Glass damping
1	3mm-2mm-1	Softening	Zero
2	2mm-2mm-1	Fast fracture	Damping: $\beta = 1.7 \cdot 10^{-7}$

The results are presented in Figure 5.12 and numerical values are found in Table C.5 in Appendix C. Note that the Base Model, which the mean deviation is calculated from, predicted the lowest HIC value. The main effects are summarized as follow.

- The model is insensitive to Mesh.

- The Stress model is an important factor. Fast fracture reduces HIC.

- The model is insensitive to Damping.

The key interaction effects are listed below.

- Glass damping interacts with Mesh. The effects of Damping is opposite for the two meshes. Zero Damping is negative for the 3mm-2mm-1 Mesh and Damping is positive for 2mm-2mm-1 Mesh.

- Adding material damping to Fast fracture is positive, while a negative effect is found for Softening.

It appears that a softening behaviour where the fracture energy is multiplied by a factor of 1.5 is too high. Fractures are not fast enough due to tension softening, and the stiffness of the laminated glass is increased. The interaction effect between Mesh and Glass damping is inconsistent, and any conclusion on this effect is hard to draw. The material damping in glass appears to have a negligible effect on numerical performance. As expected, material damping in glass seems to have a positive effect on Fast fracture since this criterion could introduce stress waves in neighbouring elements when erosion occurs. The limited number of simulations necessitates that the results are interpreted with caution, but should indicate that material damping in glass may not be required. The computational cost of adding material damping is extremely high and should be avoided if efficiency is important [57]. The detrimental effect of material damping is demonstrated by the 2mm-2mm-1 mesh, where the average computational time with material damping was 7.8 hours and without was 2 hours on 24 CPUs.
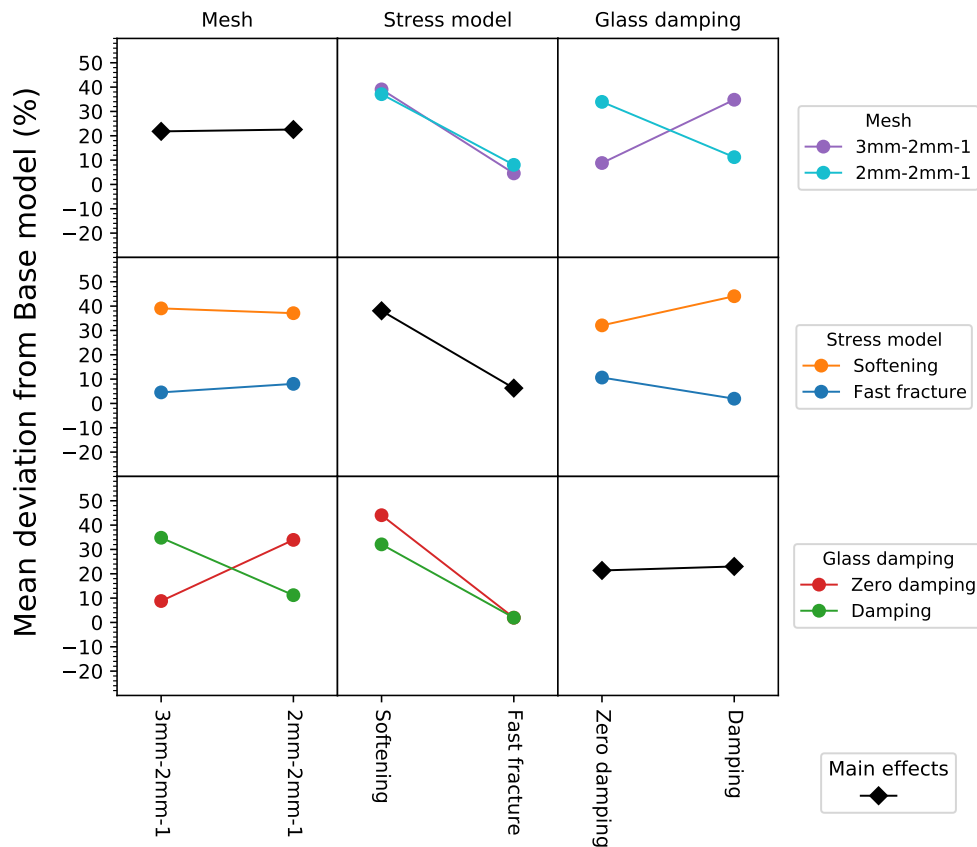
Figure 5.12: Performance measured in terms of HIC_{15}. The Base Model is 3mm-2mm-1, Fast fracture and damping, where each term corresponds to a level in Table 5.6.

5.7 Quasi-static punch test

The best performing numerical model from Section 5.4 was used to simulate the quasi-static test described in Section 2.2. The best performing model is referred to as Radial Cuts-3mm-2mm-1 and the performance of the model in the dynamic simulations is shown in Figure 5.9. The Mises plasticity PVB model was modified to not include the strain rate-dependency, such that the quasi-static simulation could be time-scaled. Only the stress versus equivalent plastic strain curve for 0.0 s^{-1} strain rate in Figure 3.3 was included in the PVB model.

The impactor was prescribed a constant velocity during the simulation instead of the initial velocity as a predefined field. The mass added to the impactor was removed such that there was no kinetic energy added to the system from the impactor. The simulations needed to be time-scaled since the duration of the quasi-static tests was around 15 minutes, which is not feasible in an explicit analysis. In order to avoid inertia forces, the impactor was accelerated to its constant velocity by using a smooth step in the initial 20% of the run time. An impactor velocity of 500 mm/s was found to give the most efficient simulations in terms of run time while still keeping the kinetic energy low compared to the total energy. The simulations can thus be considered as quasi-static.

Force versus displacement history from the simulation is plotted together with experimental data in Figure 5.13. The deformed shape of the glass pane at 24 mm impactor displacement is shown in Figure 5.14. Large deformations in the PVB interlayer were observed in the zones where the glass elements had eroded for large impactor displacement. The first fracture was observed at 2.59 mm impactor displacement and the corresponding load was 2.43 kN.

(a) Force versus displacement

(b) Force versus displacement
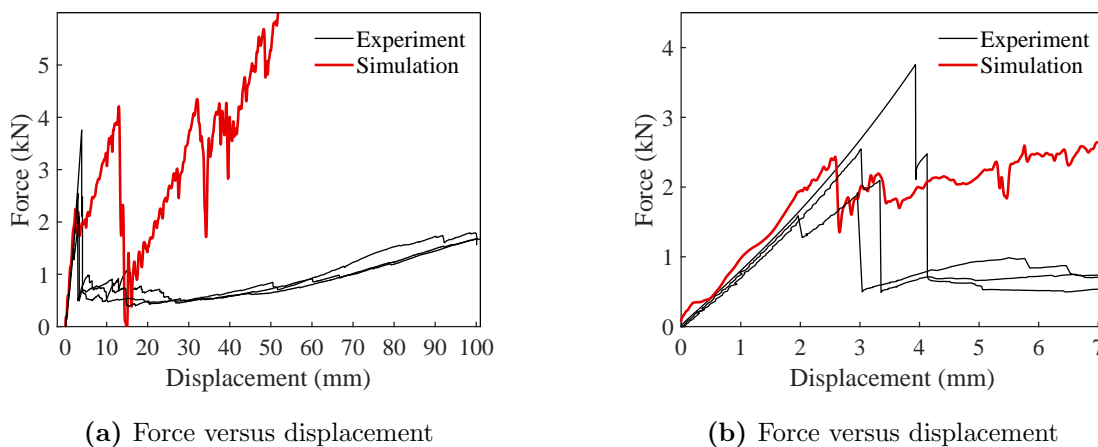
Figure 5.13: Force versus displacement from the simulation of quasi-static tests on laminated glass compared with experimental results. The complete test in (a) and the first 7 mm of displacement in (b).

<div align="center">

(a) Lower view   **(b)** Upper view

</div>
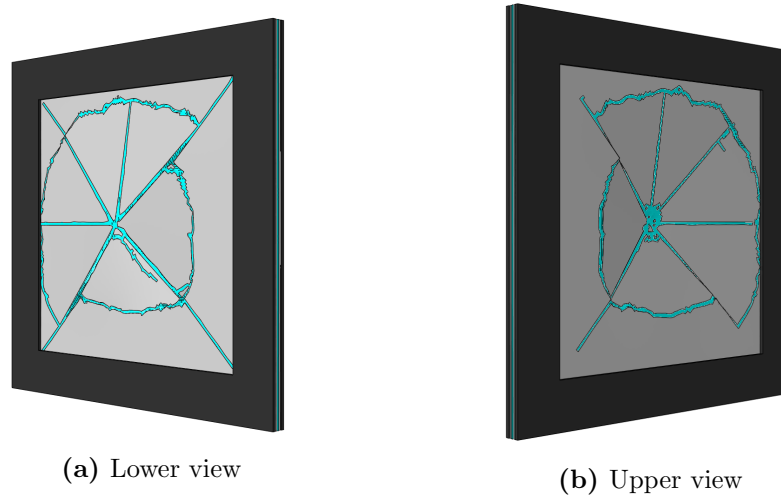
Figure 5.14: Deformed shape from quasi-static simulation at 24 mm impactor displacement.

It is clear from Figure 5.13b that the numerical model is able to simulate a behaviour which is similar to the experimental behaviour up until fracture. The load at first failure corresponds well with the experiments, but the post-fracture behaviour deviates. The numerical model is not able to simulate the sudden drop in force after the first glass failure. This is possibly caused by a slow fracture growth, as also seen in the previous dynamic simulations. Radial fractures start to grow after fracture initiation in glass pane centre at 2.59 mm displacement. The circumferential fractures, as seen in Figure 5.14, develops between 13 and 15 mm of impactor displacement. There is also a large drop in the force within this displacement interval, as seen in Figure 5.13a. The force drops to the same level as in the experiments before it increases again with a significantly higher gradient than in the experiments. It is believed that this is caused by too few fractures. The glass is fragmented into large and few pieces, and further deformation will be concentrated in zones of the interlayer where the neighbouring glass elements have eroded. Since the fragments are few and large, compared to the experiment, the deformation is concentrated in small fractions of the interlayer. The behaviour will hence be much stiffer than in the experiments, where the glass fragmented into many small pieces and the whole interlayer was working actively as a membrane. It is important to highlight that the simulation was performed without a delamination criterion between the glass and the interlayer. Such a criterion could have softened the behaviour of the laminate by allowing more of the interlayer to deform.

Figures 5.9a and 5.9c shows the fracture pattern from the dynamic simulation on the same numerical model as in the quasi-static simulation. Figures 5.9a, 5.9c and 5.14 has approximately equal impactor displacement. As seen in the figures, the quasi-static simulation deviates from the dynamic simulations by having less eroded elements in the top pane around the impactor. The fracture pattern also consists of larger pieces in the quasi-static simulation. As described in Section 2.2, there was observed less fragmentation in the quasi-static experiments compared to the dynamic experiments.

6. Numerical work - Case Studies

A series of case studies were performed in order to investigate the performance of the previously developed numerical model when exposed to different load scenarios.

6.1 Head impact on laminated glass
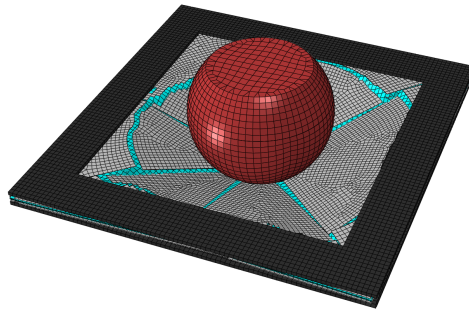
Figure 6.1: Head impact on laminated glass.

A commonly used numerical headform from the industry was used to simulate head impact on laminated glass. The headform is calibrated against a human head, and acceleration measurements inside the headform should be similar to what a real human will experience during a head impact. The mass of the headform is 4.5 kg and should be similar to an adult human head.

The numerical model for the 400 × 400 × 9.1 mm laminated glass plate with 5mm circular free glass mesh as developed in Chapter 5 was used. The following parameters were used in the Brittle Cracking model: Critical stress = 118 MPa, fracture energy = 0.59 N/mm, Brittle Failure = 0.01 mm. The simulation was run with the same impact velocity, 11.1 m/s ($\approx$ 40 km/h), as used in Euro NCAP tests [58]. The headform impacted the glass with a 90-degree impact angle. A general contact algorithm between the glass and the head form was used.

The results from the case study is presented as fracture patterns shown in Figure D.1 In Appendix D, acceleration of the headform during the impact shown in Figure D.2 in Appendix D, and the corresponding HIC_{15} value, which is 1521 $g^{2.5}$s. The numerical model of the head impact is shown in Figure 6.1.

It is observed from Figure D.1 in Appendix D that radial fractures in both top and bottom glass pane reaches the edge of the glass. This behaviour is more in accordance with the

experiments, where all initial radial fractures reached the glass edge. Fewer eroded elements were observed in the centre of the top plate than in the simulation with a rigid impactor in Section 5. It is believed that a softer headform will distribute the impact load over a larger region compared to a rigid impactor. Fewer elements will hence fail in the centre of the plate. As a consequence, the unloading of the plate just after the element erosion will not be seen. The continuous contact between the glass and the headform will again lead to continuously loading of the plate and most likely faster fracture growth.

The fracture patterns in Figure D.1 in Appendix D looks qualitatively good. The general trends with initially radial fractures followed by circumferential fractures are the same as might be expected from an experiment. A HIC_{15} value of 1521 $g^{2.5}$s will give a brown rating in a Euro NCAP head impact test, [58], which is the second worst rating. Head impact at 40 km/h on every location on a windshield, which is more than 165 mm from the supporting frame, shall give a HIC_{15} value less than 650 $g^{2.5}$s. A windshield is less stiff than the laminated glass used in this thesis because of thickness, size and boundary conditions. A poor rating on this type of laminated glass is plausible since it is far stiffer than a regular automobile windshield.

6.2   Head impact on laminated windshield
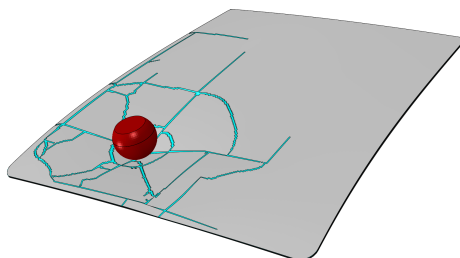
Figure 6.2: Head impact on a laminated windshield.

A case study was performed on a numerical model with geometry and dimensions similar to an automotive windshield. The laminated windshield had a doubly curved geometry with an approximate size 1490 mm × 1250 mm, and a total thickness of 4.5 mm. The dimensions are similar to the windshield used in the numerical and experimental studies conducted by Evensen and Rudshaug [47]. The laminate consisted of one 1.6 mm thick glass layer faced towards the coupe, a 0.8 mm thick PVB interlayer and a 2.1 mm thick glass layer faced towards the surroundings. The glass dimensions can be shown in Figures D.3 and D.4 in Appendix D. The numerical model with headform and windshield is shown in Figure 6.2.

The glass layers were modelled with shell elements, and the PVB interlayer was modelled with one volume element over the thickness. The mesh was structured and was not made to trigger any specific fracture pattern. Simulations with two different meshes were run, one with 5 mm glass elements and one with 8 mm glass mesh. The Brittle Cracking material parameters were customized for each mesh, and the numerical values are presented in Table 6.1. The PVB interlayer was modelled with the strain rate-dependent Mises plasticity model used in Chapter 5. Tie constraints were used between the glass and the interlayer. The windshield was supported by a 4 mm high and 30 mm wide rubber band. A tie constraint was used between the inner glass and the rubber support because windshields are glued to the supporting metal frame in real-life use. The rubber band is meant to model the glue, and the tie constraint is meant to model the adhesion in the glue. The lower side of the rubber band is fixed in all directions.

Table 6.1: Element dimensions and Brittle Cracking parameters from simulations of head impact on windshield.

	Mesh 1	Mesh 2
Glass element dimensions	$\approx 8 \times 8$ mm^2	$\approx 5 \times 5$ mm^2
PVB interlayer element dimensions	$\approx 8 \times 8 \times 0.8$ mm^3	$\approx 2.5 \times 2.5 \times 0.8$ mm^3
Critical stress	118 MPa	118 MPa
Fracture energy	0.944 N/mm	0.590 N/mm
Failure displacement	0.016 mm	0.010 mm

The numerical headform described in Section 6.1 was used in the simulations. Six different impact targets were defined and are shown in Figure D.5 in Appendix D. Simulations were run with an impact velocity of 11.1 m/s and 90-degree impact angle on these targets. Note that the impact angle differs from the Euro NCAP test protocol, [58], where the angle should be 65 ± 2 degrees relative to the ground reference line. A 90-degree impact angle relative to the windshield was selected since no ground reference line was defined relative to the windshield. General contact was used between the glass and the impactor. In addition to the simulations with the headform, one simulation on Target Position 1 with Mesh 2 was performed with a rigid impactor. The rigid impactor had the same geometry and mass as the headform, but was modelled as discrete rigid.

The estimated HIC$_{15}$ values from the simulations are shown in Table 6.2. Fracture patterns and acceleration versus time plots are shown in Figures D.6 - D.24 in Appendix D. The fracture patterns in the outer glass from simulations on Target Position 1 are additionally shown in Figure 6.3. The simulations were run for 30 ms and the fracture patterns are taken from the end of the simulation. A CFC method [50] was used to filter the numerical results in the acceleration versus time plots. The computational time with Mesh 1 was in average 2.1 hours and 48 hours with Mesh 2. All simulations were run with 4 CPUs on the same

computer.

Table 6.2: HIC_{15} estimations from simulations of head impact on different target positions.

Target position	HIC_{15} $(g^{2.5}s)$		
	Mesh 1 Headform	Mesh 2 Headform	Mesh 2 Rigid
1	286	346	286
2	262	389	
3	272	366	
4	346	404	
5	307	387	
6	311	378	

(a) Mesh 1 - Headform   (b) Mesh 2 - Headform   (c) Mesh 2 - Rigid
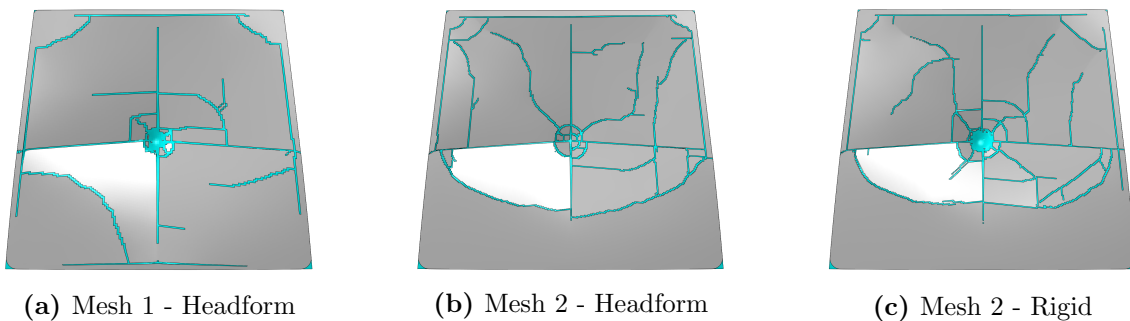
Figure 6.3: Fracture patterns from head impact simulations on target position 1.

Simulations with both meshes show the same general trends as observed in previous simulations. There are in general more fractures in simulations with Mesh 2 than Mesh 1. All simulations with Mesh 1 had an area with eroded elements where the headform had contacted the glass. This was not the case with Mesh 2, and it can thus be argued that simulations with Mesh 2 show a more realistic fracture pattern. There are some deviations between the estimated HIC_{15} values from the different meshes. The same deviations are also seen in the acceleration versus time plots in Appendix D.2, which the HIC_{15} values are obtained from. In general, simulations with Mesh 2 estimates a higher HIC_{15} than simulations with Mesh 1. It might be expected that larger elements would result in a stiffer behaviour and thus a higher HIC_{15}. It is believed that the erosion of all the glass elements in the contact zone in simulations with Mesh 1 causes the lower HIC_{15} values. Verifying the actual HIC_{15} values are difficult without performing experimental tests.

There is no consistency in which target positions that have the lowest HIC_{15} value between the two meshes, as shown in Table 6.2. Target positions closer to the boundaries seems to have a higher HIC_{15} value in both meshes. This is plausible since the windshield is stiffer in these regions. All the estimated HIC_{15} values are below Euro NCAP's requirement for automobile windshields. In a real car, the suspensions and the elastic chassis will allow the

boundary of the windshield to move. The HIC_{15} values might be even lower in head impact tests on a windshield mounted on a car.

The fracture patterns from simulations with both rigid and elastic imapctor on Target Position 1 are very similar. The difference is the area around the impact target, where excessive erosion occurs with a rigid impactor. The HIC_{15} value is also lower with a rigid impactor. This might support the argument as to why HIC_{15} estimations from Mesh 2 is higher than Mesh 1, where the major difference was the erosion of elements around the impact target.

Several combined numerical and experimental studies have been performed on head impacts on laminated automobile windshields. Alter et al. [11] used a non-local failure criterion, while Gao et al. [26] and Wang et al. [53] used an intrinsic cohesive zone approach to model the failure of glass. There are deviations in windshield geometry, headform geometry, impact velocity and boundary conditions between the simulations in this thesis and the mentioned studies. Direct comparison is therefore not possible.

The acceleration versus time curves from the experiments in the literature have one or two high-magnitude, short-duration peaks followed by a long-duration peak with lower magnitude. The same peaks are recognized in the idealized behaviour shown in Figure 1.2. The same trends are seen in the simulations in this thesis, but the second long-duration peaks are in general somewhat larger in magnitude than in the experiments from the literature. The interlayer is the only load-carrying component in this phase of the impact in the idealized behaviour. The slow fracture growth in the simulation will also cause the glass to contribute during this phase of the impact, and the behaviour is therefore likely to be too rigid. The simulations from the literature seem to reproduce the experimental behaviour better. This might be caused by the differences in the glass failure model. It is important to highlight that there are several differences between the simulations in this thesis and the experiments in the literature. The fracture patterns from the simulations in this thesis looks similar to the fracture patterns from the simulation in the study done by Alter et al. Gao et al. and Wang et al. used a different meshing technique with elements oriented in a circular pattern around the impact target. They obtained fracture patterns with several radial and circumferential fractures, which was more in line with their experiments.

The model is able to simulate the general behaviour of head impacts on laminated windshields, but the numerical results can not be verified without experimental tests. Choosing a mesh similar to Mesh 2 instead of Mesh 1 will give a more realistic fracture pattern, but it will also require a significant increase in the computational cost. This case study also shows the difference between using a soft elastic headform as impactor instead of a rigid one. The problem with excessive element erosion around the impact target may be overcome by using a soft elastic impactor when the mesh is sufficiently refined.

6.3 Blast load on laminated glass

A simulation with a blast load was performed in order to investigate the versatility of the developed numerical model. A blast load is caused by a shock wave from an explosion hitting a structure. It is recognized as a rapid increase in pressure in a very short period of time followed by a decay in pressure. In an idealized blast load, the pressure increases instantaneously from the atmospheric pressure, P_0, to the peak reflected overpressure, P_r. The pressure then decays towards P_0. This phase is called the positive phase of the blast load. After the pressure decays to P_0, the pressure drops below the atmospheric pressure before it again increase to P_0. This phase is called the negative phase of the blast load, [15].

The blast load in the simulation was modelled as a time-dependent pressure load that followed a Friedlander curve with the same parameters used in the studies conducted by Osnes et al. [25], which was fitted from experimental data. The blast had a maximum reflected overpressure of 237.7 KPa and 21.09 ms duration of the positive phase. The complete time versus pressure data are presented in Table D.1 in Appendix D. The Friedlander curve only describes the positive phase of a blast load. There exist more advanced methods to simulate blast loads, which also includes the negative phase and fluid-structure interaction. It was chosen to only run the simulation with the Friedlander curve, because it can be applied easily to the existing numerical model.

The blast load was applied to the side of the glass which will be referred to as the backside. A different fracture pattern than in the impact simulations may be expected, since the blast load will load the glass in a different way. The glass was therefore modelled with 5 mm shell elements and structured mesh, in order to not trigger the fracture in an unrealistic direction. The PVB interlayer and the rubber band at the support were modelled in the same way as in Section 6.1. All the material parameters were equal, including the parameters in the Brittle Cracking model.

The results from the blast load simulation are presented as the development of fractures in the front- and backside glass in Figure 6.4. The fractures in the front glass developed to the situation seen in Figure 6.4a in 0.30 ms. The development of fractures in the back glass was slower. The maximum midpoint displacement was 50.1 mm at 5.6 ms.

Osnes et al. [25] performed simulations with the same setup and the same pressure versus time curve as in the blast load simulation in this thesis and compared the results with experimental tests. Osnes et al. used a node-splitting technique to simulate the glass failure and modelled the glass with 4 mm × 4 mm × 3.8 mm 40-node quadratic interpolated pen-

(a) t = 1.05 ms   **(b)** t = 4.22 ms   **(c)** t = 21.09 ms

(d) t = 1.05 ms   **(e)** t = 4.22 ms   **(f)** t = 21.09 ms
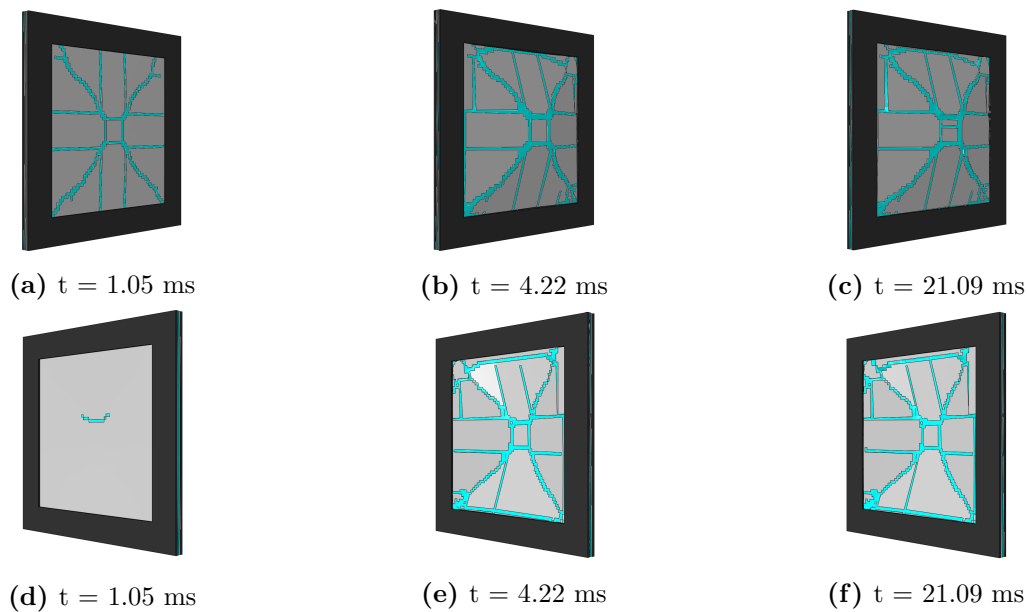
Figure 6.4: Fracture development during the blast load. Frontside glass pane in (a)-(c) and backside glass pane in (d)-(f).

tahedron elements. The node-splitting simulation had a maximum midpoint displacement of around 90 mm at 6 ms. A midpoint displacement of above 120 mm was observed in the experiment.

The fracture initiates at around the same time in both the node-splitting and the element erosion simulation. The post-failure behaviour is on the other hand different. It is seen that there are a lot more fractures with node-splitting than in with element erosion. There are almost no changes in the fracture pattern in the element erosion simulation after 3 ms, while there is a significant development of fragments between 3 ms and 6 ms in the node-splitting simulation. Too large and too few fragments in the element erosion simulations will lead to a too stiff behaviour, which might explain why there is a lower midpoint displacement.

The interlayer deformation will be localized in the zones where the neighbouring glass elements have eroded. As seen from Figure 6.4, these zones work like hinges and the laminated glass gets a trapezoidal-shaped deformation pattern. This will give an inaccurate estimation of displacement of most points on the glass when it is known that the laminated glass gets a bell-shaped deformation pattern in the experiment. The midpoint is most likely one of the points where the displacement is underestimated.

The simulation with element erosion is able to catch the general trends in a blast load experiment. The fracture initiates at approximately the same time as in the experiment and fractures along the diagonal develops quickly. However, the laminated glass will get a too stiff behaviour due to fewer fractures and fragments.

7. General discussion

The main effort in this thesis has been to explore the capabilities of using commercially available tools in the finite element (FE) code Abaqus to model the behaviour of glass exposed to impact loading. The experiments gave valuable information about typical failure modes in glass. Low-velocity impact tests and quasi-static punch tests were performed. Performing experimental testing on glass is challenging. The stochastic fracture strength of glass will require a large number of repetitions of each test in order to perform a statistical analysis of the results. The glass is additionally sensitive to the experimental setup. Smaller variations in the response for increasing impact velocities were observed for the laminated glass, while opposite observations were made on the monolithic glass. Verification of these observations by statistical analysis could be valuable knowledge in the design process of windshields and should be a topic for further work.

The experiments and the simulations showed that the PVB interlayer provides the laminated glass valuable properties in the post-fracture phase. The PVB interlayer retains glass shards and maintains a load-carrying capacity in the post-fracture phase, while the monolithic glass experience complete failure and produce dangerous shards. Laminated glass is therefore suited for applications where both the transparency of glass and energy-absorbing properties are needed.

Available FE tools and techniques are increasing every year. Industry-needs and scientific curiosity drive the progress and evolution of new numerical methods. Therefore, not only is the user required to be competent on the use of a FE software, but must also know which software or techniques that are appropriate for a given problem. The numerical work on laminated glass in Chapter 5 was based on experimental tests performed on relatively thick laminated glass with a fully clamped boundary. The exposed non-clamped area is additionally small compared to full-scale windshields. The industry needs efficient and accurate numerical tools to simulate head impact on windshields. Therefore, the question is whether or not the numerical models developed to simulate the experimental setup in this thesis applies to full-scale-windshields. The experimental setup appears to provide different numerical challenges than the low-velocity impact on a full-scale windshield. Since the thesis does not include experimental low-velocity impact tests on windshields, it is hard to verify whether or not the developed model performs better on a more flexible windshield. It is believed that a full-scale windshield is more flexible because of the boundary conditions, component size, plate thickness, and type of impactor used.

The experimental test setup for the dynamic low-velocity impact tests was chosen because it allowed for repeatable and predictable testing in a well-defined system. A drawback with the drop tower setup is the limitation on the size of the test component. Since the area spanned by a full-scale windshield is significantly larger compared to the 300×300 mm^2 area in the clamping frame. When the difference in the spanned impact area is large, the discrepancy in stiffness could be alleviated by other measures. The numerical work on windshields in Section 6.2 show promising results in combination with the developed model. Use of thinner laminated glass and a soft impactor appears to alleviate some of the numerical challenges encountered in Chapter 5.

Modelling failure in a brittle material such as glass with element erosion is a challenging task. Element erosion removes the failed element such that the crack width is equal to the element size. Since elements are removed from the simulation, the ability to transfer compression forces is lost. The experiments could indicate that the compression forces contribute to limiting the rotation between glass shards and that this effect drives further fracturing. Severe fracturing and fragmentation are vital for the post-fracture phase in simulations. However, element erosion may lead to nonphysical behaviour because of excessive element erosion around the impact zone. On the other hand, if there were few fractures, the behaviour in the simulations was very stiff compared to the physical behaviour observed in the experimental work. Hence, the challenge is to find a balance between creating fractures and avoiding excessive element erosion.

The mesh is an important parameter in simulations of glass exposed to low-velocity impacts. Circular oriented glass mesh resulted in a faster fracture growth and yielded more realistic fracture patterns. Creating a glass mesh which triggers a correct fracture pattern requires knowledge about the fracture pattern. Prediction of the fracture pattern in cases with complex geometry and boundary conditions can be a challenging task. A simulation method which requires precise knowledge of the fracture pattern to ensure accurate results is not optimal. Choosing an interlayer mesh which has similar or smaller sized elements than the glass mesh was found to be important for obtaining proper results.

The numerical work on laminated glass in Chapter 5 highlighted several challenges in modelling failure in laminated glass. As explained earlier, the clamped boundary, component size, thickness of the laminated glass and aluminium impactor contributes to a stiff experimental setup, which is a tremendous numerical challenge since the fracturing of the glass should occur rapidly. Several techniques were attempted to alleviate the challenge of slow fracture growth in the numerical simulations. These include mesh refinement of both the glass and PVB. Turning off element erosion in the impacted side of the laminate to allow for compression forces. The material model, Brittle Cracking, for glass was also investigated. None of the numerical techniques were able to alleviate the problem of slow fracture

growth. However, the problem of excessive element erosion in the impact zone was partly avoided. The Brittle Cracking model combined with element erosion should be verified against full-scale windshield experiments to see if it performs better on a softer component. Novel methods like cohesive zone modelling, node-splitting and a non-local failure criterion in glass could represent the future of modelling fracture in glass. As of today, there are some challenges and drawbacks with using the novel methods on an industrial scale. They are often computationally costly and require experimental verification to be calibrated correctly. The element erosion method combined with a local failure criterion is easy-to-implement and computationally efficient, which can explain why the industry prefers it as of today.

The head injury criterion (HIC) is the standard measurement used by Euro NCAP for evaluating pedestrian and passenger safety in new cars. Therefore, the automotive industry must be able to predict HIC for low-velocity impacts on windshields to pass Euro NCAP evaluations and further improve the current design. Hence, this thesis has chosen to use HIC as the primary measurement when comparing results between numerical simulations and experiments. HIC includes both the average magnitude of the acceleration of the impactor and the duration of the impact. As seen in Equation 1.1, the average acceleration is raised to the power of 2.5. The error in HIC will also be raised to the power of 2.5 relative to the error in acceleration measurements. Small variations in accelerations may lead to large differences in predicted HIC values. Another important factor that should be considered when using HIC as a measurement is that it does not describe the physical mechanism of laminated glass failure. Therefore, sound engineering judgement should be used to verify that the predicted HIC value stems from a proper physical description of the problem. It is believed that this is important to ensure not only accurate but also reliable models.

Delamination between the glass and the interlayer is a part of the structural behaviour of laminated glass. The use of element erosion allows the interlayer elements to deform without restrictions in the areas with eroded glass elements. A delamination criterion is therefore believed to be less important when element erosion is used. It is still a possibility for more accurate results in some of the simulations performed in this thesis if a delamination criterion was included. A delamination criterion is believed to be more important in situations with large deformations, such as in the blast load case study and the simulation of the quasi-static experiment.

The material properties of glass have been considered as homogeneously distributed in order to limit the number of parameters in the numerical studies. This is a major simplification. The fracture strength of glass is stochastic and is determined by size, density and orientation of microscopic surface flaws. It is easier to compare different simulation results when the stochastic properties of glass are excluded from the analysis. The changes in the results from adjusting one parameter can thus only be caused by the parameter itself and not by stochas-

tic material behaviour. The strain rate-dependency of the glass strength is not considered in the simulations either. The strain rates in the different dynamic tests are considered to be within the same range, while there should be expected a difference in the strength of significance between the dynamic tests and the quasi-static tests. Since each test was only repeated three times, it is hard to validate this difference and the actual glass strength.

As of today, element erosion combined with local failure criteria is the most efficient way of modelling fracture in laminated glass for industrial applications. Novel methods are often limited by high computational costs and advanced material calibration. New, accurate and efficient numerical tools are likely to become available on an industrial-scale, as the computational power increases and the research on glass develops.

8. Concluding Remarks

The work conducted in this thesis consists of both experimental and numerical work and is summarized as follows.

- **Dynamic experimental tests on monolithic and laminated glass**
  Low-velocity impact tests in a drop-tower were performed on monolithic and laminated glass. All the tests with glass failure showed the same fracture behaviour with initial radial fractures from the centre followed by circumferential fractures. Increased impact velocity caused more fragmentation of the glass. The fragmentation of the laminated glass was more severe compared to the monolithic glass.

- **Quasi-static experimental tests on laminated glass**
  Three quasi-static punch tests were performed on laminated glass, and the fractures initiated in the centre of the glass pane and showed similar behaviour as in the dynamic tests. The following three phases can describe the quasi-static tests: no fractures, fractures in one glass pane and fractures in both glass pane. Bending of the glass panes is the dominating deformation mechanism in the first two phases, while membrane stretching of the interlayer is dominating the third phase. Large deviations in the load at first fracture between the three tests were observed.

- **3D-DIC and displacement measurements**
  3D-DIC and digital cameras were used to track optical targets on the glass panes during the dynamic and the quasi-static tests. The impactor displacement was also obtained from the force measurements in the dynamic tests, and from the testing machine in the quasi-static tests. Both methods yielded coinciding displacement results.

- **Finite element model and pre-fracture behaviour**
  A finite element model of the dynamic tests was developed. The glass was modelled as linear elastic without any failure criterion. Simulations were run with different impact velocities for both monolithic and laminated glass. The numerical results were compared with the pre-fracture phase in the dynamic tests and showed that the simulations were able to reproduce the pre-fracture behavior.

- **Simulations of low-velocity impact on monolithic glass**
  Glass failure was modelled with the built-in Brittle Cracking model in Abaqus. A factorial design study was performed where the influence of different input parameters in the Brittle Cracking model and mesh types were investigated. The mesh type had the largest influence on the results. A mesh with circular oriented elements was found to give the best results. Simulations with the Brittle Cracking model were able

to reproduce the general trend from the experiments with initially radial fractures followed by circumferential fractures. The fracture growth was found to be around 40 times slower in the simulations compared to the experiments. There were also fewer fractures in the simulations compared to the experiments.

- **Simulations of low-velocity impact on laminated glass**
  Factorial design studies on laminated glass were performed. Meshing had the most significant influence on the simulations. A circular oriented glass mesh gave the most realistic results. An interlayer mesh which has smaller or equally sized elements as the glass mesh was found to perform best. One element over the thickness in the interlayer mesh was found to be sufficient. A strain rate-dependent Mises plasticity model gave similar results to a non-linear viscoelastic model in the post-fracture phases and was more computationally efficient. A HIC_{15} value of 198 $g^{2.5}s$ was obtained from the best performing simulation with an impact velocity of 5.8 m/s, which is 16.2% higher than in the experiments.

- **Simulations of quasi-static punch test on laminated glass**
  Time scaled simulation of the quasi-static tests was performed. The first fracture initiated at around the same time as in the experiment, but slow fracture growth caused large deviations between the simulation and the experiments.

- **Case studies**
  Simulations of head impact on laminated glass, head impact on laminated automobile windshield and blast load on laminated glass were performed. The use of a soft head-form as impactor was found to give fewer eroded elements around the impact target in the head impact simulations. All predicted HIC_{15} values from the head impact simulations on the laminated windshield fulfilled Euro NCAPs requirement.

9. Further work

The following topics are suggested for further research.

- **Perform experimental tests on either windshields or more suitable setup**
  The experimental test setup in this thesis was significantly stiffer than in a typical head impact test on a laminated windshield. The experimental behaviour was found to be challenging to reproduce in the numerical simulations. Simulations with a soft head form as impactor on a laminated windshield showed promising results. The authors suggest performing a variety of experimental tests with a less stiff test setup for further verification of the developed numerical model.

- **Non-local failure criterion**
  The non-local failure criteria proposed by Alter et al. [11] and Pyttel et al. [30] seem to predict the fast fracture growth in glass better. Head impact simulations with a non-local failure criteria will better reproduce the rapid stiffness reduction of the glass after the initial fracture, and could provide better estimations of the HIC_{15} value. The authors suggest investigating the possibilities of implementing a non-local failure criterion in Abaqus.

- **Compare element erosion with node-splitting**
  Removing elements by using element erosion is a nonphysical approach to model a fracture. This is especially true for a brittle material such as glass, where a lot of fragmentation is expected. A node-splitting technique will better model the physical behaviour of a fracture. The authors suggest running simulations where node-splitting is utilized. Comparing the results from node-splitting simulations with element erosion simulations will give better knowledge about the limitations of using element erosion.

- **Include the stochastic behaviour and the strain rate-dependency of glass**
  Glass is a stochastic material and the strength is determined by the size, orientation and density of surface flaws. The strength is additionally strain rate-dependent. Including these two factors in the numerical model are necessary for simulating the correct behaviour of glass.

- **Study the material properties of the PVB interlayer**
  The material descriptions of the PVB interlayer used in this thesis are obtained from experiments on plain PVB. The lamination process of laminated glass may influence the material behaviour of the interlayer. Investigating the behaviour of interlayer material after the autoclave process may improve the material description and further provide more realistic simulations of laminated glass.

- **Delamination** Delamination between glass and interlayer is a part of the structural behaviour of laminated glass. The delamination is especially present for large deformations. A study of how delamination can be included efficiently in the numerical model is suggested.

Bibliography

[1] Euro NCAP. About Euro NCAP. https://www.euroncap.com/en/about-euro-ncap/, 2020. Accessed on 2020-03-30.

[2] Euro NCAP. The ratings explained. https://www.euroncap.com/en/vehicle-safety/the-ratings-explained/, 2020. Accessed on 2020-03-30.

[3] Euro NCAP. Assesment Protocol – Vulnerable Road User Protection, V10.0.2. https://www.euroncap.com/en/for-engineers/protocols/vulnerable-road-user-vru-protection/, 2019. Accessed on 2020-02-14.

[4] P. Prasad and H. Mertz. The Position of the United States Delegation to the ISO Working Group on the Use of HIC in the Automotive Environment. *SAE Technical Paper Series*, 1985.

[5] J. Christensen and C. Bastien. Nonlinear Optimization of Vehicle Safety Structures. *Butterworth-Heinemann*, 2006.

[6] H. S. Norville, K. W. King, and J. L. Swofford. Behavior and strength of laminated glass. *Journal of Engineering Mechanics, Vol. 124 Issue 1, Article 46*, 1998.

[7] J. Pelfrene, J. Kuntsche, S. Van Dam, W. Van Paepegem, and J. Schneider. Critical assessment of the post-breakage performance of blast loaded laminated glazing: Experiments and simulations. *International Journal of Impact Engineering, Vol. 88, pp. 61-71*, 2015.

[8] M. A. Samieian, D. Cormie, D. Smith, W. Wholey, B. R.K Blackman, J. P. Dear, and P. A. Hooper. Temperature effects on laminated glass at high rate. *International Journal of Impact Engineering, Vol. 111, pp. 177-186*, 2017.

[9] B. Liu, T. Xu, X. Xu, Y. Wang, Y. Sun, and Y. Li. Energy absorption mechanism of polyvinyl butyral laminated windshield subjected to head impact: Experiment and numerical simulations. *International Journal of Impact Engineering, Vol. 90, pp. 26-36*, 2015.

[10] M. Larcher, G. Solomos, F. Casadei, and N. Gebbeken. Experimental and numerical investigations of laminated glass subjected to blast loading. *International Journal of Impact Engineering, Vol. 39, pp. 42-50*, 2012.

[11] C. Alter, S. Kolling, and J. Schneider. An enhanced non-local failure criterion for laminated glass under low velocity impact. *International Journal of Impact Engineering, Vol. 109, pp. 342-353*, 2017.

[12] U. Keller and H. Mortelmans. Adhesion in Laminated Safety Glass – What makes it work? *Glass Processing Days, 13–16 June '99*, 1999.

[13] W. L. Beason and J. R. Morgan. Glass Failure Prediction Model. *Journal of Structural Engineering, Vol. 110 Issue 2, pp. 197-212*, 1984.

[14] D. Z. Yankelevsky. Strength prediction of annealed glass plates – A new model. *Engineering Structures, Vol. 79, pp. 244-255*, 2014.

[15] K. Osnes, T. Børvik, and O. S. Hopperstad. Testing and modelling of annealed float glass under quasi-static and dynamic loading. *Engineering Fracture Mechanics, Vol. 201, pp. 107-129*, 2018.

[16] P. D. Linz, P. A. Hooper, H. Arora, Y. Wang, D. Smith, B. Blackman, and J. P. Dear. Delamination properties of laminated glass windows subject to blast loading. *International Journal of Impact Engineering, Vol. 105, pp. 39-53*, 2017.

[17] P. A. Hooper, B. R. K. Blackman, and J. P. Dear. The mechanical behaviour of poly(vinyl butyral) at different strain magnitudes and strain rates. *Journal of Materials Science, Vol. 47, pp. 3564-3576*, 2012.

[18] M. Timmel, S. Kolling, P. Osterrieder, and P. A. Du Bois. A finite element model for impact simulation with laminated glass. *International Journal of Impact Engineering, Vol. 37, pp. 1456-1478*, 2007.

[19] J. Xu, Y. Li, B. Li, M. Zhu, and D. Ge. Experimental study on mechanical behavior of PVB laminated glass underquasi-static and dynamic loadings. *Composites Part B, Vol. 42, pp. 302–3080*, 2001.

[20] X. Zhang, H. Hao, and G. Ma. Parametric study of laminated glass window response to blast loads. *Engineering Structures, Vol. 56, pp. 1707–1717*, 2012.

[21] M. Teotia and R. K. Soni. Applications of finite element modelling in failure analysis of laminated glass composites: A review. *Engineering Failure Analysis, Vol. 94, pp. 412-437*, 2018.

[22] J. Pelfrene, S. Van Dam, R. Sevenois, F. Gilabert, and W. Van Paepegem. Fracture Simulation of Structural Glass by Element Deletion in Explicit FEM. *Challenging Glass 5 - Conference on Architectural and Structural Applications of Glass, Ghent University*, 2016.

[23] A. Hillerborg, M. Modéer, and P.-E. Petersson. Analysis of crack formation and crack growth in concrete by means of fracture mechanics and finite elements. *Cement and Concrete research. Vol. 6, pp. 773-782*, 1976.

[24] L. Olovsson, J. Limido, J.-L. Lacome, A. G. Hanssen, and J. Petit. Modeling fragmentation with new high order finite element technology and node splitting. *The European Physical Journal Conferences 94, Article 04050*, 2015.

[25] K. Osnes, J. K. Holmen, O. S. Hopperstad, and T. Børvik. Fracture and fragmentation of blast-loaded laminated glass: An experimental and numerical study. *International Journal of Impact Engineering, Vol. 132, Article 103334*, 2019.

[26] W. Gao, R. Wang, S. Chen, and M. Zang. An intrinsic cohesive zone approach for impact failure of windshield laminated glass subjected to a pedestrian headform. *International Journal of Impact Engineering, Vol. 126, pp. 147-159*, 2019.

[27] J. Xu, Y. Li, X. Chen, Y. Yan, D. Ge, M. Zhu, and B. Liu. Characteristics of windshield cracking upon low-speed impact: Numerical simulation based on the extended finite element method. *Computational Materials Science, Vol. 48, pp. 582-588*, 2010.

[28] Z. G. Yang, M. Y. Zang, and Y. L. Cheng. Simulation of impact fracture behavior of laminated glass based on DEM/FEM and cohesive model. *Strength of Materials, Vol. 51, pp. 520-533*, 2019.

[29] D. Wei, D. Li, and Z. Zhang. Simulation Study of Low-Velocity Impact on Polyvinyl Butyral Laminated Glass Based on the Combined TCK-JH2 Model. *Applied Science, Vol. 9, Article 3204*, 2019.

[30] T. Pyttel, H. Liebertz, and J. Cai. Failure criterion for laminated glass under impact loading and its application in finite element simulation. *International Journal of Impact Engineering, Vol. 38, pp. 252-263*, 2011.

[31] A. Haufe, R. Böhm, and A. Erhart. Novel Approach to Model Laminated Glass. *LS-DYNA Forum*, 2016.

[32] Livemore Software Technology. LS-DYNA R11 Keyword Manual Vol II. http://www.lstc.com/download/manuals, 2019. Accessed on 2020-05-19.

[33] K. Osnes, O. S. Hopperstad, and T. Børvik. Rate dependent fracture of monolithic and laminated glass: experiments and simulations. *Engineering Structures, Vol. 212, Article 110516*, 2020.

[34] J. Pelfrene, S. Van Dam, and W. Van Paepegem. Numerical analysis of the peel test for characterisation of interfacial debonding in laminated glass. *International Journal of Adhesion Adhesives, Vol. 62, pp. 146-153*, 2015.

[35] M. A. Samieian, D. Cormie, D. Smith, W. Wholey, B. Blackman, J. P. Dear, and P. A. Hooper. On the bonding between glass and PVB in laminated glass. *Engineering Fracture Mechanics, Vol. 214, pp. 504-519*, 2019.

[36] Z. Lei and M. Zang. An approach to combining 3D discrete and finite element methods based on penalty function method. *Computational Mechanics, Vol. 46, pp. 609–619*, 2010.

[37] S. Chen, M. Zang, D. Wang, Z. Zheng, and C. Zhao. Finite Element modelling of impact damage in polyvinyl butyral laminated glass. *Composite Structures, Vol. 138, pp. 1-11*, 2016.

[38] Dassault Systèmes Simulia Corp. Abaqus 2019. 2019.

[39] Instron. CEAST 9300-series Droptower Impact Systems, CEAST 9300 Series Specifications. https://www.instron.us/-/media/literature-library/products/2010/02/ceast-9300-series.pdf?la=en-US, 2009. Accessed on 2020-02-07.

[40] A. Reyes and T. Børvik. Low velocity impact on crash components with steel skins and polymer foam cores. *International Journal of Impact Engineering, Vol. 132, Article 103297*, 2019.

[41] E. Fagerholt. User Manual - eCorr - Digital Image Correlation Tool. https://www.ntnu.edu/kt/ecorr, 2017. Accessed on 2020-02-18.

[42] E. Fagerholt, T. Børvik, and O.S. Hopperstad. Measuring discontinuous displacement fields in cracked specimens using digital image correlation with mesh adaptation and crack-path optimization. *Optics and Lasers in Engineering, Vol. 51 Issue 3, pp. 299-310*, 2013.

[43] NS-EN 13541: Glass in building – Security glazing – Testing and classification of resistance against explosion pressure. 2012.

[44] J. S. Bergstrom and M. C. Boyce. Constitutive modeling of the time-dependent and cyclic loadingof elastomers and application to soft biological tissues. *Mechanics of Materials, Vol. 33, pp. 523–530*, 2001.

[45] J. Bergstrom. *Mechanics of Solid Polymers*. William Andrew, 2015.

[46] T. Grue and S. Kjernlie. Modeling of windshields subjected to impact loading. *Master thesis, Norwegian University of Science and Technology, Department of Structural Engineering*, 2018.

[47] J. Rudshaug and E. Evensen. Modelling of windshields subjected to quasi-static loading. *Master thesis, Norwegian University of Science and Technology, Department of Structural Engineering*, 2019.

[48] Dassault Systèmes Simulia Corp. A cracking model for concrete and other brittle materials. https://abaqus-docs.mit.edu/2017/English/SIMACAETHERefMap/simathe-c-cracking.htm, 2017. Accessed on 2020-02-12.

[49] Dassault Systèmes Simulia Corp. Cracking model for concrete. `https://abaqus-docs.mit.edu/2017/English/SIMACAEMATRefMap/simamat-c-cracking.htm`, 2017. Accessed on 2020-02-12.

[50] Meade, MATLAB Central File Exchange. Calculate Filter Coefficients for Phaseless, Low Pass, Butterworth Filter (compliant with SAE-J211). `https://www.mathworks.com/matlabcentral/fileexchange/61852-calculate-filter-coefficients-for-phaseless-low-pass-butterworth-filter-compliant-with-sae-j211`, 2020. Accessed on 2020-06-04.

[51] Dassault Systèmes Simulia Corp. User subroutine to define characteristic element length at a material point. `http://ivt-abaqusdoc.ivt.ntnu.no:2080/v6.14/books/sub/default.htm?startat=ch01s02asb11.html#sub-rtn-uexpucharlength`, 2014. Accessed on 2020-03-11.

[52] Y. Peng, J. Yang, C. Deck, and R. Willinger. Finite element modeling of crash test behavior for windshield laminated glass. *International Journal of Impact Engineering, Vol. 57, pp. 27-35*, 2013.

[53] D. Wang, S. Chen, W. Xu, and M. Zang. Numerical modelling of impact failure of an automotive windshield glazing subjected to a dummy pedestrian headform. *International Journal of Impact Engineering, Vol. 141, Article 103564*, 2020.

[54] Dassault Systèmes Simulia Corp. Contact controls for general contact in Abaqus/Explicit. `https://abaqus-docs.mit.edu/2017/English/SIMACAEITNRefMap/simaitn-c-contactcontrolsassign.htm`, 2017. Accessed on 2020-05-04.

[55] Dassault Systèmes Simulia Corp. About contact interactions. `https://abaqus-docs.mit.edu/2017/English/SIMACAEITNRefMap/simaitn-c-contactoverview.htm`, 2017. Accessed on 2020-06-06.

[56] S. Chen, M. Zang, D. Wang, S. Yoshimura, and T. Yamada. Numerical analysis of impact failure of automotive laminated glass: A review. *Composites Part B: Engineering, Vol. 122, pp. 47-60*, 2017.

[57] Dassault Systèmes Simulia Corp. Damping. `https://abaqus-docs.mit.edu/2017/English/SIMACAEKEYRefMap/simakey-r-damping.htm`, 2017. Accessed on 2020-05-5.

[58] Euro NCAP. Pedestrian Test Protocol, V8.5. `https://www.euroncap.com/en/for-engineers/protocols/vulnerable-road-user-vru-protection/`, 2018. Accessed on 2020-02-14.

A. Appendix: Experimental work
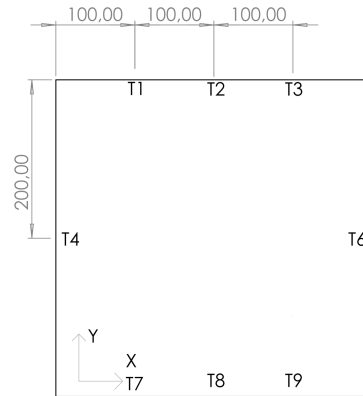
Figure A.1: Points on glass where the thickness was measured. Measurements are given in mm.
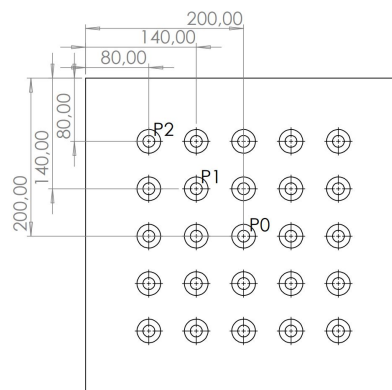
Figure A.2: Positions of optical targets. Measurements are given in mm.
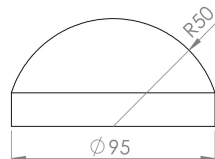
Figure A.3: Dimensions of the impactor nose used in the experimental tests. Measurements are given in mm.

Table A.1: Thickness measurements of glass in the points shown Figure (A.1).

Glass Type	Test #	T1 [mm]	T2 [mm]	T3 [mm]	T4 [mm]	T6 [mm]
Monolitic	1.1	3.80	3.79	3.80	3.81	3.81
Monolitic	1.2	3.81	3.81	3.79	3.81	3.79
Monolitic	1.3	3.81	3.80	3.80	3.81	3.79
Monolitic	2.1	3.81	3.80	3.80	3.81	3.81
Monolitic	2.2	3.80	3.80	3.80	3.81	3.81
Monolitic	2.3	3.81	3.81	3.81	3.81	3.80
Laminated	3.1	9.11	9.11	9.11	9.11	9.10
Laminated	3.2	9.10	9.11	9.10	9.10	9.10
Laminated	3.3	9.10	9.11	9.11	9.10	9.11
Laminated	3.4	9.10	9.10	9.12	9.10	9.10
Laminated	4.1	9.11	9.10	9.10	9.10	9.09
Laminated	4.2	9.09	9.09	9.09	9.09	9.08
Laminated	4.3	9.09	9.08	9.08	9.09	9.09
Laminated	5.1	9.10	9.09	9.09	9.08	9.09
Laminated	5.2	9.09	9.09	9.09	9.09	9.08
Glass type	Test #	T7 [mm]	T8 [mm]	T9 [mm]	Mean [mm]	Standard deviation, [mm]
Monolitic	1.1	3.80	3.79	3.80	3.800	0.0076
Monolitic	1.2	3.81	3.80	3.79	3.801	0.0099
Monolitic	1.3	3.81	3.80	3.79	3.801	0.0083
Monolitic	2.1	3.80	3.80	3.80	3.804	0.0052
Monolitic	2.2	3.80	3.80	3.80	3.803	0.0046
Monolitic	2.3	3.81	3.81	3.80	3.808	0.0046
Laminated	3.1	9.10	9.10	9.09	9.104	0.0074
Laminated	3.2	9.07	9.10	9.10	9.098	0.0117
Laminated	3.3	9.10	9.10	9.10	9.104	0.0052
Laminated	3.4	9.10	9.11	9.11	9.105	0.0076
Laminated	4.1	9.10	9.10	9.09	9.099	0.0064
Laminated	4.2	9.09	9.09	9.08	9.088	0.0046
Laminated	4.3	9.11	9.11	9.10	9.094	0.0119
Laminated	5.1	9.10	9.09	9.11	9.094	0.0092
Laminated	5.2	9.09	9.09	9.08	9.104	0.0119

Table A.2: Test series of glass.

Glass type	Test #	Prescribed velocity [m/s]	Measured velocity [m/s]	Fracture [Yes/No]
Monolitic	1.1	2.0	2.3999	Yes
Monolitic	1.2	2.0	2.4159	Yes
Monolitic	1.3	2.0	2.4014	Yes
Monolitic	2.1	4.0	4.2203	Yes
Monolitic	2.2	4.0	4.2218	Yes
Monolitic	2.3	4.0	4.2285	Yes
Laminated	3.1	2.0	2.4196	Yes
Laminated	3.2	2.0	2.4200	Yes
Laminated	3.3	2.0	No measurements	Yes
Laminated	3.4	2.0	2.4220	Yes
Laminated	4.1	6.0	5.8027	Yes
Laminated	4.2	6.0	5.7805	Yes
Laminated	4.3	6.0	5.7851	Yes
Laminated	5.1	1	1.7169	Yes (Only lower plate)
Laminated	5.2	0.77	1.6040	No
		0.90	1.6715	No
		0.95	1.6900	No
		1.0	1.7111	No
		1.2	1.8306	No
		10.0	9.8798	Yes

B. Appendix: Numerical work - Monolithic glass

B.1 Factorial design - Brittle Cracking and mesh
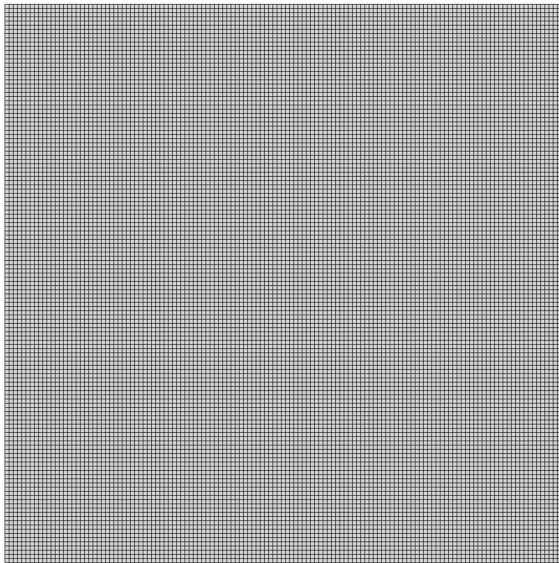
<div align="center">(a) 3 mm Structured mesh</div>
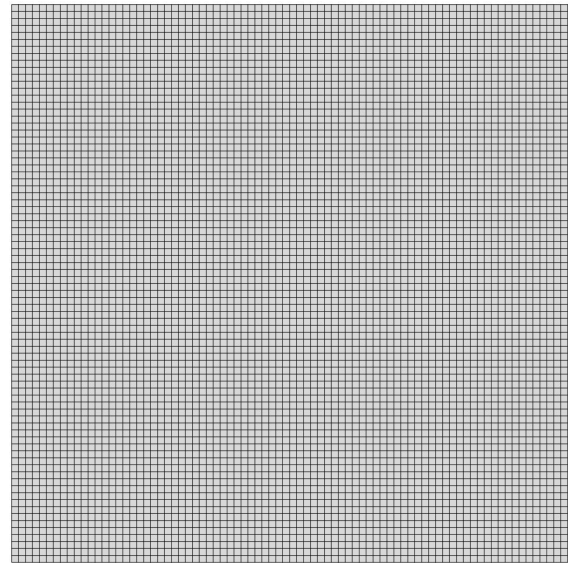
<div align="center">(b) 5 mm structured mesh</div>
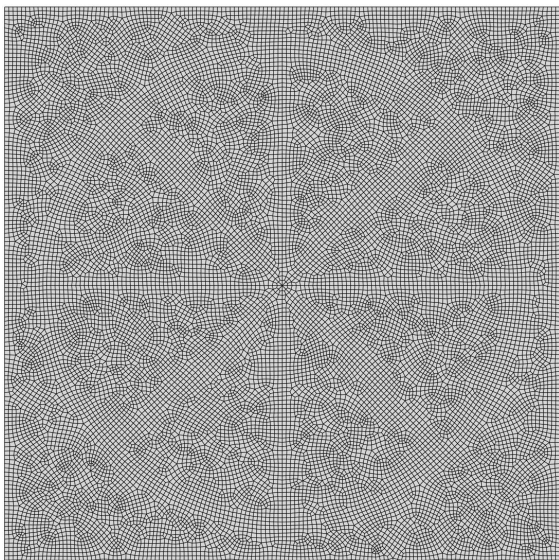
<div align="center">(c) 3 mm circular mesh</div>
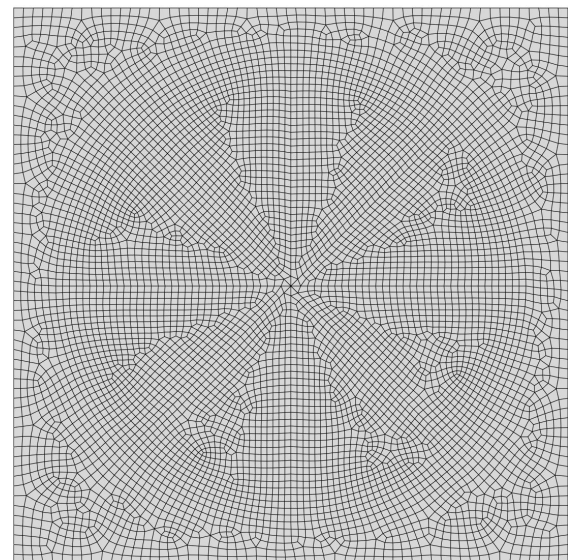
<div align="center">(d) 5 mm circular mesh</div>

Figure B.1: The four meshes in the factorial design study.

Table B.1: Results from brittle cracking factorial design study with 3 mm structured mesh.

3 mm structured mesh						
Fracture stress, (MPa)	Mode I fracture energy, (N/mm)	Failure displace-ment, (mm)	Time at fracture initiation, (s)	Fracture growth, (s)	HIC_{15} , $(g^{2.5}s)$	Fracture pattern, (grade 1-10)
100	0.27	0.001	1.25	4.12	5.62	2.75
118	0.27	0.001	1.5	6	9.71	3
140	0.27	0.001	1.63	4.99	11.57	2.25
100	0.4	0.001	1.25	6.25	8.04	3.5
118	0.4	0.001	1.5	6	9.56	2.25
140	0.4	0.001	1.63	5.12	11.60	2.25
100	0.7	0.001	1.38	5.25	8.52	3.25
118	0.7	0.001	1.5	6	9.81	2.5
140	0.7	0.001	1.63	5.87	12.94	2.25
100	0.27	0.01	1.33	4.34	5.80	3.5
118	0.27	0.01	1.5	8.5	11.73	2.5
140	0.27	0.01	1.67	8.33	19.85	2.5
100	0.4	0.01	1.33	6.84	9.53	2.5
118	0.4	0.01	1.5	8.33	11.47	2.5
140	0.4	0.01	1.67	8.33	19.85	2.5
100	0.7	0.01	1.67	8.33	12.86	2.5
118	0.7	0.01	1.5	8.5	16.21	2.5
140	0.7	0.01	1.67	8.33	22.22	2.5

Table B.2: Results from brittle cracking factorial design study with 5 mm structured mesh.

5 mm structured mesh						
Fracture stress, (MPa)	Mode I fracture energy, (N/mm)	Failure displacement, (mm)	Time at fracture initiation, (s)	Fracture growth, (s)	HIC_{15}, $(g^{2.5}s)$	Fracture pattern, (grade 1-10)
100	0.27	0.001	0.76	4.14	4.04	4.5
118	0.27	0.001	0.75	4.65	4.79	5.25
140	0.27	0.001	1.52	4.98	9.35	2.75
100	0.4	0.001	0.76	4.14	2.80	4.75
118	0.4	0.001	1.3	4.3	5.02	5
140	0.4	0.001	1.4	4.34	6.32	5
100	0.7	0.001	0.88	3.75	2.84	5
118	0.7	0.001	0.88	4.37	4.61	5
140	0.7	0.001	1.5	5.62	10.22	5
100	0.27	0.01	0.83	5	8.30	4.5
118	0.27	0.01	1	4.67	4.97	4.5
140	0.27	0.01	1.5	5.67	9.99	3.5
100	0.4	0.01	1	6.83	13.03	5.25
118	0.4	0.01	1.5	6.67	14.35	5
140	0.4	0.01	1.5	4.5	6.23	5
100	0.7	0.01	1.5	4.83	9.63	4
118	0.7	0.01	1.5	8.5	29.02	2.5
140	0.7	0.01	1.5	4.67	6.79	4.25

Table B.3: Results from brittle cracking factorial design study with 3 mm circular free mesh.
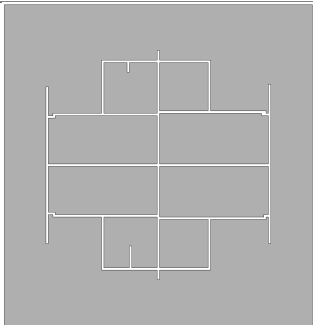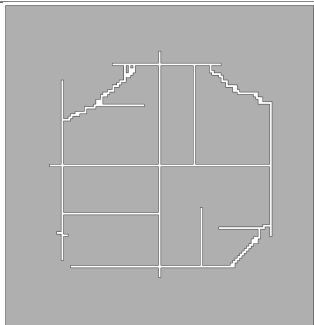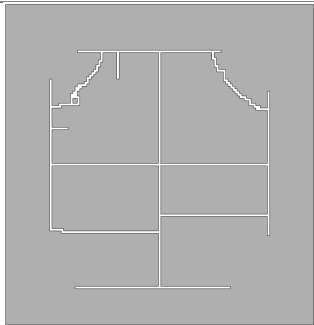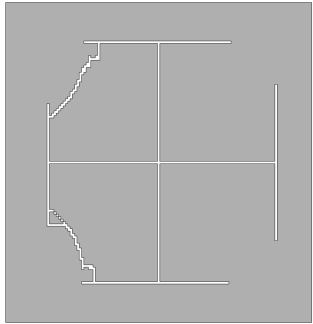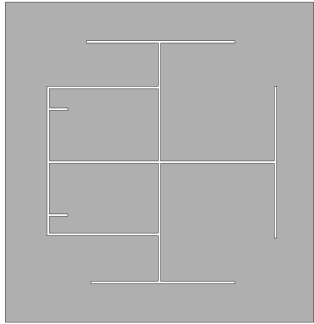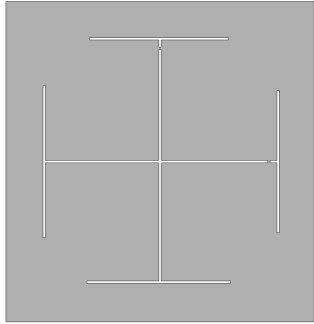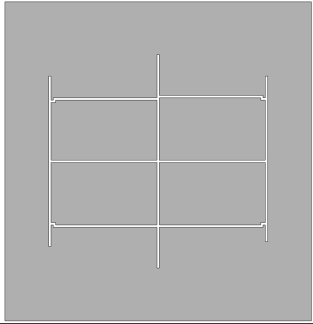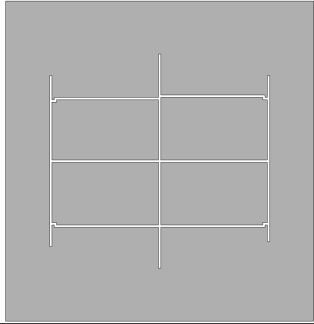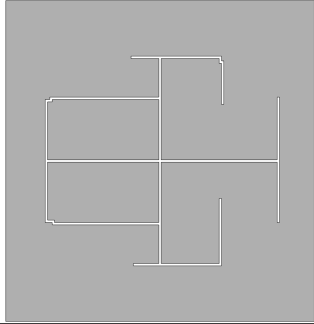
3 mm circular free mesh						
Fracture stress, (MPa)	Mode I fracture energy, (N/mm)	Failure displace-ment, (mm)	Time at fracture initiation, (s)	Fracture growth, (s)	HIC$_{15}$, (g$^{2.5}$s)	Fracture pattern, (grade 1-10)
100	0.27	0.001	1.73	9.37	5.45	3.75
118	0.27	0.001	1.73	11.27	7.29	3.5
140	0.27	0.001	1.95	11.05	19.95	3.5
100	0.4	0.001	1.73	4.37	4.70	4
118	0.4	0.001	1.73	11.27	7.87	3.5
140	0.4	0.001	1.95	11.05	19.95	3.25
100	0.7	0.001	1.73	4.57	4.60	3.5
118	0.7	0.001	1.73	8.67	8.02	2.5
140	0.7	0.001	1.95	9.55	13.12	2.75
100	0.27	0.01	1.73	4.77	5.57	4.25
118	0.27	0.01	1.73	6.07	8.40	3.25
140	0.27	0.01	1.95	11.05	19.72	3.75
100	0.4	0.01	1.73	6.72	6.83	3.75
118	0.4	0.01	1.73	11.27	21.55	2.75
140	0.4	0.01	1.95	11.05	19.72	3.25
100	0.7	0.01	1.52	5.63	8.09	3.75
118	0.7	0.01	1.73	11.27	13.50	3.75
140	0.7	0.01	1.95	11.05	20.87	2.75
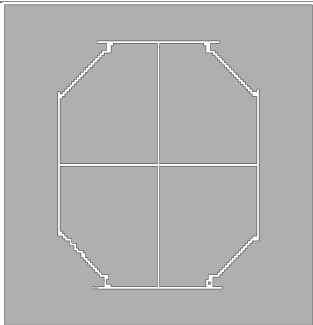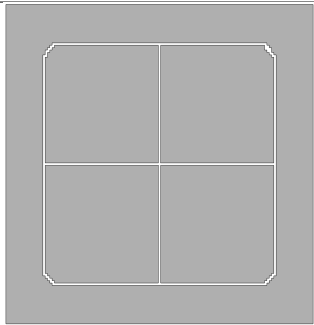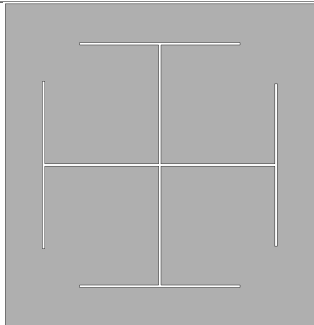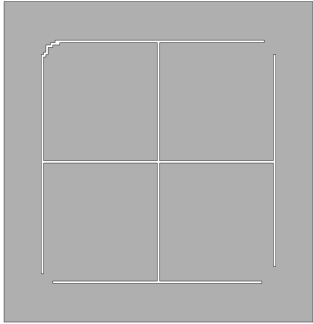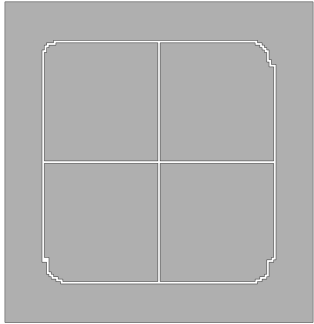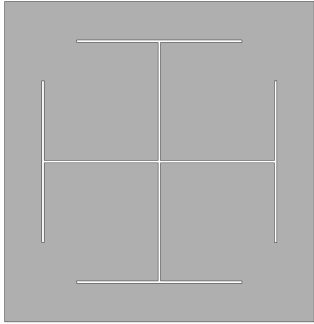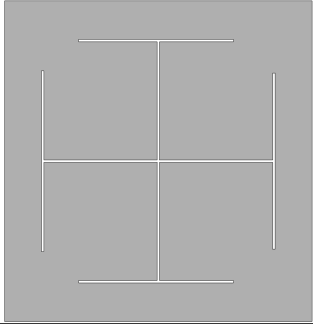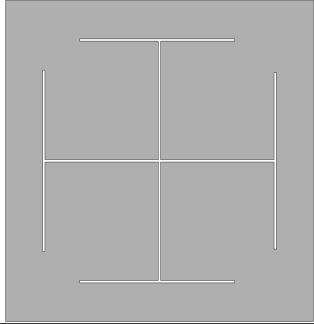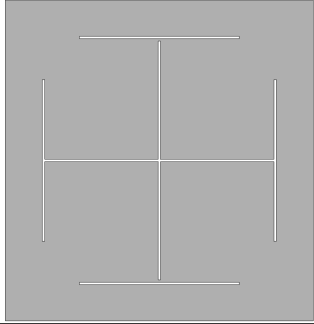
Table B.4: Results from brittle cracking factorial design study with 5 mm circular free mesh.

5 mm circular free mesh						
Fracture stress, (MPa)	Mode I fracture energy, (N/mm)	Failure displacement, (mm)	Time at fracture initiation, (s)	Fracture growth, (s)	HIC_{15}, $(g^{2.5}s)$	Fracture pattern, (grade 1-10)
100	0.27	0.001	1.43	3.42	2.46	4.75
118	0.27	0.001	1.71	3.86	5.16	5.25
140	0.27	0.001	1.71	5	7.95	4.75
100	0.5	0.001	1.43	4	4.28	5.25
118	0.5	0.001	1.71	3.86	5.21	5
140	0.5	0.001	1.71	4.86	7.95	5.25
100	0.7	0.001	1.57	5.86	6.55	5.75
118	0.7	0.001	1.71	3.86	5.36	4.5
140	0.7	0.001	1.71	8.29	28.39	3.25
100	0.27	0.01	1.43	3.86	4.00	5.25
118	0.27	0.01	1.71	3	2.97	3.75
140	0.27	0.01	1.86	5.71	15.93	4.25
100	0.5	0.01	1.43	4.28	5.69	5
118	0.5	0.01	1.71	4.15	7.80	5
140	0.5	0.01	1.71	4.72	7.34	4.5
100	0.7	0.01	1.57	4.43	5.64	5
118	0.7	0.01	1.71	3.58	5.07	4.5
140	0.7	0.01	1.86	5.85	16.34	4.75
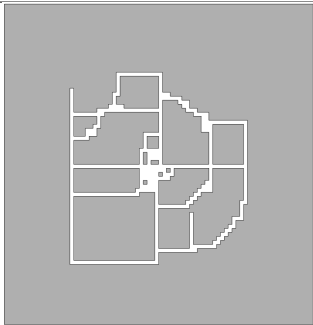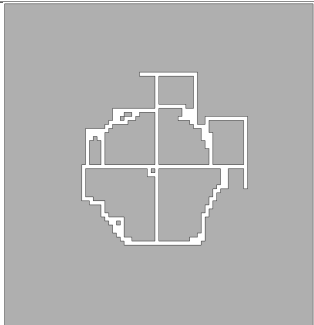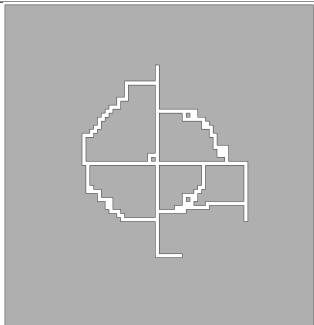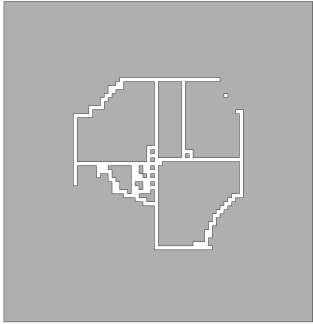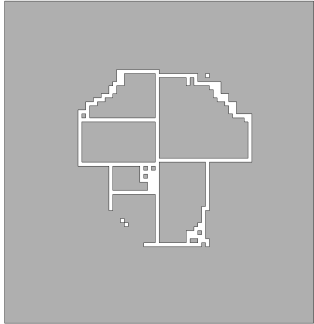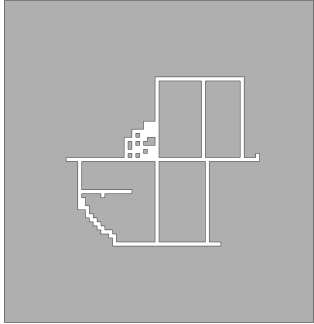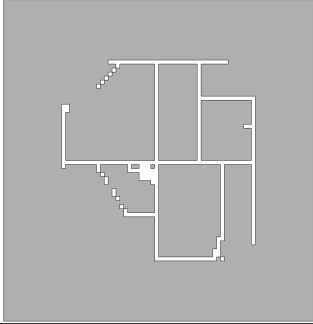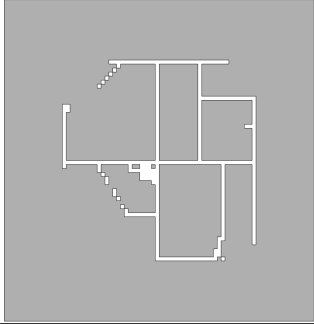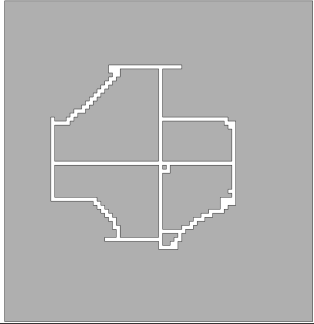
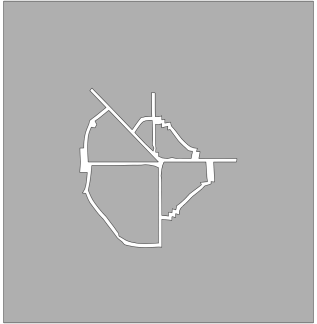**Table B.5:** Fracture pattern from 3 mm structured mesh. Failure displacement = 0.001 mm.

Fracture stress	Mode I fracture energy		
	0.27 N/mm	0.5 N/mm	0.7 N/mm
100 MPa			
118 MPa			
140 MPa			
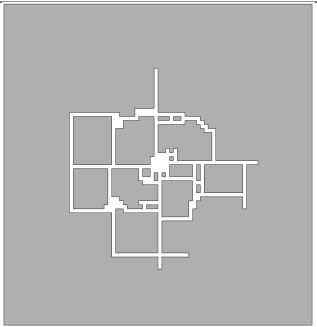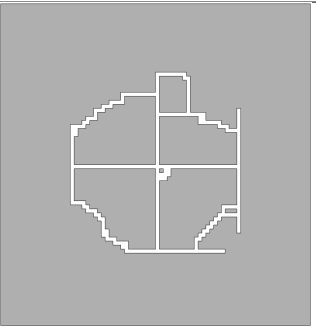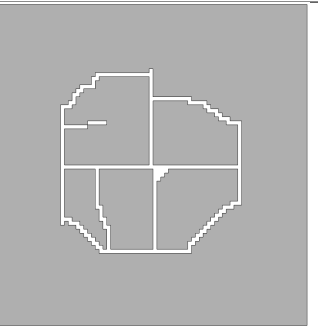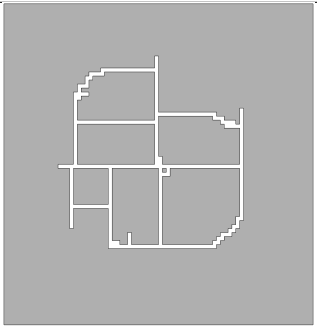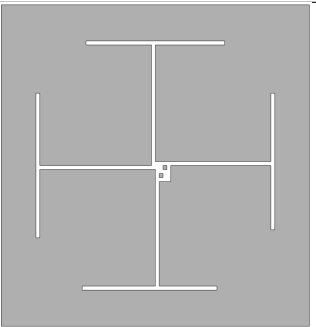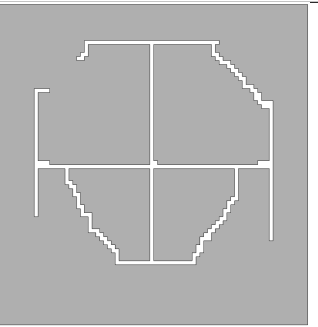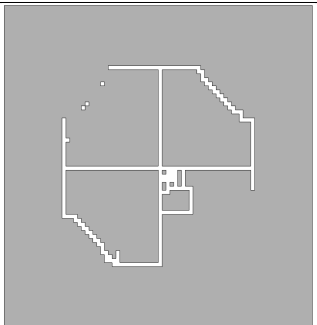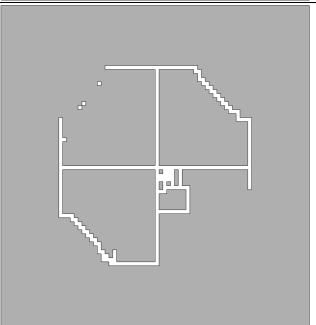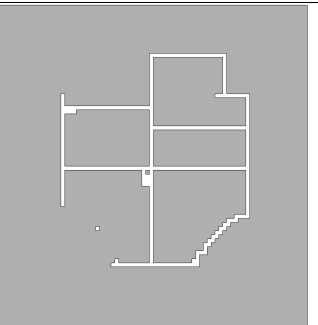
Table B.6: Fracture pattern from 3 mm structured mesh. Failure displacement = 0.01 mm.

Fracture stress	Mode I fracture energy		
	0.27 N/mm	0.5 N/mm	0.7 N/mm
100 MPa			
118 MPa			
140 MPa			
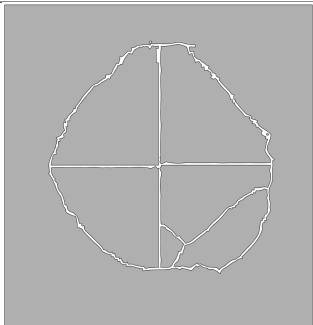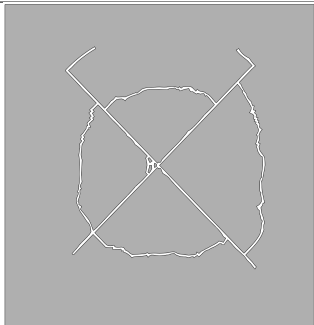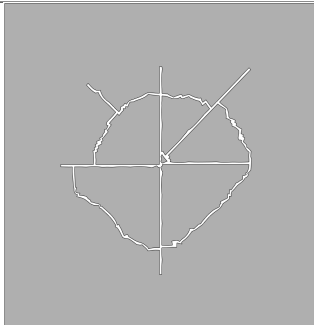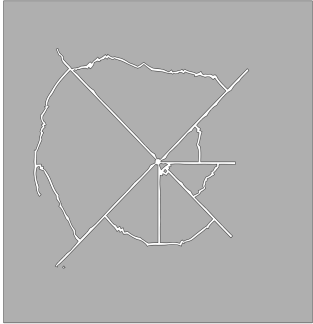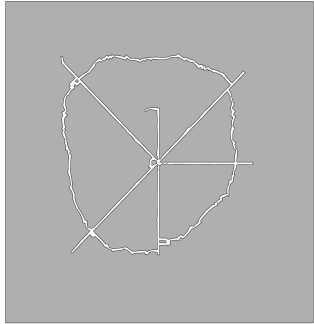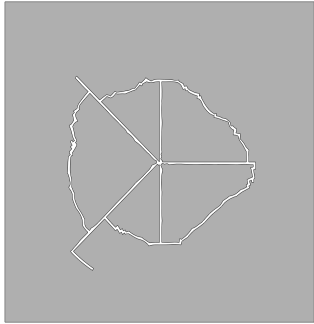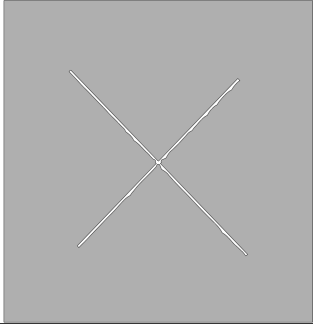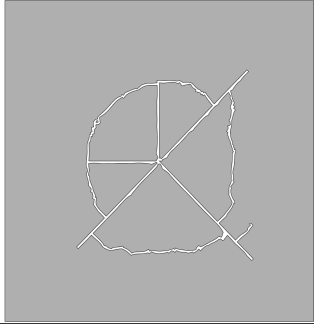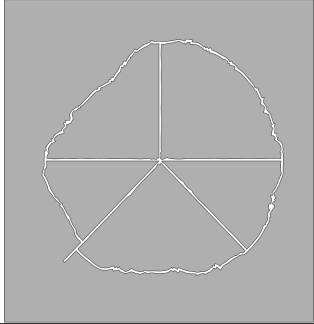
Table B.7: Fracture pattern from 5 mm structured mesh. Failure displacement = 0.001 mm.

Fracture stress	Mode I fracture energy		
	0.27 N/mm	0.5 N/mm	0.7 N/mm
100 MPa			
118 MPa			
140 MPa			
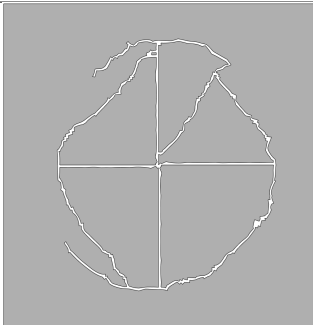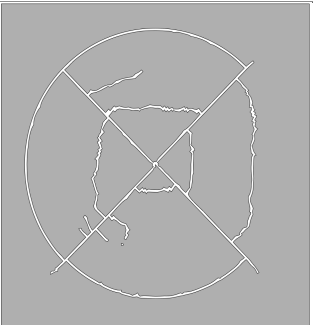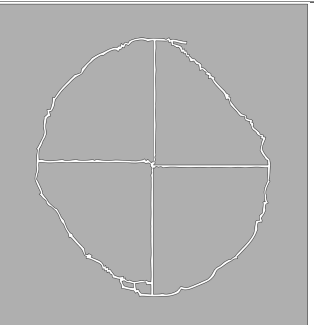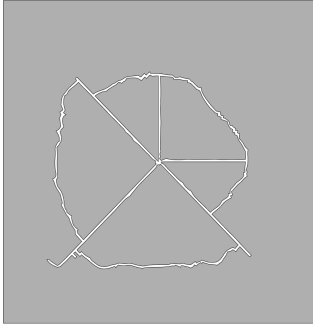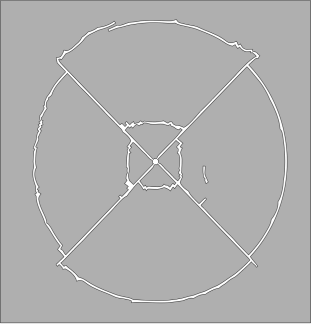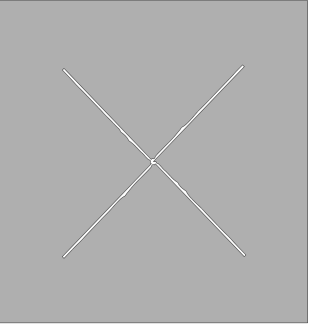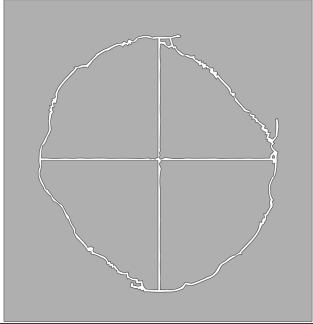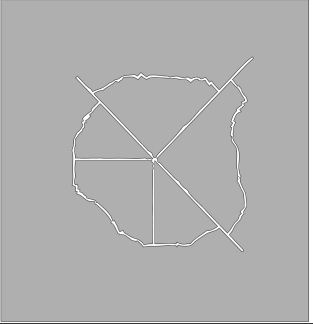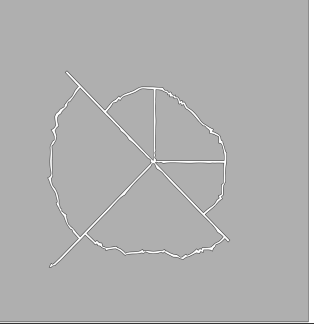
Table B.8: Fracture pattern from 5 mm structured mesh. Failure displacement = 0.01 mm.

Fracture stress	Mode I fracture energy		
	0.27 N/mm	0.5 N/mm	0.7 N/mm
100 MPa			
118 MPa			
140 MPa			
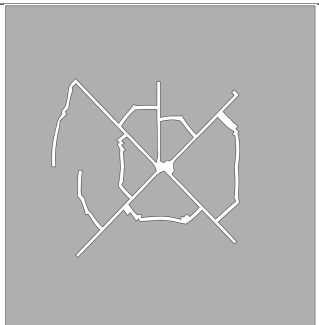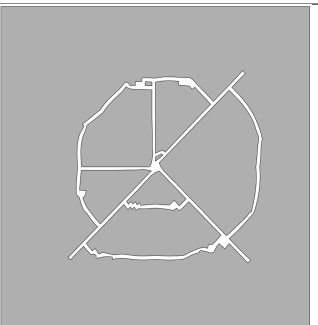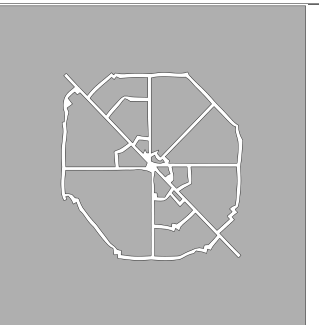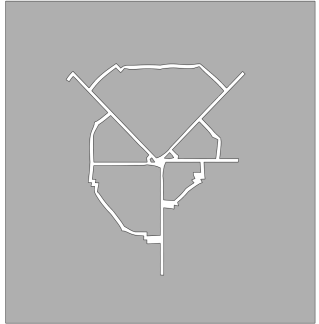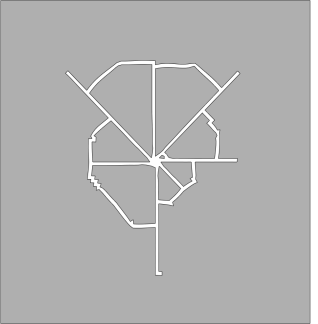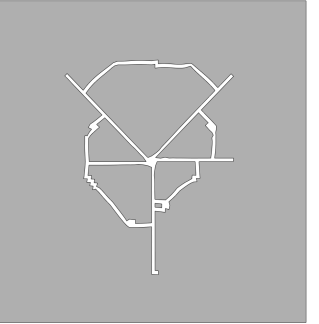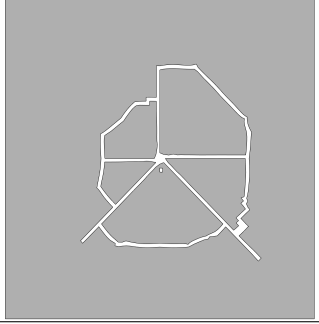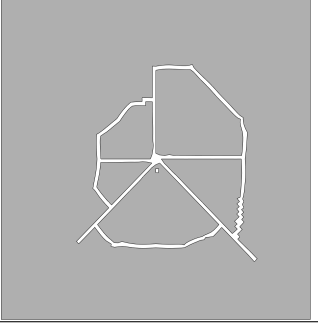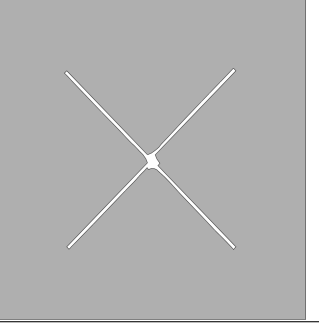
Table B.9: Fracture pattern from 3 mm circular free mesh. Failure displacement = 0.001 mm.

Fracture stress	Mode I fracture energy		
	0.27 N/mm	0.5 N/mm	0.7 N/mm
100 MPa			
118 MPa			
140 MPa			

Table B.10: Fracture pattern from 3 mm circular free mesh. Failure displacement = 0.01 mm.
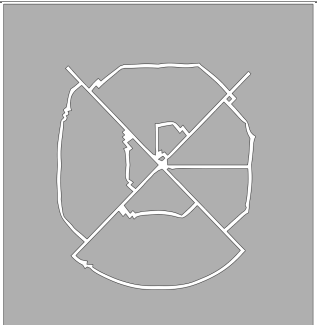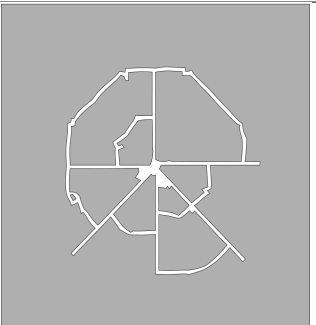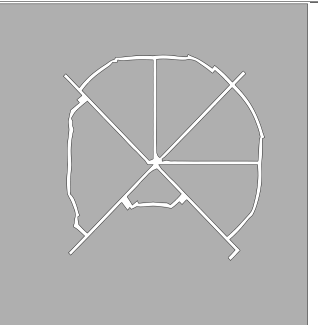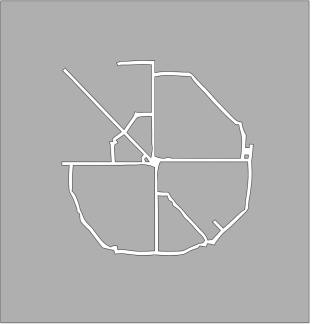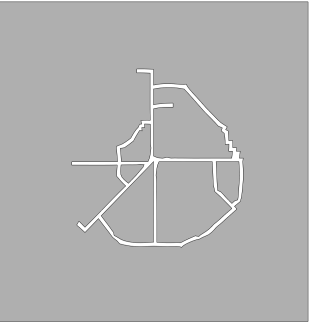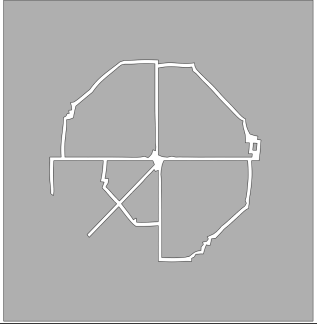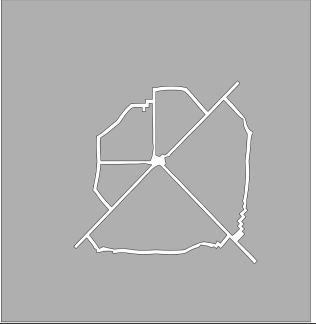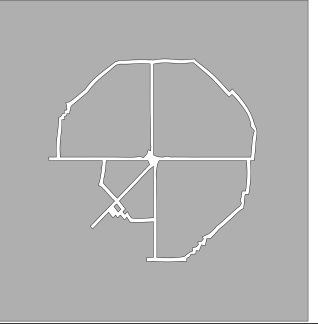
Fracture stress	Mode I fracture energy		
	0.27 N/mm	0.5 N/mm	0.7 N/mm
100 MPa			
118 MPa			
140 MPa			

Table B.11: Fracture pattern from 5 mm circular free mesh. Failure displacement = 0.001 mm.

Fracture stress	Mode I fracture energy		
	0.27 N/mm	0.5 N/mm	0.7 N/mm
100 MPa			
118 MPa			
140 MPa			

Table B.12: Fracture pattern from 5 mm circular free mesh. Failure displacement = 0.01 mm.
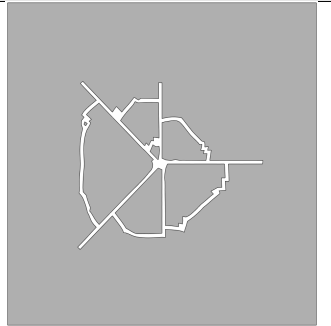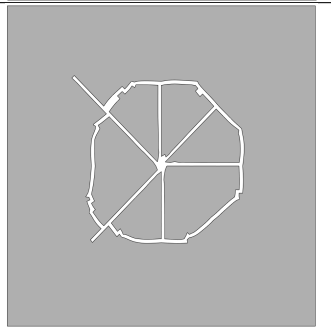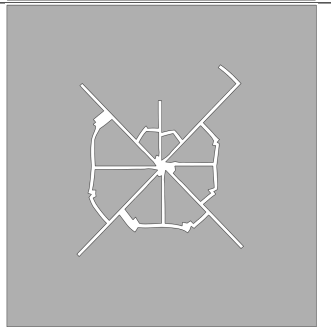
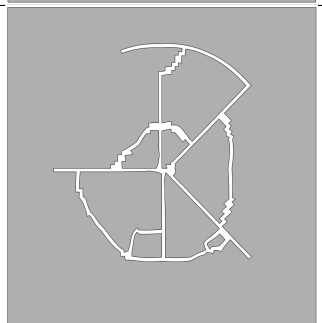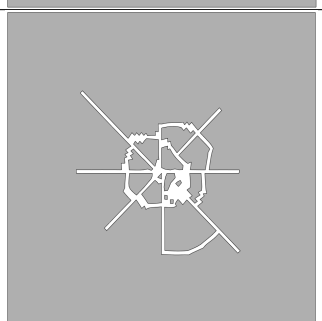| Fracture stress	Mode I fracture energy		
	0.27 N/mm	0.5 N/mm	0.7 N/mm
100 MPa			
118 MPa			
140 MPa			
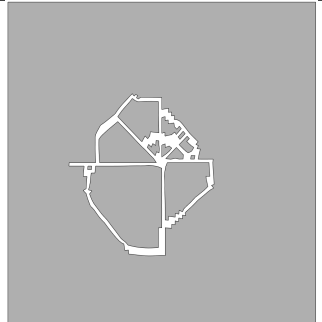
Figure B.2: Energy balance from a typical simulation in the factorial design study.

B.2 Integration order and number of integration points

Table B.13: Results from integration order and number of integration points factorial design study.

Integration order	Integration points	HIC$_{15}$ (g$^{2.5}$s)	Fracture pattern
Reduced	5	5.08	
Reduced	7	5.22	
Reduced	9	4.61	

Table B.14: Results from integration order and number of integration points factorial design study.

Integration order	Integration points	HIC_{15} $(g^{2.5}s)$	Fracture pattern
Full	5	2.88	
Full	7	3.88	
Full	9	1.96	

Table B.15: Run time for the different simulations in the factorial design study of integration order number of integration points.

	Run time per simulated time	
	Reduced integration	Full integration
5 integration points	58 s/ms	157 s/ms
7 integration points	67 s/ms	186 s/ms
9 integration points	76 s/ms	225 s/ms

B.3 Volume elements

Table B.16: Element dimensions and Brittle Cracking parameters from simulations with volume elements.

Mesh	Element dimensions	Critical stress	Fracture energy	Failure displacement
1	$5 \times 5 \times 0.95$ mm^3	118 MPa	0.590 N/mm	0.010 mm
2	$3 \times 3 \times 0.63$ mm^3	118 MPa	0.477 N/mm	0.0081 mm
3	$1 \times 1 \times 0.63$ mm^3	118 MPa	0.112 N/mm	0.0019 mm

C. Appendix: Numerical work - Laminated glass

C.1 Factorial design - Main parameters

Table C.1: Results from Main parameters factorial design for structured mesh.

Factorial Design - Main Parameters							
Structured							
Glass Mesh	Brittle Failure	PVB Model	Contact	HIC_{15}	t_1	t_2	Max Displacement
(-)	(-)	(-)	(-)	$(g^{2.5}s)$	(s)	(s)	(mm)
5 mm	On	N-L viscoelastic	GC	198	0	13.7	34.5
5 mm	On	N-L viscoelastic	STS	233	0	10.0	31.3
5 mm	On	Mises plasticity	GC	216	0	11.9	33.5
5 mm	On	Mises plasticity	STS	316	0	12.3	32.2
5 mm	Top Off	N-L viscoelastic	GC	188	0	14.8	36.9
5 mm	Top Off	N-L viscoelastic	STS	557	0	7.9	18.5
5 mm	Top Off	Mises plasticity	GC	445	0	9.9	23.1
5 mm	Top Off	Mises plasticity	STS	485	0	9.0	20.1
3 mm	On	N-L viscoelastic	GC	391	0	11.1	29.2
3 mm	On	N-L viscoelastic	STS	280	0	8.5	26.4
3 mm	On	Mises plasticity	GC	299	0	10.9	30.7
3 mm	On	Mises plasticity	STS	454	0	9.5	25.4
3 mm	Top Off	N-L viscoelastic	GC	378	0	6.9	22.8
3 mm	Top Off	N-L viscoelastic	STS	540	0	5.4	17.2
3 mm	Top Off	Mises plasticity	GC	378	0	6.9	22.8
3 mm	Top Off	Mises plasticity	STS	541	0	8.6	18.8

Table C.2: Results from Main parameters factorial design for Circular mesh.

Factorial Design - Main Parameters							
Circular							
Glass Mesh	Brittle Failure	PVB Model	Contact	HIC_{15}	t_1	t_2	Max Displacement
(-)	(-)	(-)	(-)	$(g^{2.5}s)$	(s)	(s)	(mm)
5 mm	On	N-L viscoelastic	GC	273	0	12.7	31.7
5 mm	On	N-L viscoelastic	STS	243	0	9.7	29.7
5 mm	On	Mises plasticity	GC	171	0	15	37.1
5 mm	On	Mises plasticity	STS	332	0	11.2	29.1
5 mm	Top Off	N-L viscoelastic	GC	416	0	11.8	26.6
5 mm	Top Off	N-L viscoelastic	STS	388	0	9.4	20.3
5 mm	Top Off	Mises plasticity	GC	371	0	11.9	27.8
5 mm	Top Off	Mises plasticity	STS	356	0	10.9	23.4
3 mm	On	N-L viscoelastic	GC	267	0	12.6	30.9
3 mm	On	N-L viscoelastic	STS	378	0	8.5	24.3
3 mm	On	Mises plasticity	GC	205	0	13.5	34.1
3 mm	On	Mises plasticity	STS	238	0	8.6	29.6
3 mm	Top Off	N-L viscoelastic	GC	385	0	11.5	25.1
3 mm	Top Off	N-L viscoelastic	STS	464	0	7.9	18.9
3 mm	Top Off	Mises plasticity	GC	322	0	11.6	26.9
3 mm	Top Off	Mises plasticity	STS	535	0	9.3	19.8

C.2 Factorial design - Mesh Parameters

Table C.3: Results from Mesh parameters factorial design for Circular Free mesh.

Factorial Design - Mesh Parameters						
Circular Free						
Glass size (mm)	PVB size (mm)	NOE PVB thickness (-)	HIC_{15} $(g^{2.5}s)$	t_1 (s)	t_2 (s)	Max displacement (mm)
5	5	1	332.7	0.0	11.4	27.7
5	5	3	308.1	0.0	11.1	28.1
5	4	1	298.2	0.0	10.1	26.8
5	4	3	331.6	0.0	11.2	27.0
5	3	1	345.4	0.0	11.0	26.4
5	3	3	305.8	0.0	10.7	27.5
5	2	1	338.9	0.0	11.5	27.4
5	2	3	367.5	0.0	11.3	26.2
3	5	1	335.9	0.0	11.0	27.0
3	5	3	324.4	0.0	11.2	26.4
3	4	1	437.5	0.0	10.5	25.0
3	4	3	286.82	0.0	8.4	25.9
3	3	1	293.7	0.0	11.3	27.0
3	3	3	267.6	0.0	11.7.	27.7
3	2	1	265.0	0.0	10.0	25.8
3	2	3	297.8	0.0	12.2	28.8
2	5	1	346.9	0.0	10.2	26.1
2	5	3	322.8	0.0	9.7	25.1
2	4	1	339.5	0.0	10.7	25.6
2	4	3	251.9	0.0	10.1	26.2
2	3	1	309.3	0.0	11.7	28.2
2	3	3	253.0	0.0	12.0	28.6
2	2	1	317.7	0.0	11.7	27.5
2	2	3	287.6	0.0	11.7	28.5

Table C.4: Results from Mesh parameters factorial design for Radial Cuts mesh.

Factorial Design - Mesh Parameters						
Radial Cuts						
Glass size (mm)	PVB size (mm)	NOE PVB thickness (-)	HIC_{15} ($g^{2.5}s$)	t_1 (s)	t_2 (s)	Max displacement (mm)
5	5	1	324.8	0.0	12.3	27.7
5	5	3	339.4	0.0	11.0	26.5
5	4	1	311.7	0.0	8.4	26.0
5	4	3	457.0	0.0	10.9	26.4
5	3	1	335.9	0.0	11.6	26.5
5	3	3	251.0	0.0	11.0	27.2
5	2	1	232.3	0.0	8.1	26.8
5	2	3	291.1	0.0	10.6	26.5
3	5	1	356.1	0.0	11.3	26.9
3	5	3	240.8	0.0	10.8	26.5
3	4	1	230.9	0.0	11.9	28.4
3	4	3	263.9	0.0	7.4	26.3
3	3	1	251.6	0.0	12.2	28.1
3	3	3	289.9	0.0	6.6	25.5
3	2	1	198.1	0.0	12.6	29.9
3	2	3	241.7	0.0	5.4	27.5
2	5	1	340.9	0.0	9.8	25.6
2	5	3	312.0	0.0	10.8.	26.7
2	4	1	261.1	0.0	11.7	28.7
2	4	3	267.7	0.0	11.9	28.7
2	3	1	248.3	0.0	12.8	31.5
2	3	3	266.4	0.0	12.2	29.3
2	2	1	252.4	0.0	11.5	28.3
2	2	3	275.6	0.0	11.5	26.6

C.3 Stress softening and material damping

Table C.5: Results from Brittle Cracking in laminated glass factorial design

Mesh	Stress model	Material damping	HIC_{15}	t_1	t_2	Max displacement
(-)	(-)	(-)	$(g^{2.5}s)$	(s)	(s)	(mm)
3mm-2mm-1	Softening	Zero	272.0	0.0	11.6	26.6
3mm-2mm-1	Softening	Damping: $\beta = 1.7 \cdot 10^{-7}$	425.1	0.0	10.2	23.6
3mm-2mm-1	Fast fracture	Zero	273.4	0.0	12.3	27.6
3mm-2mm-1	Fast fracture	Damping: $\beta = 1.7 \cdot 10^{-7}$	250.7	0.0	12.2	27.5
2mm-2mm-1	Softening	Zero	390.2	0.0	11.3	27.9
2mm-2mm-1	Softening	Damping: $\beta = 1.7 \cdot 10^{-7}$	297.12	0.0	12.3	28.5
2mm-2mm-1	Fast fracture	Zero	281.2	0.0	12.6	30.1
2mm-2mm-1	Fast fracture	Damping: $\beta = 1.7 \cdot 10^{-7}$	260.4	0.0	12.5	29.2

C.4   Energy output
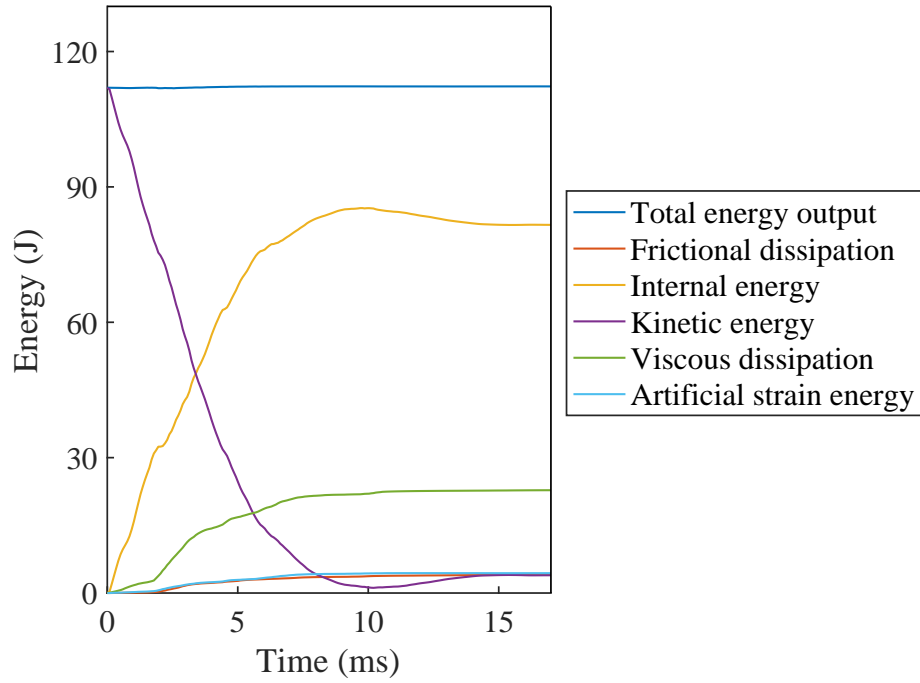
Figure C.1: Energy balance for the best configured model with impact velocity 5.8 m/s. The configuration is Radial Cuts-3mm-2mm-1,

D. Appendix: Numerical work - Case studies

D.1   Head impact on laminated glass
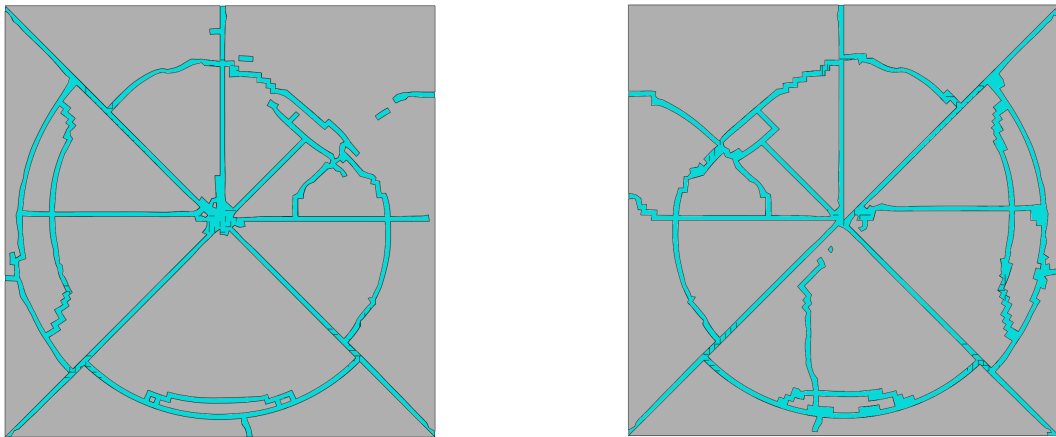
(a) Upper glass plate after impact seen from above.   **(b)** Lower glass plate after impact seen from below.

Figure D.1: Fracture pattern in upper and lower glass after impact on laminated glass.
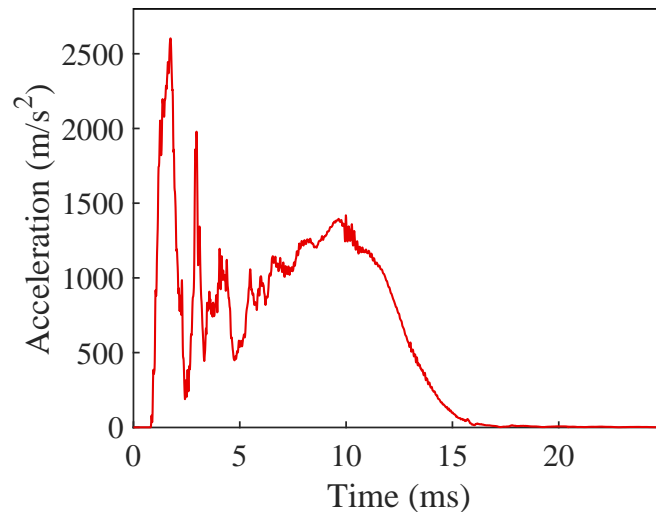
Figure D.2: Acceleration of headform during impact.

D.2   Head impact on laminated windshield
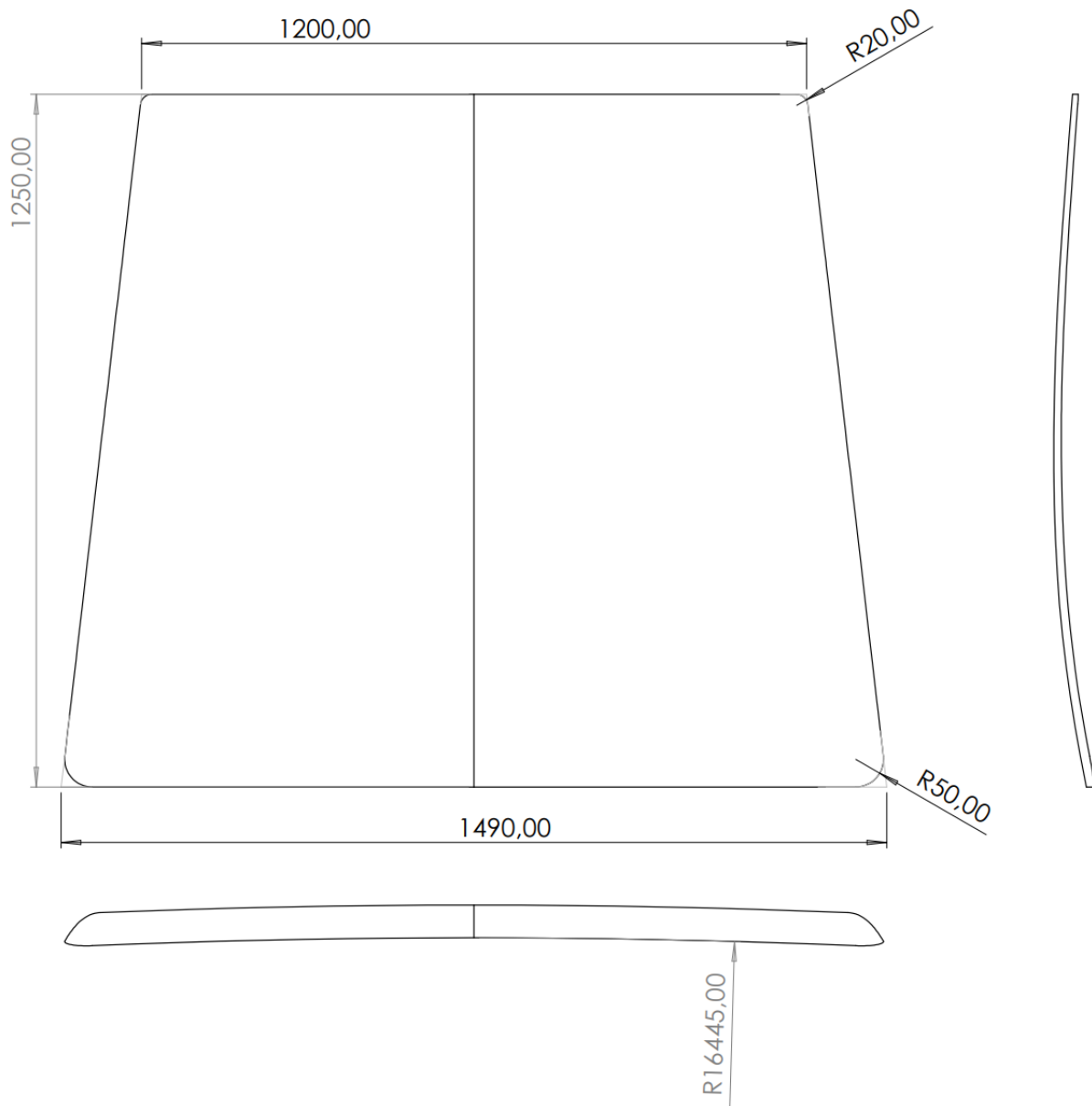
Figure D.3: Dimensions of windshield used in the case study. The measurements are given in mm.
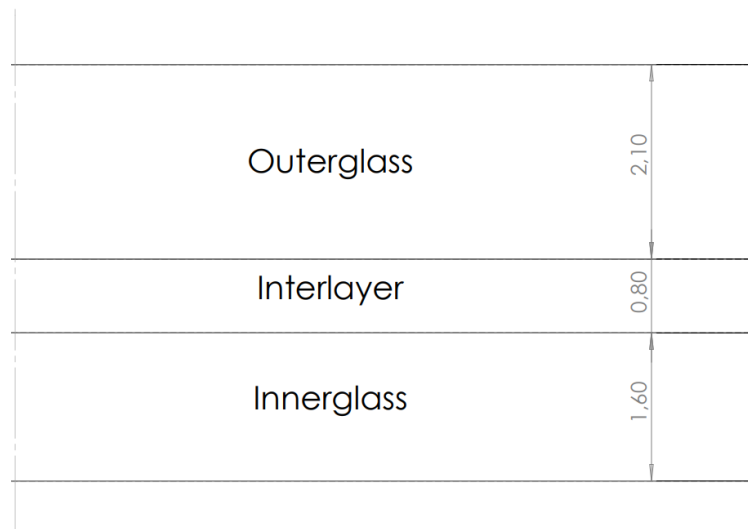
Figure D.4: Cross section measurements of the laminated windshield used in the case study. The measurements are given in mm.
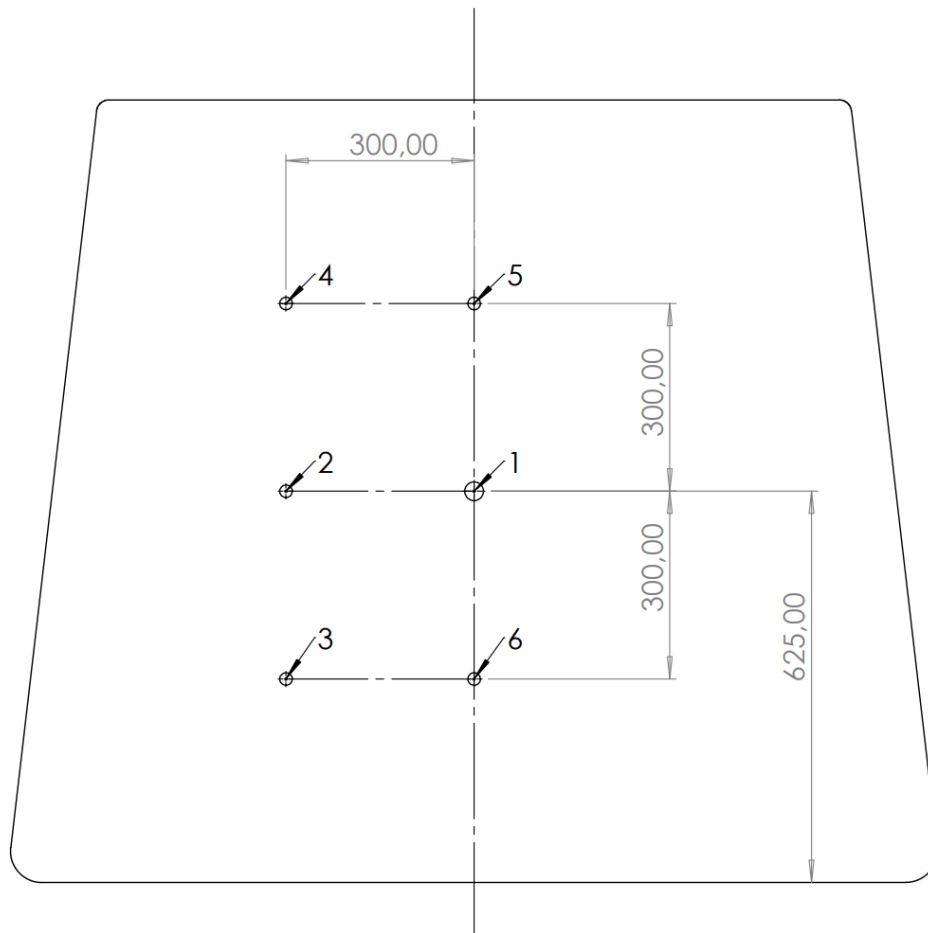
Figure D.5: Positions of impact targets on windshield. The measurements are given in mm. Impact target nr. 1 is recognized as the center of the windshield.

(a) Outerglass

(b) Innerglass
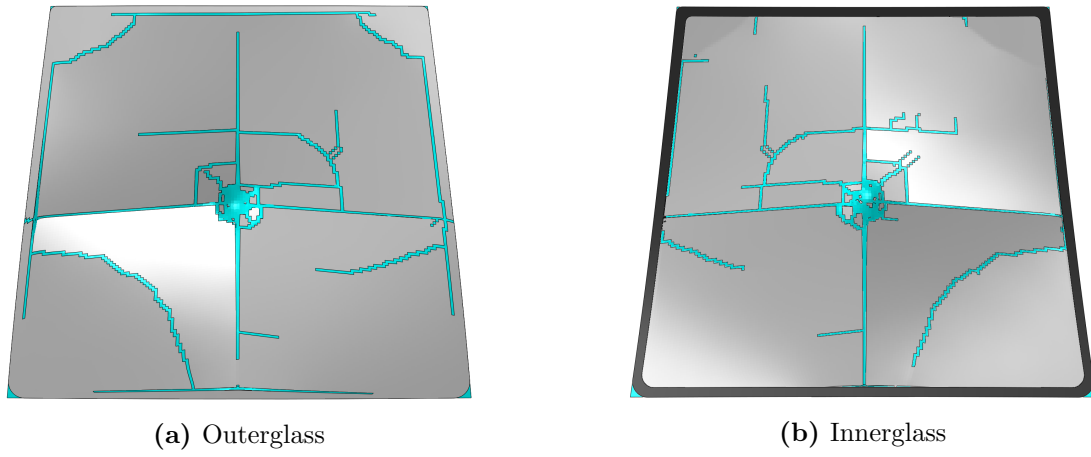
Figure D.6: Fracture pattern from simulation of head impact on target position 1 with Mesh 1.

(a) Outerglass

(b) Innerglass
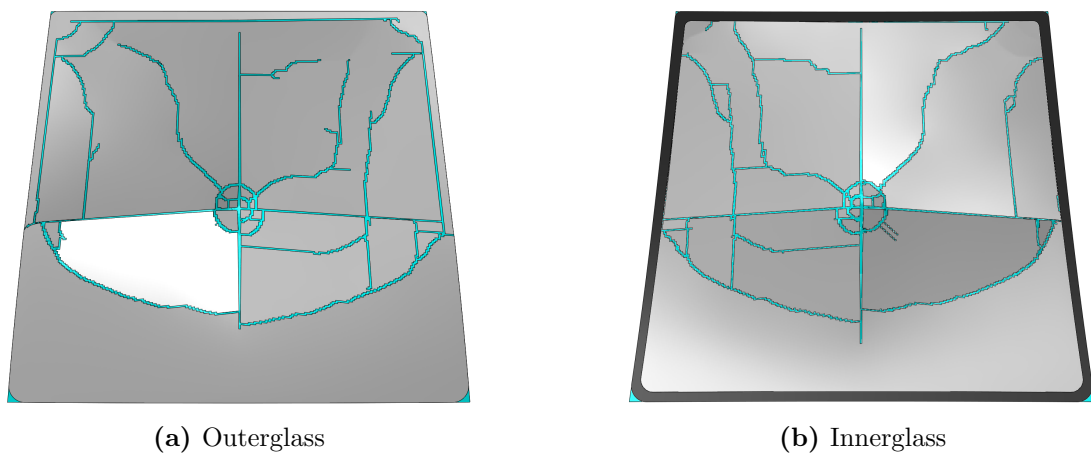
Figure D.7: Fracture pattern from simulation of head impact on target position 1 with Mesh 2.

(a) Outerglass

(b) Innerglass
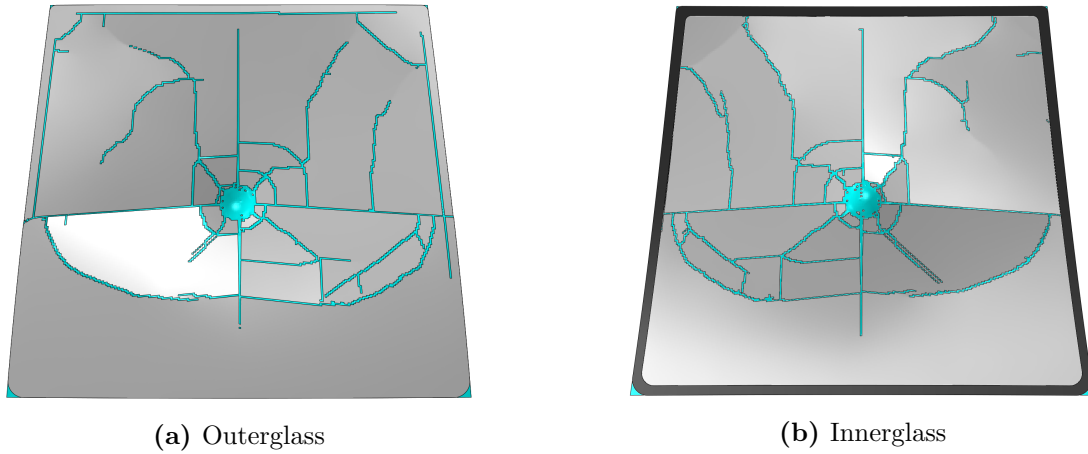
Figure D.8: Fracture pattern from simulation of head impact on target position 1 with Mesh 2 and a rigid impactor.
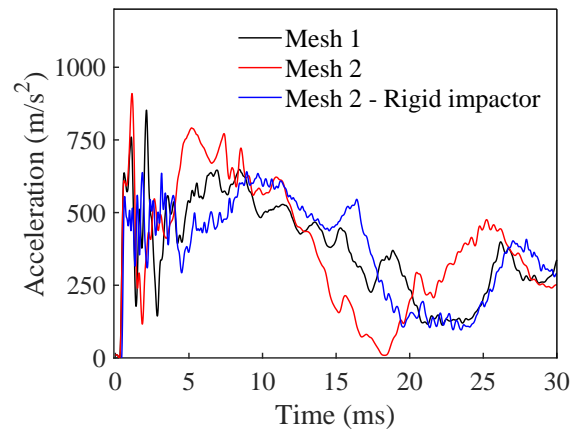
Figure D.9: Time versus acceleration of headform from simulation of head impact on target position 1.

(a) Outerglass

(b) Innerglass
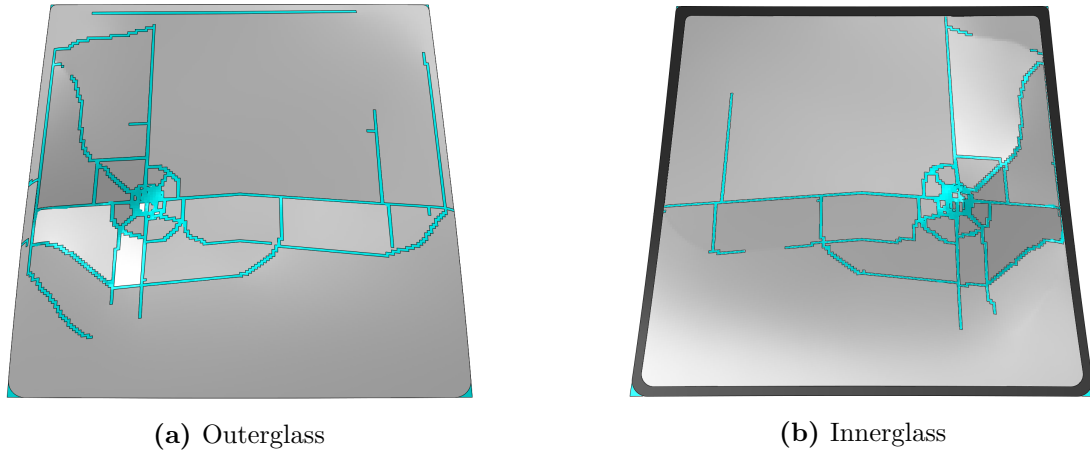
Figure D.10: Fracture pattern from simulation of head impact on target position 2 with Mesh 1.

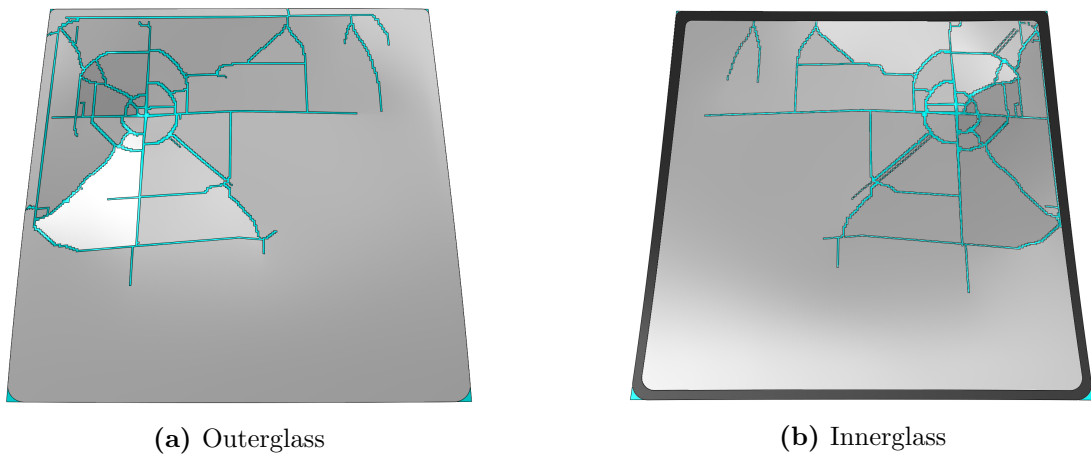**(a)** Outerglass

(b) Innerglass
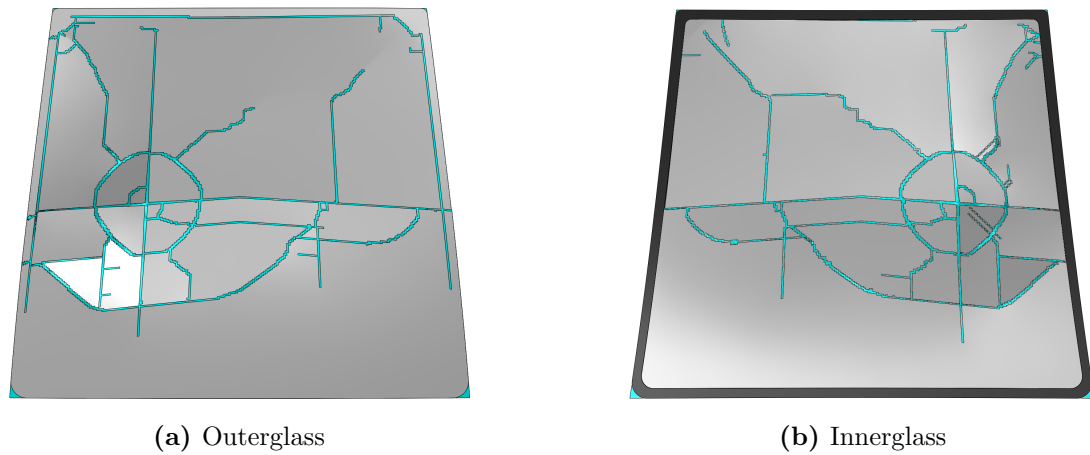
Figure D.11: Fracture pattern from simulation of head impact on target position 2 with Mesh 2.
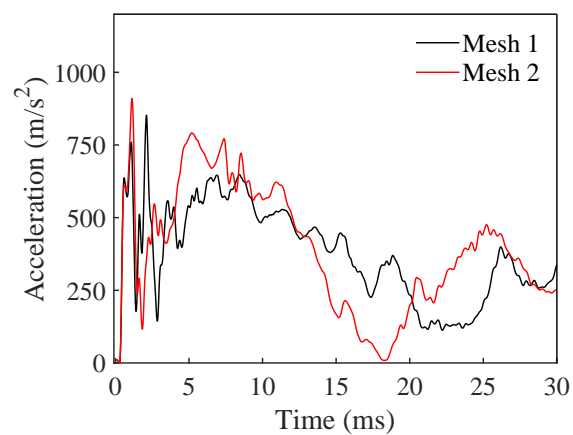
Figure D.12: Acceleration versus time of headform from simulation of head impact on target position 2.

(a) Outerglass

(b) Innerglass
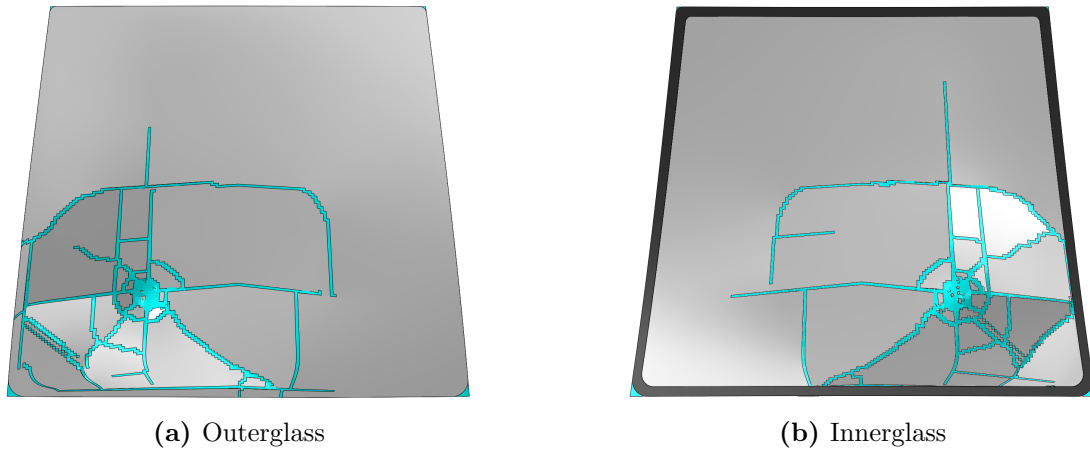
Figure D.13: Fracture pattern from simulation of head impact on target position 3 with Mesh 1.

(a) Outerglass

(b) Innerglass
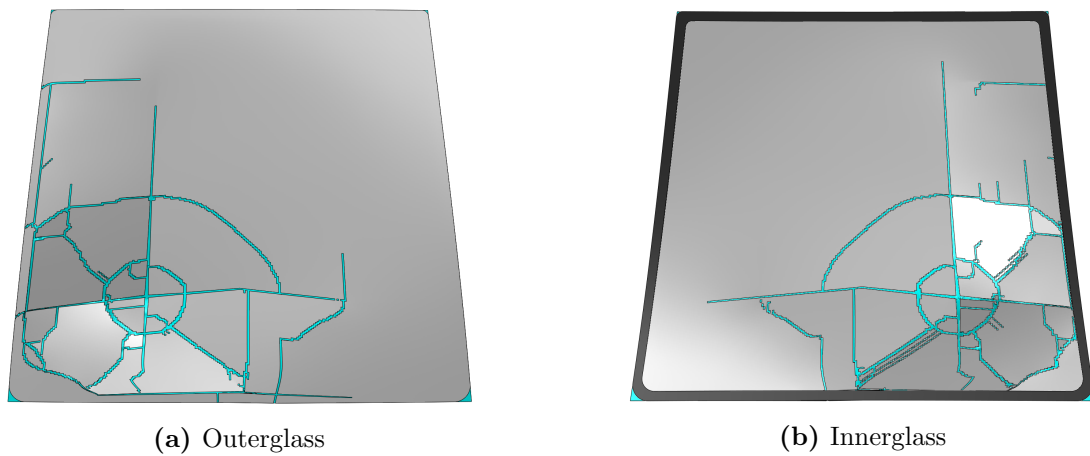
Figure D.14: Fracture pattern from simulation of head impact on target position 3 with Mesh 2.
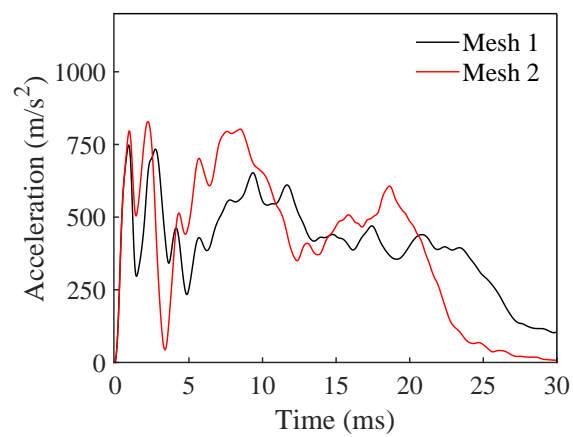
Figure D.15: Acceleration versus time of headform from simulation of head impact on target position 3.

(a) Outerglass

(b) Innerglass
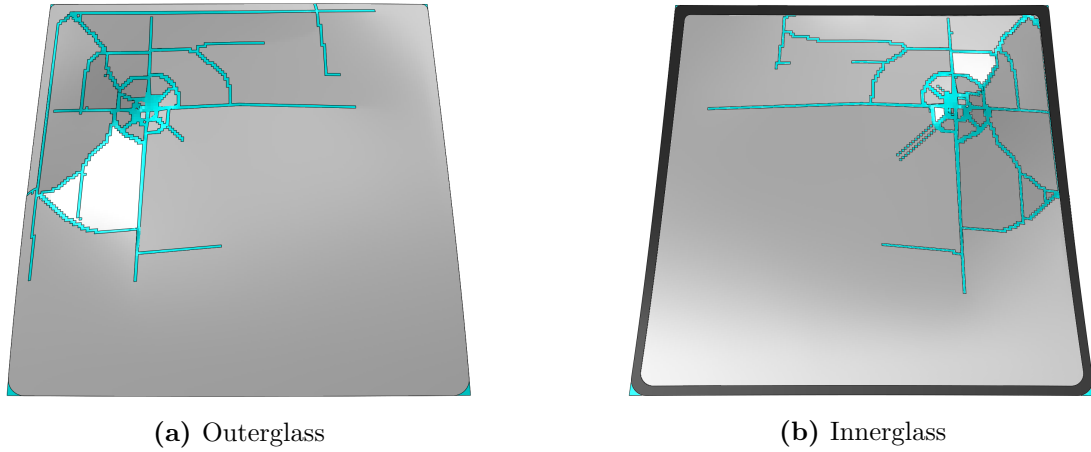
Figure D.16: Fracture pattern from simulation of head impact on target position 4 with Mesh 1.

(a) Outerglass

(b) Innerglass

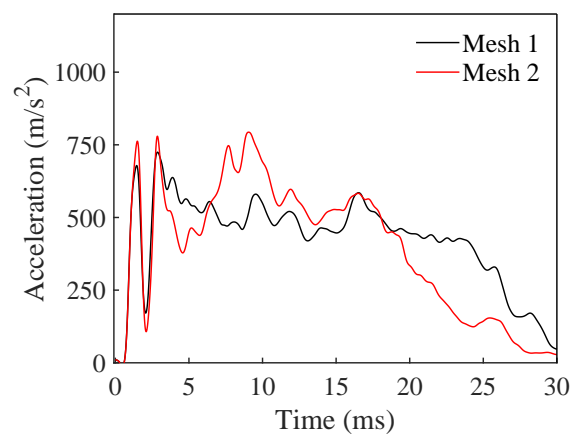**Figure D.17:** Fracture pattern from simulation of head impact on target position 4 with Mesh 2.
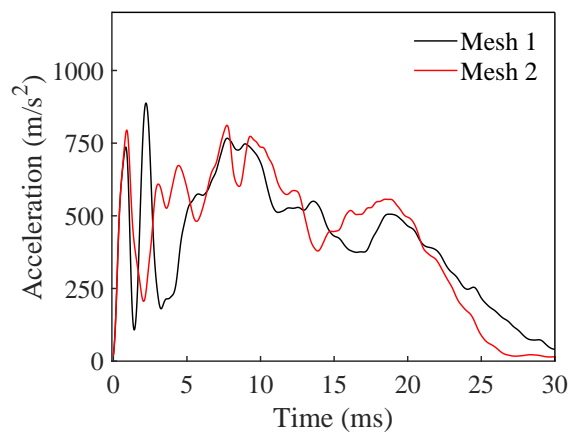
Figure D.18: Acceleration versus time of headform from simulation of head impact on target position 4.

(a) Outerglass

(b) Innerglass
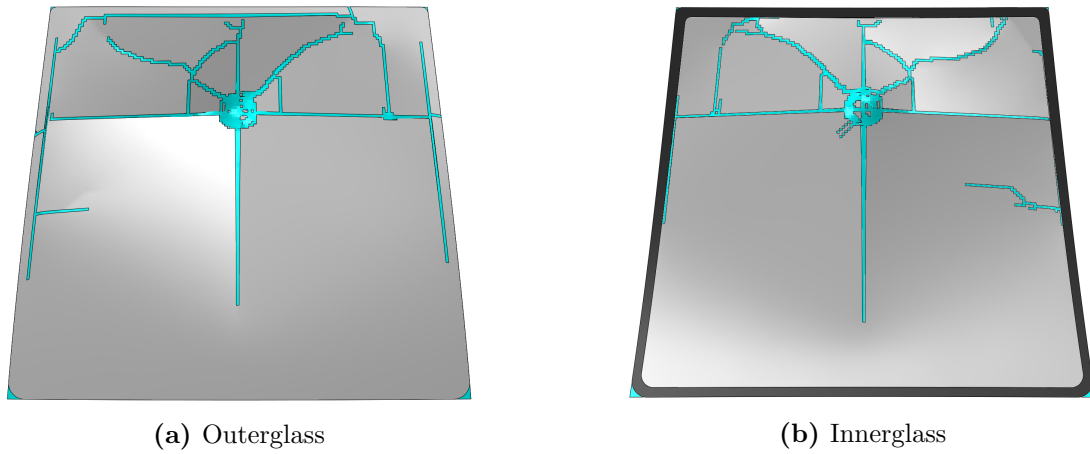
Figure D.19: Fracture pattern from simulation of head impact on target position 5 with Mesh 1.

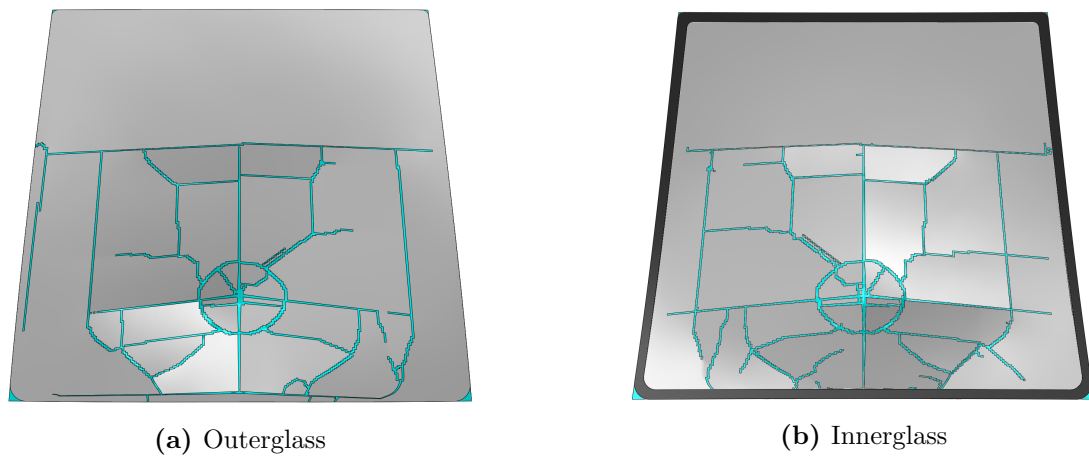
(a) Outerglass

(b) Innerglass
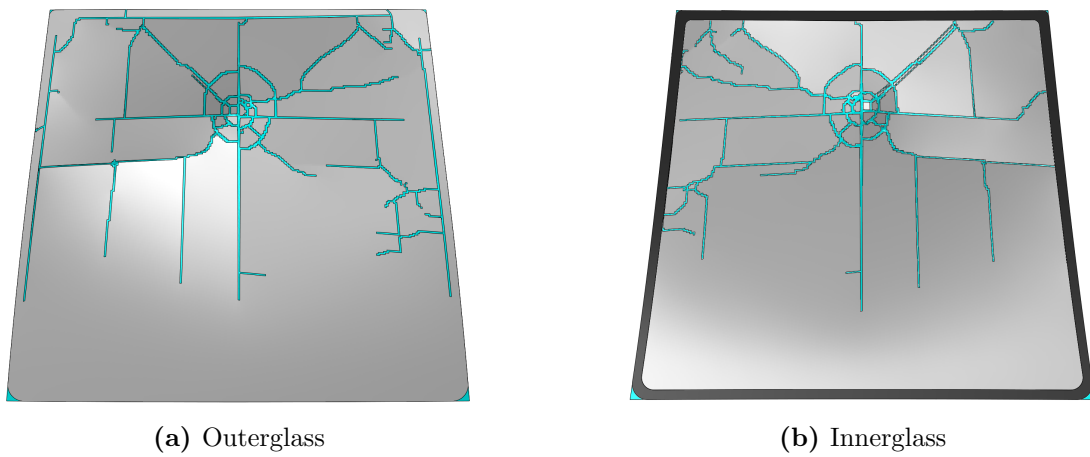
Figure D.20: Fracture pattern from simulation of head impact on target position 5 with Mesh 2.

Figure D.21: Acceleration versus time of headform from simulation of head impact on target position 5.

(a) Outerglass

(b) Innerglass
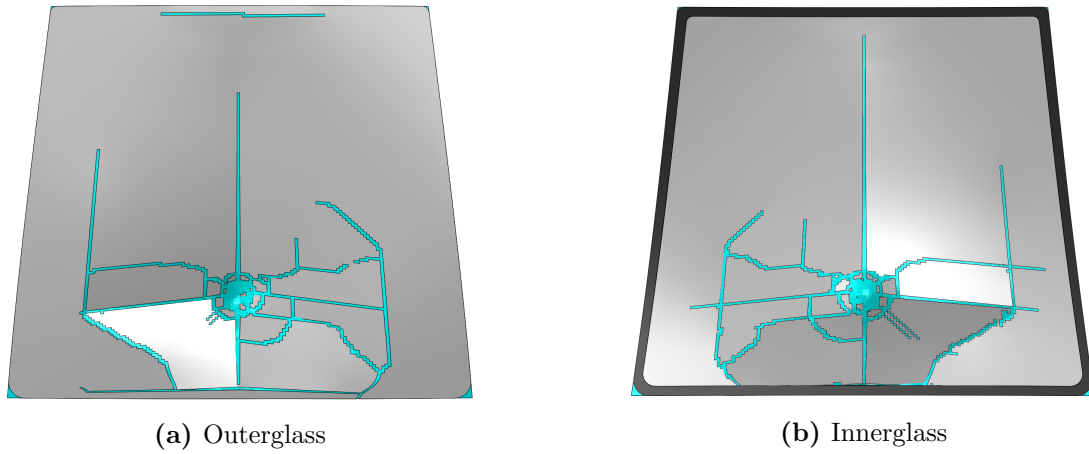
Figure D.22: Fracture pattern from simulation of head impact on target position 6 with Mesh 1.

(a) Outerglass

(b) Innerglass

Figure D.23: Fracture pattern from simulation of head impact on target position 6 with Mesh 2.
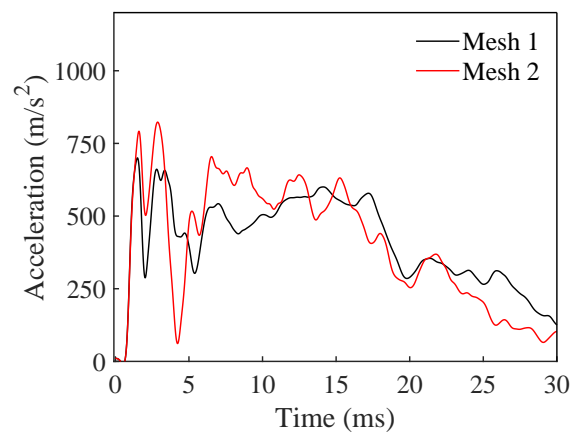
Figure D.24: Acceleration versus time of headform from simulation of head impact on target position 6.

D.3 Blast load on laminated glass

Table D.1: Pressure versus time data used for model the blast load in Abaqus, [25].

Time (ms)	Pressure (kPa)
0	237.7
1.11	208.31
2.22	182.
3.33	158.46
4.44	137.42
5.55	118.65
6.66	101.92
7.77	87.027
8.88	73.796
9.99	62.06
11.1	51.668
12.21	42.486
13.32	34.389
14.43	27.268
15.54	21.02
16.65	15.556
17.76	10.793
18.87	6.6559
19.98	3.0786
21.09	0